



**TECHNISCHE  
UNIVERSITÄT  
DRESDEN**

---

Decomposition of weak optically stimulated  
luminescence signals and its application in  
retrospective dosimetry at quartz

---

**MASTERARBEIT**

zur Erlangung des akademischen Grades

**Master of Science**

vorgelegt von

**Dirk Mittelstraß**

**geboren am 19.05.1983 in Freital**

INSTITUT FÜR KERN- UND TEILCHENPHYSIK

FAKULTÄT PHYSIK

BEREICH MATHEMATIK UND NATURWISSENSCHAFTEN

TECHNISCHE UNIVERSITÄT DRESDEN

2019



Eingereicht am 27. November 2019

1. Gutachter: Prof. Dr. Arno Straessner
2. Gutachter: Prof. Dr. Johannes Heitmann

## **Abstract**

The probably most common application in retrospective dosimetry is the dating of geomorphologic and historic events. An often used method is optical stimulated luminescence (OSL) dating. The accuracy of quartz OSL dating results relies strongly on the dominance of the thermally stable and easy-to-bleach 'fast' signal component. If this component does not dominate the initial OSL signal in a given data set, systematic errors are likely. These originate in the signal contribution of insufficiently bleached or thermally unstable traps. To solve this issue, a new approach for mathematical component separation is presented. First, we identify the number of signal components and their decay constants. We do this by creating one global OSL decay curve from all records of a given data set and apply a multi-component exponential decay fitting method. Second, we deploy the found decay constants in an algebraic decomposition algorithm and divide every single OSL record into its signal components. We test the accuracy, precision and robustness of the proposed procedures by comprehensive simulations and evaluate the results by statistical methods. The simulations demonstrate the mathematical reliability of the method in the majority of scenarios. The new approach is then applied in a standard dating protocol and tested at some geomorphological relevant data sets. Also a new protocol for simplified measurement conditions is tested. The usefulness of the method as reliable and rapid data analysis tool in quartz OSL dating is demonstrated.

## **Kurzdarstellung**

Die wahrscheinlich häufigste Anwendung der retrospektiven Dosimetrie, ist die Datierung von geomorphologischen und historischen Ereignissen. Eine gebräuchliche Methode ist die Datierung von Quarzen mittels optisch stimulierter Lumineszenz (OSL). Ihre Genauigkeit hängt jedoch von der Dominanz der thermisch stabilen und einfach zu bleichenden ‚schnellen‘ OSL Signalkomponente ab. Dominiert diese nicht das Anfangssignal einer OSL Messung, sind systematische Fehler durch thermisch instabile oder unzureichend gebleichte Signalanteile wahrscheinlich. Um dieses Problem zu lösen, wird ein neuer Ansatz zur mathematischen Auftrennung der Signalkomponenten vorgestellt. Zuerst bestimmen wir die Anzahl der Signalkomponenten und ihre Zerfallskonstanten über ein nichtlineares Regressionsverfahren. Danach verwenden wir die ermittelten Zerfallskonstanten um in einem algebraischen Verfahren jede einzelne OSL Kurve zu zerlegen. Die Genauigkeit und Robustheit dieser Verfahren testen wir mit Hilfe umfassender Simulation, die wir statistisch auswerten. Die Simulationsergebnisse zeigen die Zuverlässigkeit der Methode. Wir testen den neuen Ansatz auch im Rahmen eines üblichen Datierungsprotokolls an einigen geomorphologischen Datensätzen. Es zeigt sich seine Nützlichkeit als zuverlässiges und anwenderfreundliches Werkzeug zur Datenanalyse bei der OSL Datierung von Quarz.

# Contents

<b>1 Introduction</b>	<b>1</b>
<b>2 Fundamentals: Quartz as luminophore and dosimeter</b>	<b>3</b>
2.1 Defect physics.....	3
2.2 Dose information storage and read out.....	4
2.3 OSL signal components .....	8
<b>3 Method: Component-wise dose calculation</b>	<b>11</b>
3.1 Step 1 – Evaluation of component number and decay constants.....	13
3.2 Step 2 – Single curve decomposition.....	21
3.3 Step 3 – Component-wise dose calculation.....	30
<b>4 Method verification: Simulated OSL curves</b>	<b>35</b>
4.1 Step 1 reliability .....	36
4.2 Step 2 reliability .....	43
4.3 Signal background dependence .....	49
<b>5 Application: Automated sample analysis</b>	<b>52</b>
5.1 Example analysis.....	53
5.2 Re-evaluation of some standard SAR data sets .....	60
5.3 Omit thermal treatment in measurement protocol.....	63
<b>6 Conclusion and Outlook</b>	<b>67</b>
<b>Bibliography</b>	<b>71</b>
<b>List of figures</b>	<b>77</b>
<b>List of tables</b>	<b>78</b>
<b>Appendix</b>	<b>79</b>

# Acronyms

aliquot	Subsample on a single sample carrier
CW-OSL	Continuous wave OSL: The stimulation light intensity stays constant during measurement
DE	Differential evolution: A genetic algorithm to solve starting value issue for nonlinear regression models
$D_e$	Equivalent dose: Artificial dose equivalent to the dose which caused the natural luminescence signal of one aliquot
HELA	Hybrid evolutionary-linear algorithm: Variant of the differential evolution algorithm specialized on multi-component decay models
IRSL	Infrared stimulated luminescence
LM-OSL	Linearly modulated OSL: The stimulation light intensity rises linearly with time
OSL	Optical stimulated luminescence
OTOR	One trap one recombination centre: Simple model for luminescence in crystals
package	Function library in R
PMT	Photomultiplier tube
<b>R</b>	Statistical programming language
SAR	Single-aliquot regenerative-dose protocol: Standard measurement protocol in luminescence dating
SNR	Signal-to-noise ratio of a measurement
TL	Thermoluminescence

# Notation

Package names, software functions, scripts and code snippets are indicated by `Courier New`

<code>function()</code>	<b>R</b> function part of the <code>OSLdecomposition</code> package programmed for this thesis
<code>package::function()</code>	<b>R</b> function part of another package
<code>script.Rmd</code>	Data evaluation script programmed as <code>Rmarkdown</code> document

# 1 Introduction

Let us think about the crystal lattice of an insulator and its energy band model. An insulator can be seen as a semiconductor with a wide band gap. Its crystal lattice may contain defects with defect states located deep in the band gap. If these defect states are not clustered with energy exchanging path-ways like recombination centres or crystal surfaces, they can be long-term stable. A defect state can have a lifetime in the order of millions of years at ambient temperature levels, if its energy level is located sufficiently deep in the band gap. Under usual environmental conditions, there are just a few ways to change such a defect state directly: By exposing it to ionizing radiation or optical light of sufficient photon energy, by heating it up to high enough temperatures or by recrystallizing the sample.

Now let us think about a crystal in nature, for example a sand grain laying on a beach or a mineral grain inside a freshly fired brick. During the extensive stimulation with wide-bandwidth sun light or the heating process, any charge carrier trap below the conduction band will be emptied. After the brick has cooled or after the sand grain is buried, deep traps will be filled with charge carriers only by ionizing radiation. Sources of ionizing radiation are cosmic rays as well as environmental or artificial radioactivity. With the accumulation of radiation the concentration of filled traps increases. This concentration is therefore a measure of time and radiation history since the grain has been buried or the brick has been burned. This basic principle allows for emergency dosimetry [1], [2], thermochronometry [3] and especially retrospective dosimetry. The most common applications of retrospective dosimetry are archaeological and geomorphological dating [4]–[6].

But how can we measure the concentration of filled traps in a given sample? One way of doing that is to measure them directly by electron-spin resonance (ESR) spectrometry [7], [8]. Another way is to measure the concentration indirectly by stimulating them. The released charge carriers might recombine under the emission of luminescence light. The intensity of the emitted luminescence light is proportional to the concentration of filled traps. We can either stimulate thermally (= thermoluminescence (TL) [9]), radiologically (= radioluminescence (RL) [10]) or optically (= optical stimulated luminescence (OSL) [11], [12]).

One sample material often used for OSL dating is natural quartz ( $\alpha$ -SiO<sub>2</sub>). Quartz is suitable for the process because of its crystallographic purity and its vast occurrence. Quartz OSL dating is a standard tool in investigating stratigraphic sequences of sediments [13], [14]. Most sediments are rich in sand (or entirely made of it), and most sands are rich in quartz grains. Thus, one can reconstruct the chronology of rivers, coastlines, glaciers and dunes with quartz OSL dating. And this does not just work on Earth, but also on Mars [15], [16], at least in theory.

The history of natural quartz as dosimeter and chronometer goes back to the 1970s when Wintle, Huntley and others investigated the use of thermoluminescence dosimetry for dating sediments [17]. But in 1985, Huntley *et al.* [18] showed that instead of TL, rather OSL of natural quartz samples is a viable method for dating quartz-rich sediments. The following two decades may be seen as the golden age of quartz luminescence research, bringing many new insights and ending up in a standard protocol for quartz OSL dating. In 2000, Murray and Wintle [19] published their 'continuous wave optical stimulated luminescence single aliquot regenerative dose protocol' or CW-OSL SAR protocol or just SAR protocol. It established itself quickly as a standard protocol and was adapted for other minerals and methods than OSL of quartz, most notably infrared stimulated luminescence (IRSL) of feldspars [20]. But the native SAR protocol and many of its predecessors share one fundamental flaw: They do not resolve for the different types of contributing defects and their different physical properties. This adds sample-related systematic errors to the data analysis process and jeopardizes dating results. Many experimental and mathematical solutions to this problem have been published over the last 20 years, but none of them established itself as new standard. Some approaches rely too much on bright OSL signals, which, for quartz, are often not given; other approaches just try to calibrate the errors out of the protocol without actually addressing the underlying issues. Most approaches, however, are simply too complex and time-consuming to be adapted in a geo-scientist's everyday life.

In this thesis, I want to present a new mathematical approach which is not just easy-to-use because of its emphasis on automation, but also stands on a robust theoretical foundation. My hope is that it will not only improve current quartz OSL dating techniques, but will also open a new scientific pathway towards future research.



## 2 Fundamentals: Quartz as luminophore and dosimeter

Silica, as defined by their chemical sum formula  $\text{SiO}_2$ , are the second most common minerals on earth (after feldspars), making up 12.6% of the weight of the Earth's crust [21]. The most abundant  $\text{SiO}_2$ -modification in the lithosphere is crystalline  $\alpha\text{-SiO}_2$  or 'low quartz' which is commonly known just as 'quartz'. The crystal structure of  $\alpha\text{-SiO}_2$  is built from  $[\text{SiO}_4]^{4-}$  tetrahedra, sharing each corner with another tetrahedron. This structure leads to trigonal-trapezohedral symmetry [22] which is the reason for the piezo-electricity of quartz and also allows the diffusion of  $\text{Na}^+$ ,  $\text{Li}^+$  and  $\text{H}^+$  cations along the c-axis, which is relevant for the luminescence processes. All luminescence processes in quartz are related to crystal defects.

### 2.1 Defect physics

The most frequent trace element in quartz is aluminium with contents in the order of 100 to 1000 ppm while only few other elements show significant contents above 1 ppm. The particular concentrations vary largely between quartz samples, depending on their origin and variety [22], [23]. The main cause of the relatively high purity of most quartz samples is the small ionic radius of the  $\text{Si}^{4+}$  ions (0.42 Å) which is matched closest by  $\text{Al}^{3+}$  ions (0.5 Å) [21]. Accordingly, the most frequent point defects (besides E' oxygen vacancies) are Si-substituting Al-defects:  $[\text{AlO}_4]^0$  with a bound hole  $h^+$  or some cation  $\text{M}^+$  providing charge neutrality at thermal equilibrium.  $[\text{AlO}_4]^0$  and its ionized counterpart  $[\text{AlO}_4]^-$  serve as recombination centres in all major luminescence emissions [24], [25].

Another important class of point defects is the substitution of  $\text{Si}^{4+}$  with  $\text{Ge}^{4+}$  or  $\text{Ti}^{4+}$  (= X) which is stabilized by some interstitial alkali ion  $\text{Li}^+$  or  $\text{Na}^+$  (=  $\text{M}^+$ ), forming the defect pair class  $[\text{X}/\text{M}^+]^+$ . Theories about their contribution to luminescence dosimetry phenomena are inconsistent and part of on-going discussions, see chapter 5 of Chen and Pagonis [26]. Itoh *et al.* [27] suggest them as positively charged meta-stable defect state in the irradiation-to-OSL process.

**Table 2.1:** Dominant irradiation and OSL defect mechanisms in quartz after Itoh *et al.* [27]

Process	Mechanism
Irradiation	$[\text{AlO}_4/\text{M}^+]^0 \rightarrow [\text{AlO}_4]^- + \text{M}^+$ $\text{M}^+ + \text{X} \rightarrow [\text{X}/\text{M}^+]^+$
Optical stimulation	$[\text{X}/\text{M}^+]^+ \rightarrow [\text{X}/\text{M}^+]^0 + h^+$ $[\text{AlO}_4]^- + h^+ \rightarrow [\text{AlO}_4/h^+]^0 + h\nu (\sim 3.4 \text{ eV})$

More comprehensive reviews of the defect physics of quartz can be found for example in Götze [22], Preusser *et al.* [23] and most recently in Chen and Pagonis [26].

## 2.2 Dose information storage and read out

Independent from the exact defect mechanics, a variety of kinetic models based on phenomenological observations has been developed. The simplest model, yet conveniently explaining major TL and OSL phenomena, is the one-trap-one-recombination-centre model (OTOR) used as theoretical fundament by Chen and McKeever [28] and Chen and Pagonis [29] in their textbooks about TL and OSL modelling. The OTOR model illustrates how a solid state dosimeter (not just quartz) can be described. It simplifies the defect physics to an energy band model with a large band gap, one electron trap and one recombination centre. Kinetic properties are assigned to both types of defects: A defect concentration and charge carrier transition probabilities into and from the conduction band and valence band. A set of rate equations is derived from these kinetic properties. This set of rate equations can be solved with regards for any desired scenario, like the accumulation of dose information under irradiation or the excitation of TL or OSL under various types of stimulation. Note that for all cases, apart from some trivial ones, these equation systems have to be solved numerically. The transition probabilities in the kinetic model can be linked to actual physical parameters like the energy level in the band gap or the photo-ionisation cross-section, via secondary equations. Thus, the OTOR model allows us to explain the mechanics of OSL dating.

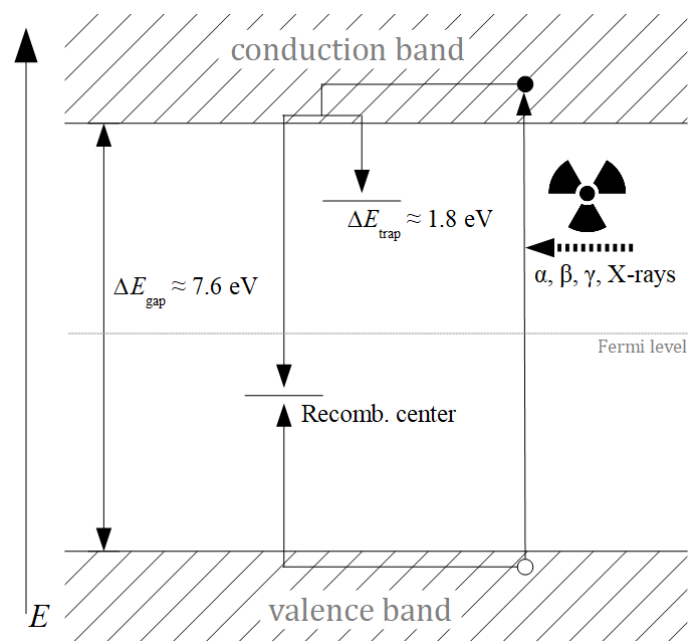


**Figure 2.1:** OTOR model: Irradiation events generate electron-hole pairs. Holes move into recombination centres, electrons move partly into electron traps and partly recombine.

How is the dose information stored? We assume that the crystal is at the time point zero at its thermal equilibrium. This means, most defect states below the Fermi level are filled with electrons, while defect states above the Fermi level are mostly empty. In retrospective dosimetry, this time point zero equals the point in time of burial after bleaching by sun light or extensive heating, or the point in time of (re-)crystallization. To alter this stable state, high energy processes are necessary. All high energy processes which occur in nature are related either to cosmic rays or to environmental radioactivity. These irradiation events produce electron-hole pairs in the valence band with a certain rate (= dose rate). The holes activate the recombination centres, the electrons either fall into an electron trap or recombine with a hole in a recombination centre. The chance for an electron going one way or the other, depends on the transition probabilities and the concentration of available traps/recombination centres. With elapsing time, more and more electron traps are being filled and the likelihood of an electron transition is slowly shifting towards the recombination centres. The concentration of filled electron traps approaches a saturation level, or more exactly, they approach an equilibrium with the thermal decay. In case of the main dating-relevant trap type of quartz, the thermal lifetime at room temperature is in the range of several million years. The increase of the trapped-electron concentration level can be described with an exponential growth curve with a saturation level depending on dose rate and temperature. We will apply such a curve function later in chapter 3.3. If we know the dose rate of this process, we can set each unit of dose equal to a particular time span. If we can reconstruct the accumulated dose in the sample, we can estimate the time elapsed since the crystal left thermal equilibrium. Together with the information on the environmental dose rate, it is then possible to calculate the age of the sample.

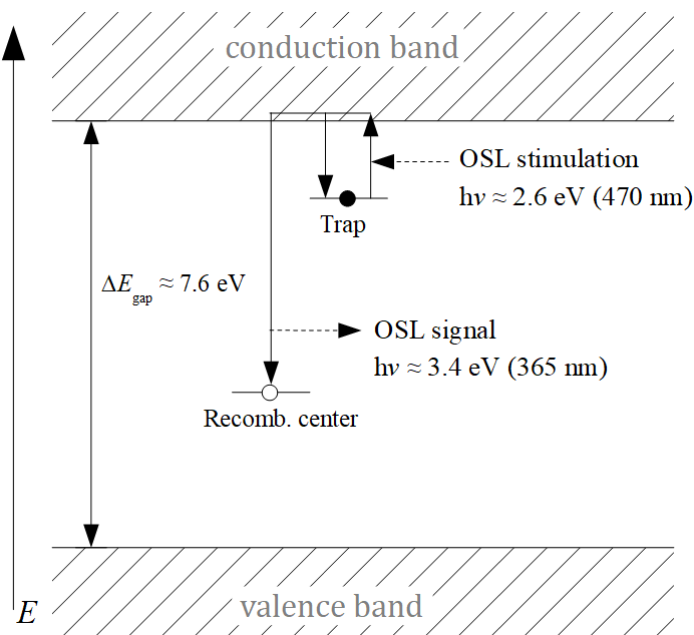


**Figure 2.2:** OTOR model: Optical stimulation with sufficient photon energy lifts trapped electrons into the conduction band. They partly recombine under photon emission and partly fall back into the electron trap.

To gather information about the accumulated dose, we have to measure the concentration of filled electron traps. When performing OSL measurements, we do this by stimulating the sample with photons of a certain minimum energy. In case of quartz OSL, the trap of interest is located about 2 eV below the conduction band (the exact value depends on the reference). Thus, we need at least yellow light to lift electrons into the conduction band. Common are blue (470 nm = 2.64 eV) and green (532 nm = 2.33 eV) stimulation. In the OTOR model, the transition probability for this process is defined by the optical excitation rate  $\lambda$ . This excitation rate is in turn given by the product of photon flux and photo-ionisation cross-section of the trap. The photo-ionisation cross-section depends on the stimulation photon energy and the sample temperature and is for quartz discussed in detail by Singarayer and Bailey [30], [31]. In the publications by Chen and others the optical excitation rate is mostly denoted  $f$ . We will stay with the common notation for decay constants  $\lambda$  because the values for  $\lambda$  we will evaluate with the methods introduced later are not necessarily equal to the physical optical excitation rate.

Some delocalised electrons may fall back into the trap (= retrapping) while others recombine under the emission of photons (in the near-UV respectively at about 3.4 eV in the case of quartz). The recombination process is several orders of magnitude faster than the electron depletion [32]. So the likelihood of which way an electron goes is only determined by the defect concentrations and the transition probabilities. Chen and Leung [33] simulated OSL signals for the OTOR model under the assumption of continuous optical stimulation with constant intensity (= CW-OSL). They found that the resulting curves can be very well approximated with stretched exponential equations:

$$I(t) = I_0 e^{-\left(\frac{t}{\tau}\right)^\beta} \quad 0 \leq \beta \leq 1 \quad (2.1)$$

Here,  $I_0$  is the initial signal at the start of stimulation and  $\tau$  is the lifetime of the signal, not equal but in the same order of magnitude as the inverse of the optical excitation rate  $\lambda$ . The ‘stretching’ parameter  $\beta$  has no particular physical meaning, but decreases when the likelihood of retrapping increases.

A special case occurs when for the conduction-band electrons the likelihood of retrapping is negligible compared to the likelihood of recombination. This is the case when the product of concentration and transition probability of available recombination centres is much larger than the same product for electron traps. Then OTOR model simulations approximate first order kinetic behaviour (see chapter 5.3 in Chen and McKeever [28]). The stretching parameter  $\beta$  in equation (2.1) becomes  $\beta = 1$ , the lifetime  $\tau$  becomes  $\tau = \frac{1}{\lambda}$  and the initial signal  $I_0$  becomes  $I_0 = n_0 \lambda$ :

$$I(t) = n_0 \lambda e^{-\lambda t} \quad (2.2)$$

Here,  $n_0$  is the concentration of filled electron traps at the start of the stimulation. Equation (2.2) is assumed to sufficiently describe the major OSL signal components of quartz, as we will see in the next chapter. The necessary dominance of the recombination centres arises from the defect physics of quartz. As we discussed previously,  $[\text{AlO}_4]$  defects are identified as major luminescing recombination centres. Other defects, which are assumingly related to the electron traps in the OTOR model, are most likely much lower concentrated. However, the links between kinetic models and actual defect physics are difficult to draw, as for example the disparity in the type of charge carriers between the Itoh *et al.* theory (see table 2.1) and the OTOR model demonstrates.

To evaluate the natural dose of a sample, we still have to account for several unknowns: the concentration of defects, the transition probabilities and the conversion rate between dose rate and electron-hole production. The simplicity of the two-defect OTOR model does not hold for actual quartz samples either. In practice, a quartz dosimetry approach does also have to account for retrapping effects of shallow traps and for alternative non-luminescent recombination and trapping pathways. The issue of unknown defect concentrations and unknown conversion and transition rates is solved by setting the natural-dose luminescence intensity into relation with artificial-dose luminescence intensities. Other issues can be settled by thermal treatment and normalization measurement steps. The exact strategy depends on the chosen measurement protocol. The by far most common measurement protocol in quartz OSL dosimetry, is the SAR protocol. It was first suggested by Murray and Roberts [34], defined in detail by Murray and Wintle [19] and comprehensively reviewed by Wintle and Murray [35]. The SAR protocol was also reviewed and discussed in German language in my bachelor thesis in 2013 [36] which can be found on the enclosed CD.

However, despite its widespread use, one issue the SAR protocol does not account for, is the occurrence of multiple OSL signal components.

## 2.3 OSL signal components

The OTOR model for quartz assumes one dominant recombination centre and one electron trap. However, experimental quartz OSL decay curve shapes cannot be accurately described by this model. In 1994, Smith and Rhodes [37] were the first to systematically investigate the shape of CW-OSL decay curves of quartz. They found, that OSL curves can be sufficiently well described by three independent exponentially decaying signal components. Bailey *et al.* [38] investigated this further and Bailey [39] published in 2001 his kinetic luminescence model of quartz. Like the OTOR model, it is built upon a set of rate equations but includes 5 electron traps and 4 recombination centres. Bailey enhanced his model later [40] and Pagonis *et al.* [41] and Friedrich *et al.* [42] published improved versions of Bailey's model to better account for thermally transferred charge carriers and radioluminescence curve shapes. Friedrich *et al.* [43] as well as Peng and Pagonis [44] give brief overviews of the developed quartz models and both working groups provide **R** software solutions for creating luminescence simulations with these models. All these models have one thing in common: They describe at least two OSL-contributing electron traps with about two orders of magnitude smaller defect concentration as the major recombination centres. For these two electron traps, the approximation (2.2) holds according to the models, at least under default SAR conditions (470 nm stimulation, 125 °C sample temperature).

Multiple independent OSL signal components with first order kinetics were also confirmed by another measurement method. In 1996, Bulur [45] introduced a new OSL technique: linearly modulated (LM) OSL. Here, the stimulation intensity increases linearly during OSL measurements. Thus, signal components occur as peak-shaped curves. In case of first-order kinetics, the position of the maximum is directly proportional to the photo-ionisation cross-section of the related trap and the intensity of the maximum is directly proportional to concentration of filled traps at beginning of the measurement. This allows easy by-hand parameter estimation of rapidly decaying OSL components but also simplifies the analysis methods to determine slowly decaying components. In consequence, a variety of studies investigated the quartz OSL components, using the LM-OSL technique. Bulur *et al.* [46] found that a quartz measured under SAR conditions can be sufficiently well described by four signal components of first order kinetics. In this thesis, we will call these four OSL components in accordance to the literature: fast, medium, slow1 and slow2. Later studies analysed collections of different quartz samples and confirmed the 4-component nature of quartz LM-OSL measurements [30], [47], [48]. They found also additional slowly decaying components and, for a few samples, an ultrafast component [49]. While the specific photo-ionisation cross-section estimates were not identical for all quartz samples, they show some similarities pointing to equal physical origins. A brief overview over multiple studies and their findings is provided by Durcan and Duller [48], but also in my bachelor thesis [36].

But why is signal component separation desirable for standard dating measurements? In the SAR protocol, the integral of the initial  $\sim 0.5$  s of the CW-OSL signal is defined as luminescence intensity value. This value is corrected for the signal background observed in the last few seconds of the stimulation. For most samples, the initial measurement signal is dominated by the Fast component which is well suited for dating applications because of its thermal stability and insensitivity against charge transfers between traps. Nevertheless, in some samples, the medium component contributes significantly to the initial signal. The medium component is less thermally stable and more sensitive to capture thermally released electrons which leads to erroneous natural dose estimations [50]–[52]. More specifically: The age of old samples might be underestimated and the age of young samples might be overestimated because of the contribution of the medium component to the initial signal. Potential initial signal contributions of slowly decaying components might also lead to systematic errors in the dose evaluation procedure. The decomposition of the CW-OSL signal can improve the accuracy and reliability of quartz OSL dating results. In addition, OSL decomposition can gather valuable information about the defect setting of a sample or even enable new kinds of measurement protocols, like we will see in chapter 5.3.

In consequence, a variety of decomposition approaches were proposed so far. These approaches can be divided into two categories. The first category contains advanced measurement and/or data analysis methods:

- Substituting the CW-OSL measurements in the SAR protocol with LM-OSL measurements. Fitting routines can be applied to identify the signal components. The dose evaluation is then performed component-wise [46].
- Mathematical transformation of CW-OSL curves into LM-OSL curves or other spectral representations [53], [54]. Then the above approach can be applied.
- Fitting of CW-OSL curves by nonlinear regression [55], [56]. We will apply this method in chapter 3.1 as part of our new approach.
- Calculating and displaying the natural dose measurement channel-wise. The resulting  $D_e(t)$ -plot allows the evaluation and eventually fitting of the ‘true’ dose value [18], [50], [57], [58].
- Stimulating discretely the fast component only [59], [60].

All these approaches rely on sufficiently good signal-to-noise ratios (SNR) which are often not given for natural quartz samples. Furthermore, they are more or less time-consuming and complex in use. In consequence, they are not applicable in routine OSL dating. To account for this problem, a few simpler approaches were also proposed:

- Estimate the point of measurement time when 50% of the medium component had been emitted. Correct the bulk signal before this point of time by subtracting the bulk signal after this point of time. This erases the medium component from the initial bulk signal.

The approach is known as ‘early light background subtraction’ and probably the most common used component-issue-correcting approach [61], [62]. We will include this approach later in our application tests in chapter 5 for comparison purposes.

- Assume a 3-component model and estimate the points of measurement time when particular components are dominant. Solve then a simple relation to estimate the fast component contribution to the initial signal (the ‘Fast ratio’) [48].
- Assume a 3-component model, smooth the CW-OSL curve, define three intervals of component dominance and estimate the fast and medium signal intensity by solving two relation equations [63].

The accuracy of these approaches relies on the exact knowledge of the OSL decay curve model. The necessary decay constants to build a model are taken from literature. However, the actual decay constants may differ, as well as the number of components. The reliability of the calculated natural doses is therefore sample-dependent. Furthermore, these approaches cannot be applied easily to not-standard measurement conditions.

It is the goal of this thesis to develop and test a new approach which is able to unite the advantages of methods in both categories without sharing their disadvantages. Therefore, we define the following requirements:

- 1) Identify the number of components and their decay constants on a sample-to-sample basis.
- 2) Allow component-resolved dose calculation, even for samples with low-SNR measurements.
- 3) Allow automated component and dose evaluation, without inherent need for user interaction.
- 4) Be applicable for a large variety of instrumental and measurement conditions.



### 3 Method: Component-wise dose calculation

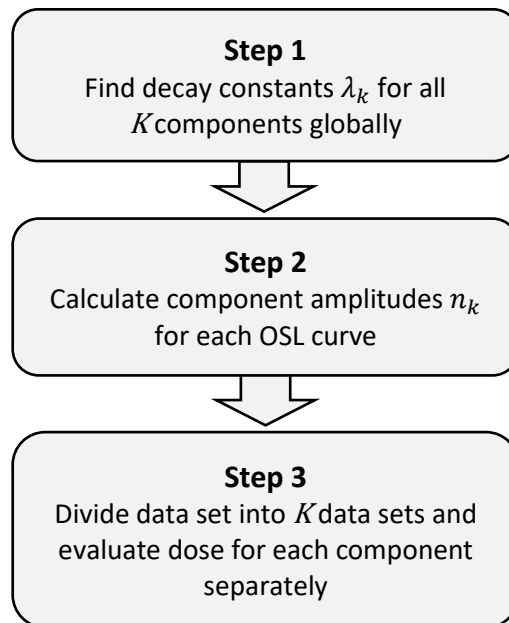


**Figure 3.1:** General workflow of signal component-wise quartz OSL dose calculation approach

The basic idea is summarized in figure 3.1. We divide the dose calculation approach into three major steps. The first step determines the number of signal components and the decay constants. This is achieved by combining all OSL records of a data-set to one global OSL curve. Because a data set usually consists of a few hundred OSL records, multi-exponential regression is enabled even for data sets with low SNR. A statistical test decides which number of components describes the global curve adequately without over-fitting it.

Step two calculates the integrated signal (i.e. signal intensity) of every component in each OSL curve. This is reduced to a quasi-linear regression problem by inheriting the decay constants from step one. Two noise-robust methods how to solve this, will be presented and compared.

Step three takes the component intensities to build dose-signal curves and calculates the naturally received dose. This is done for every component and every aliquot separately. From the resulting set of natural doses, the sample age can be calculated by applying statistical models, which will not be covered in this thesis.

## Software framework

The method for component-wise retrospective dose calculation presented in the following, is realized by a set of software functions. These are programmed in the statistical programming language **R** [64]. The functions programmed as part of this master thesis are bundled in a function library (e. g. 'package') named `OSLdecomposition`. How to use the package is shown in appendix A.1. As some algorithms were already realized by others, functions from the packages `Luminescence` [65], [66] and `numOSL` [56] were also deployed. Code generated graphics, as for example all graphs in this thesis, were realized with `ggplot2` [67]. Specific data analysis tasks were handled with `Rmarkdown` [68]. It enables automatic reporting and interactive scripting and was used for all simulation tests and all data evaluation purposes.

## Basic assumptions

The mathematical approaches developed in this thesis are built upon a set of assumptions. The fundamental assumption is that any CW-OSL signal  $I(t)$  of quartz can be described as sum of exponential decays of first order:

$$I(t) = \sum_{k=1}^K n_k \lambda_k e^{-\lambda_k t} \quad (3.1)$$

Every summand models one OSL signal component. We assume the number of components  $K$  and the decay parameters  $\lambda_k$  as constant throughout the whole measurement sequence and therefore for all CW-OSL records in a given data set of one sample. We also assume the amplitude  $n_k$  of a component as direct proportional to the amount of charge carrier releases of one specific defect state transition type.

The devices commonly used for quartz OSL measurements use PMTs in photon counting mode [69]. Every data point in an OSL record returns the number of photons detected in a corresponding time interval. Hence, OSL records are not described by continuous signal curves as in (3.1) but by series of integrals  $I_i$  over equidistant time intervals  $\Delta t$ . We integrate equation (3.1) and get:

$$I_i = \int_{(i-1)\Delta t}^{i\Delta t} I(t) dt = \sum_{k=1}^K n_k (e^{-\lambda_k (i-1)\Delta t} - e^{-\lambda_k i\Delta t}) \quad i = 1, 2, 3, \dots, N \quad (3.2)$$

All math outlined in step 1 and 2 assumes the correctness of (3.2) and all regression and decomposition functions are based on this particular formula.

Eventually appearing detection background or detector non-linearity was not considered during the development of the method but will be discussed in chapter 4.3. Nonetheless, it is highly recommended to background-corrected measured data before applying the methods outlined in this thesis. For more information about detector-related systematic errors, see [69]–[72].

### 3.1 Step 1 – Evaluation of component number and decay constants

One major goal of this thesis is to provide OSL signal decomposition even for measurements with weak signals. Fitting equation (3.2) with unknown values of  $n_k$  and  $\lambda_k$  to a low-SNR curve can fail, depending on the used algorithm and the accuracy of the start parameters. The probability of failure increases with increasing number of components  $K$ . As additional problem, we have to determine the correct number of components  $K$  first. Bluszcz and Adamiec [55] provide a strategy to obtain  $K$  and the component parameters without any prior knowledge of the sample and without start parameters  $n_k$  and  $\lambda_k$  necessary. We will adapt their strategy. But as they state, fitting of low SNR curves may miss components. Therefore, an approach to increase SNR prior to fitting is necessary.

#### Global average curve

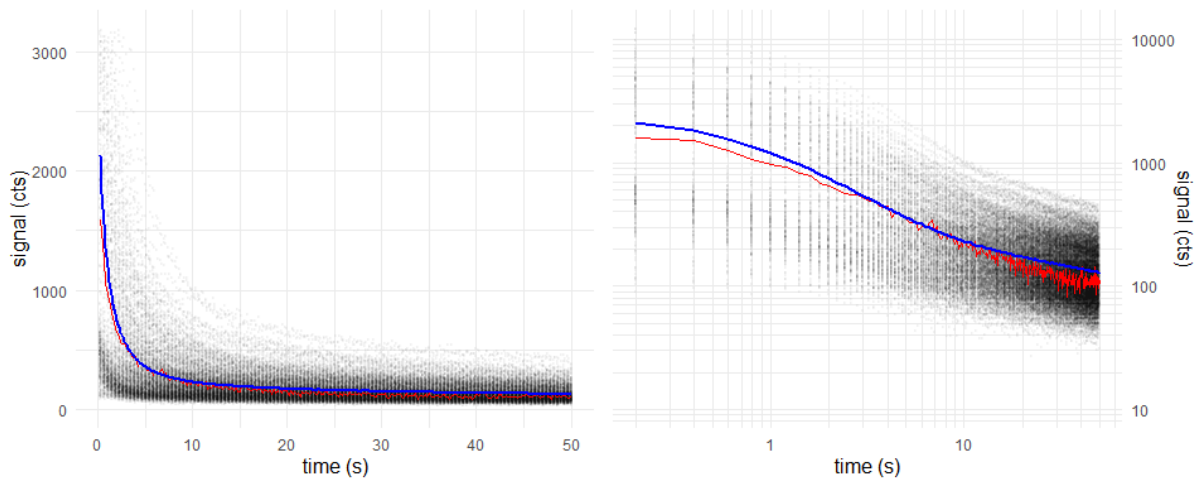


**Figure 3.2:** Global arithmetic mean OSL curve of sample BK8; 280 records; Channel width = 0.2. **Grey:** data points from all records. **Blue:** Average curve of all records (“global mean curve”); **Red:** first record (natural dose OSL from aliquot 1); Left: linear axes; Right: double-logarithmic axes.

The OSLdecomposition function `sum_OSLcurves()` returns a sufficient-SNR curve by calculating one global arithmetic mean OSL curve from all  $M$  CW-OSL curves a data set:

$$\bar{I}_i = \frac{1}{M} \sum_{m=1}^M I_{i,m} \quad (3.3)$$

The mean signal values  $\bar{I}_i$  has in the same order of magnitude as their corresponding signal values  $I_i$  in the majority of CW-OSL curves of the data set. But the standard deviation  $\bar{\sigma}_i$  per data point of the global curve signals will be much smaller than the single curve error  $\sigma_i$  per data point. If we assume that the uncertainty of a single data point is just caused by the shot noise

$\sigma_{\text{shot}} = \sqrt{I_i}$  and an unknown instrumental noise  $\sigma_{\text{detection}}$  (dark current noise; stimulation background noise), then we can estimate the noise  $\bar{\sigma}_i$  in the arithmetic mean curve and prove the SNR increase:

$$\begin{aligned}\bar{\sigma}_i &= \frac{1}{M} \sqrt{\sum_{m=1}^M \sigma_{i,m}^2} = \frac{1}{M} \sqrt{\sum_{m=1}^M (I_{i,m} + \Delta t \sigma_{\text{detection}}^2)} \\ \bar{\sigma}_i &\approx \frac{1}{M} \sqrt{M(\bar{I}_i + \Delta t \sigma_{\text{detection}}^2)} \approx \frac{\sigma_i}{\sqrt{M}} \\ \sigma_i^2 &= \frac{I_i + \Delta t \sigma_{\text{detection}}^2}{M} \\ \bar{\sigma}_i &\ll \sigma_i\end{aligned}\tag{3.4}$$

Typical OSL SAR data sets consist of a few hundred OSL records. The signal uncertainty and therefore the SNR in the global mean curve can be expected to be at least one order of magnitude better than in an average single OSL curve of its data set. This allows us to fit (3.2) with high chances of success and high precision in calculating  $\lambda_1 \dots \lambda_K$  even if the single curves provide only low-SNR signals.

Using the global mean curve to determine the decay constants is mathematically allowed because we assume  $\lambda_1 \dots \lambda_K$  as global constants. Thus the values of the term  $(e^{-\lambda_k(i-1)\Delta t} - e^{-\lambda_k i \Delta t})$  in equation (3.2) remain static throughout the data set and just vary with the indices  $i$  and  $k$ . The only parameters varying from OSL curve to OSL curve are the signal amplitudes  $n_1 \dots n_K$ . And these will be determined later in step 2 by a different method.

## Multi-component exponential decay fitting

The function `fit_OS�curve()` fits equation (3.2) to the global average OSL curve and returns the number of components and their decay constants. The basic workflow is outlined in figure 3.3. In cycles with increasing number of components, the decay constants are evaluated by a sophisticated least squares curve fitting algorithm. In the end of each cycle, a complete set of decay parameters and a minimisation value  $\chi^2$  is returned.  $\chi^2$  is also a measure of fit quality. A statistical criterion, the  $F$ -value, checks if  $\chi^2$  is significantly decreased compared to the previous cycle. If the  $F$ -value lies below a pre-set threshold value, the fitting curve found in the actual cycle is considered as over-fitted. Then the parameter set of the previous cycle is given back by `fit_OS�curve()`. If the fitting procedure stops before  $F$  falls below the threshold, the parameters of the last successful fit are given back.

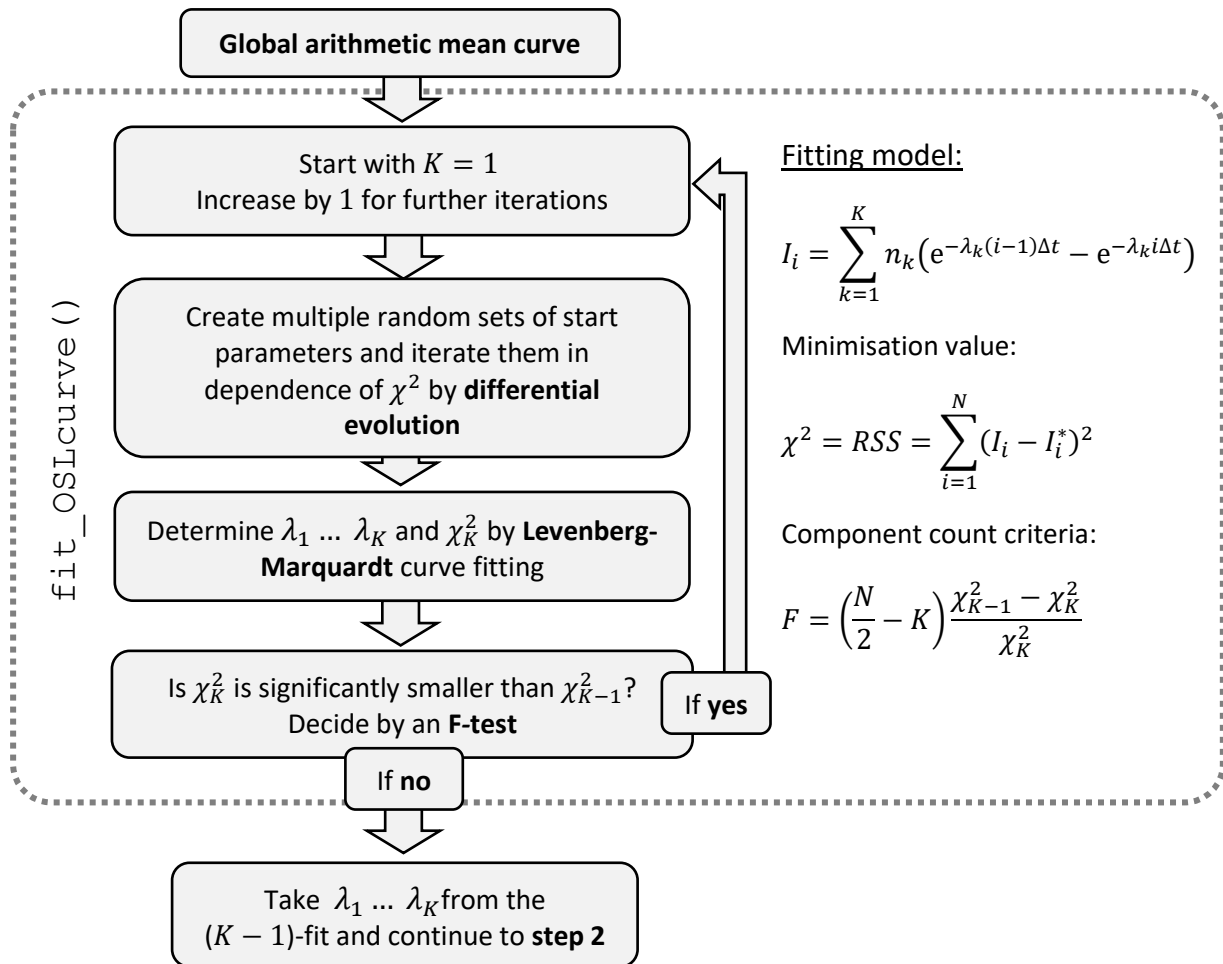


**Figure 3.3:** Workflow of multi-component exponential decay fitting (step 1 procedure): Evaluation of decay constants and number of components. The equations and their notation are explained in the following paragraphs.

We will deploy the procedure formulated by Bluszcz and Adamiec [55]. Their fitting algorithm to return the decay parameters for a specific number of components was realized in **R** by Peng *et al.* [56]. Peng *et al.* programmed the function `numOSL::decomp()` which is used as core of `fit_OSLcurve()`. They used the FORTRAN MINPACK library [73] to perform a Levenberg-Marquardt curve fitting [74]. Peng *et al.* [56] also realized HELA (for 'hybrid evolutionary-linear algorithm') to solve the starting value problem.

## Solving the starting value problem by differential evolution

Proposed by Bluszcz and Adamiec [55], HELA is a variant of the differential evolution (DE) algorithm formulated by Storn and Price [75]. Differential evolution algorithms define a vector space for the parameters in question. In this parameter space, multiple sets of parameter (vectors) are created randomly. These vectors undergo mutations and also new vectors are created by recombination. For each vector is  $\chi^2$  calculated by an external function call. This external function call makes the DE approach independent from the fitting model. The vectors with the smallest  $\chi^2$  are taken into the next generation while the others are dismissed. This is repeated until a stop condition is fulfilled. As stop condition serves usually an iteration counter or a significance test. The parameters of the final vector are very likely close to the global minimum of  $\chi^2$ .

To suit the multi-component exponential decay model better, Bluszcz and Adamiec introduced with HELA some changes [55]:

- 1) The component amplitudes  $n_1 \dots n_k$  are not part of the DE parameter space. Instead they are calculated by linear regression as part of the  $\chi^2$  calculation. This halves the necessary parameters per vector and increases performance.
- 2) The commutability of the terms in equation (3.2) lead to vectors with commuted parameters but identical model solutions. To prevent confusion of the DE algorithm, an operator sorting the parameters inside the vector is added.
- 3) Negative values for the amplitudes are forbidden to prevent unphysical solutions. Vectors which lead to negative amplitudes are altered until all amplitudes are equal or larger than zero.

## Minimisation of $\chi^2$

The final parameter values returned by HELA are used as starting values of a Levenberg-Marquardt (LM) curve fitting (see Kelley [74] for a detailed description of LM fitting). Although the improvements compared to the HELA calculated values are marginal [55], more precise values of the decay constants can be evaluated this way.

We use  $\chi^2$  as minimisation value for HELA and LM fitting.  $\chi^2$  is defined as residual square sum weighted by the signal error  $\sigma_i$  [76], [77]:

$$\chi^2 = \sum_{i=1}^N \frac{(I_i - I_i^*)^2}{\sigma_i^2} \quad (3.5)$$

$\chi^2$  is a measure of the deviation between the data point values  $I_i$  and the expected values  $I_i^*$  calculated from the fitting model. The signal variance  $\sigma_i^2$  in equation (3.5) is user-defined. A straight-forward approach is to use the definition from the common Pearson's Chi-square test. Then, we can set the variance equal to the expected value  $\sigma_i^2 = I_i^*$  if we assume that the signal values obey Poisson statistics,  $\chi^2$  becomes:

$$\chi^2 = \sum_{i=1}^N \frac{(I_i - I_i^*)^2}{I_i^*} \quad (3.6)$$

This assumes that the signal values are determined just by the number of observed detection events (=counts). And the noise is the statistical uncertainty in the occurrence of these events. In optical measurements, this is known as photon shot noise [78]. Note that equation (3.6) just holds, if the signal background and other sources of noise (like dark noise or excess noise) are negligible and the measurement data is unprocessed.

In another approach, we could simplify equation (3.5) by ignoring the signal variance and set  $\sigma_i^2 = 1$ :

$$\chi^2 = \sum_{i=1}^N (I_i - I_i^*)^2 = \text{RSS} \quad (3.7)$$

Here,  $\chi^2$  is not weighted and is equal to the residual sum of squares (RSS). The RSS is the default type of minimisation value in many regression algorithms [79].

These two approaches are selectable when running `numOSL::decomp()`, which performs HELA and LM fitting. But neither (3.6) nor (3.7) describe the uncertainty in the global mean OSL curve correctly. From (3.4) we conclude that a sufficient estimate for the signal error of the global mean curve is given by the combination of shot noise and detection noise  $\sigma_{\text{detection}}^2$  normalized by the channel width  $\Delta t$  and reduced by the number of OSL curves  $M$ :

$$\chi^2 = \sum_{i=1}^N \frac{(I_i - I_i^*)^2}{\frac{I_i^*}{M} + \frac{\Delta t \sigma_{\text{detection}}^2}{M}} \quad (3.8)$$

The type of variance we select, determines the shape of the  $\chi^2$  function. As a consequence, the  $\chi^2(\lambda_1 \dots \lambda_K, n_1 \dots n_K)$  hypersurface in the parameter space is individual for each type of variance and so will be the outcome of HELA and LM fitting at a particular curve. The 'correct' hypersurface given by equation (3.8) is not available because it is not incorporated in `numOSL::decomp()`. Incorporating it would mean re-programming HELA and LM fitting, which was not done in this thesis because of its time-consuming complexity.

But equation (3.9, next section) will show that the global minimum of  $\chi^2$  depends just on the true parameter values and not on the type of signal variance. The simulation results in chapter 3.1

will confirm this. While the accuracy is independent of the variance definition, the precision is not. If we chose the  $\sigma_i^2 = 1$  case (3.7), data points with high signal values will be weighted higher in the  $\chi^2$  calculation. Thus, fast decaying components will be calculated with better precision than in the other cases. If we chose the  $\sigma_i^2 = I_i^*$  case (3.6), data points with low signal values will have a higher weight in the  $\chi^2$  calculation and slow decaying components will be calculated with better precision. If we chose (3.8) for  $\chi^2$  calculation, the weighting will be somewhere in between.

Because the fast component is of most interest in quartz dating applications, we chose the  $\sigma_i^2 = 1$  approach given in equation (3.7) as default in this thesis.

## Error calculation

The function of  $\chi^2$  can also be used to calculate the error values of the decay parameters. Given that the number of data points is sufficiently large,  $\chi^2$  can be separated into independent quadratic functions for each parameter  $\lambda_k$  and  $n_k$ . Regarding the decay constant  $\lambda_k$ , we can rewrite equation (8.8) in Bevington and Robinson [76] and get:

$$\chi^2 = \frac{(\lambda_k - \lambda_k^*)^2}{\sigma_k^2} + C \quad (3.9)$$

Here  $\lambda_k^*$  is the value of  $\lambda_k$  related to the minimum of  $\chi^2$ ,  $\sigma_k^2$  is the uncertainty of this value in matching the unknown true value and the constant  $C$  depends on the  $\chi^2$ -functions of the other signal components. We can rewrite (3.9) and set  $\chi_{\min}^2 = C$ . If we chose  $\lambda_k$  now in a way, that the value of  $\chi^2$  is increased by one compared to the minimum, we get the 1- $\sigma$ -error of  $\lambda_k$ .

$$\sigma_k^2 = \frac{(\lambda_k - \lambda_k^*)^2}{\chi^2 - \chi_{\min}^2} \quad (3.10)$$

We can achieve accurate error estimations by equation (3.10) only if  $\chi^2$  is calculated correctly. But the correct  $\chi^2$ -definition (3.8) is not available in the **R** function we use. Therefore, the method as realized for this thesis, is not able to provide accurate error estimations of the calculated decay constants.

## F-test

So far, we discussed the strategy of finding the correct decay constants for a given number of components. But how to find the number components which represents best the OSL curves of a sample? Bluszcz and Adamiec [55] propose to use a statistical test, the *F*-test [76], [77], [80]. To understand the *F*-test, we have to understand the distribution of possible  $\chi^2$  values in case of a perfect fitted model. This  $\chi^2$  distribution depends just on the degrees of freedom, assuming the variance term in (3.5) is chosen correctly. The degrees of freedom  $n$  are given by the number of data points  $N$  minus the number of fitting parameters ( $2K$  in our model). The expected value of  $\chi^2$  in a perfect fit is proportional to number of degrees of freedom. The *F*-distribution is defined



by the ratio of two  $\chi^2$  distributions divided by their degrees of freedom. Thus, the ratio of two particular values  $\chi_A^2$  and  $\chi_B^2$ , divided by their degrees of freedom  $n_A$  and  $n_B$ , gives us the value  $F_{AB}$ , which is part of the  $F$ -distribution:

$$F_{AB} = \frac{\chi_A^2/n_A}{\chi_B^2/n_B} \quad (3.11)$$

The position of  $F_{AB}$  in the  $F$ -distribution gives us the probability whether both  $\chi^2$  values differ just by chance or differ because  $\chi_A^2$  was not obtained from an adequately fitted curve. We can use this relationship to estimate the significance in fit improvement between two models. We can also prove the significance of an additional term in a model. Applied to our multi-exponential decay model (3.2) with  $K$  components, we get equation (8) in Bluszcz and Adamiec [55]:

$$F = \frac{(\chi_{K-1}^2 - \chi_K^2)/2}{\chi_K^2/(N - 2K)} \quad (3.12)$$

If  $F$  is large, then  $\Delta\chi^2$  was not  $\chi^2$ -distributed, which means that the additional component improved the fitting significantly. If  $F$  is low, then the fitting wasn't improved significantly. We can now define a threshold value for  $F$  to decide whether we keep the additional term or not. It is common to choose a threshold value that guarantees a probability of less than 5 % that the  $\chi^2$ -decrease happened just by chance [55], [76], [79]. Looking at an  $F$ -distribution table like C.5 and C.6 in Bevington and Robinson [76], we get threshold values of about  $F_{\text{threshold}} = 3 \pm 1$ , depending on the particular number of degrees of freedom. But as the case studies in chapter 5.2 will show, 5 components or more are needed to reach such low  $F$ -values. This is not practicable because 1) the fitting procedure might break before reaching this level of fitting quality and 2) more components lead to decreased SNR in the method we will introduce in the next chapter. In practice, most OSL curves are sufficiently fitted with 3 or 4 components. So in accordance with the simulation and application results shown later in this thesis, threshold values of at least  $F_{\text{threshold}} \geq 50$  are recommended.

Also the occurrence of five or more components might not be physically justified due to inaccuracies in the multi-exponential decay model (3.2) when applied on the global mean curve:

- 1) The photon flux inside a sample grain determines its OSL decay constants. But the photon flux will vary from grain to grain due to variations in reflectance, transmittance and layer density. A similar effect has the inhomogeneity of the OSL stimulation. About 20 % variation in stimulation intensity over the sample area is common [81], [82].
- 2) We assume first order kinetics for all OSL components. This does not take potential re-trapping and photo-transfer effects in account which could lead to higher-than-first order kinetics and therefore stretched exponential component curve shapes. This is especially true for slow decaying components [83].
- 3) The lifetime of the recombination process is assumed to be zero while studies show it is mostly in the range of 30 to 45  $\mu\text{s}$  and up to 200  $\mu\text{s}$  for some recombination signal

components [32]. The resulting luminescence inertia can lead to a weaker than expected first data point in measurements with high stimulation intensity and small channel widths.

- 4) Other technical parameters like sample temperature, LED stimulation transient shape, LED temperature (LED peak wavelengths are quite sensitive to temperature changes) and sample carrier reflectance might also change during the measurement sequence of one sample

Another issue when considering the threshold value of  $F$  is the accuracy of the  $F$ -distribution. The  $F$ -distribution assumes that obtained values of  $\chi^2$  are actually following a  $\chi^2$ -distribution. This requires the accurateness of the variance term in equation (3.5). But because we neglected the weighting factor by using the RSS as  $\chi^2$  in equation (3.7), two effects happen: 1) all  $\chi^2$  values are scaled up or down by an unknown factor. 2) the  $\chi^2$ -distribution is skewed in an unknown manner. Luckily, the unknown scaling factor disappears when calculating  $F$  in (3.11) or (3.12). And the unknown skewness can be considered as weak effect due the reduced bandwidth in the  $\chi^2$ -distribution because of the large number of degrees of freedom. In addition, the logarithmic behaviour of  $F$  helps to separate 'good' from 'bad' fits independent from the exact value of  $F$ . Nonetheless, as Hedderich & Sachs [80] state, other significance tests will deliver more accurate results under the circumstance of inaccurate  $\chi^2$ -distributions.

## 3.2 Step 2 – Single curve decomposition

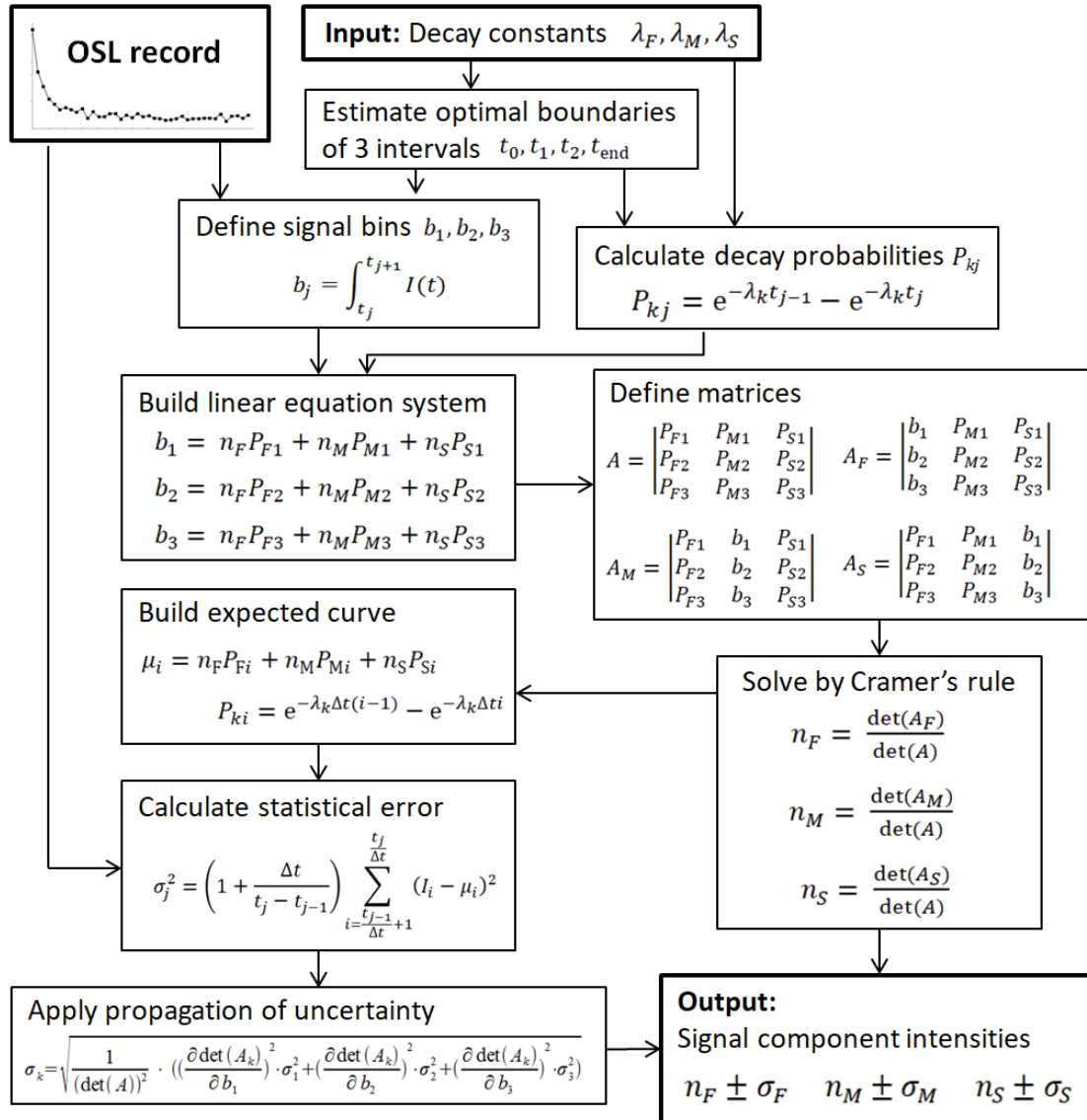


**Figure 3.3:** Workflow of OSL decomposition process for three components. Here,  $j$  is the interval and bin index,  $k$  is the component index. The CW-OSL record is assigned by `decompose_SARdata()`, the decay constants are provided by `fit_OSLcurve()`, the intervals are determined by `calc_OSLintervals()` and calculation process is performed by `decompose_OSLcurve()`.

In step 2 of the method, we calculate the signal intensity of each in step 1 found component for every CW-OSL record in a given data set. The signal intensity is related to the dose the sample received prior the measurement of the OSL record. We will use the intensity values resulting from step 2 later in step 3 to build signal-dose curves.

Like step 1, step 2 is based on the integral equation (3.2) of a multi-component exponential decay. But with the decay constants  $\lambda_k$  now known, we can define the trap release probability  $P_{ik}$  to simplify equation (3.2):

$$I_i = \sum_{k=1}^K n_k P_{ki} \quad i = 1, 2, 3, \dots, N \quad (3.13)$$

$$P_{ki} = e^{-\lambda_k(i-1)\Delta t} - e^{-\lambda_k i \Delta t}$$

Because this equation needs just the channel number  $i$  and the channel width  $\Delta t$  as input parameter, we are able to calculate the decay probability  $P_{ik}$  for each component  $k$  in each channel without considering the measured signal itself. The sum of all  $P_i$  from one component, from the start of the measurement at  $t = 0$  to infinity  $t = \infty$  must be  $\sum P = 1$ . In consequence, the pre-factor  $n_k$  must be equal to the fully integrated signal intensity of its component  $k$ . Thus, the value  $n_k$  should be directly proportional to the concentration of filled traps related to the observed signal. And the concentration of filled traps is related to the accumulated dose, which is the information we want to obtain. Thus, the goal must be to gather  $n_k$  as accurate and precise as possible. One approach to do that derives directly from equation (3.13).

Equation (3.13) applied on all channels of one single OSL record, produces a linear equation system with  $N$  equations and  $K$  unknown variables  $n_1 \dots n_K$ . There are many ways to solve such an equation system in a convenient and robust way. The approach described in the following, reduces the equation system to  $K$  equations and solves them based on determinants. This algebraic solution will allow us an analytical determination of the intensity errors.

The procedure proposed in the following is a further development of the ideas presented in my bachelor thesis [36] and the subsequent conference talk [84]. A general introduction of the used methodology is provided by chapter 7 and appendix B in Bevington and Robinson [76].

Later, in chapter 4.2 we will test the method by simulation for its accuracy, precision and robustness. In these simulations, we will also test a nonlinear regression method provided by the **R** function `stats::nls()`. This allows us to compare the determinant based approach with an alternative approach. The alternative approach will give us a least-square estimate, obtained with the Gauss-Newton minimization algorithm. It will turn out that both problem solving methods have advantages and disadvantages while showing a similar overall-performance. The simulation tests in chapter 4.2 will also show that the best results will be given when we refine the determinant-based results by a nonlinear regression and apply then the error estimation algorithm of the determinant-based approach. Nonetheless, we will not discuss the nonlinear regression method in this thesis. A comprehensive description of the method and the used **R** function is provided by Ritz and Streibig [79]. Both decomposition algorithms were programmed respectively wrapped in the function `decompose_OSLcurve()`. Both methods need input conditions, which are provided by the function `calc_OSLintervals()`.

## CW-OSL decomposition by determinants

First, we reduce equation (3.2) to a system of  $K$  equations. Thus, we can accumulate the data points of a CW-OSL record into  $K$  signal bins to improve signal-to-noise ratio. For simplicity, we will discuss the following method at the example of a 2-component case. But for cases with more components, the approach will be the same. The 2-component case will be defined by an arbitrary fast decaying component and an arbitrary slow decaying component. The decay constants  $\lambda_F$  and  $\lambda_S$  of both components are known while their component intensities  $n_F$  and  $n_S$  are unknown. We divide the CW-OSL curve into two intervals: The first interval begins at  $t_0 = 0$  and ends at some time  $t_1$ . The interval boundary  $t_1$ , like any other interval boundary, has to be a multiple of the channel time  $\Delta t$ . This way, we assure that no data point is shared by two intervals. The second interval begins at  $t_1$  and ends at  $t_{\text{end}}$ , the end of the optical stimulation. The signal bins  $b_1$  and  $b_2$  created from these intervals are calculated by:

$$b_1 = \int_{t_0}^{t_1} I(t) dt = \sum_{i=1}^{\frac{t_1}{\Delta t}} I_i \quad b_2 = \int_{t_1}^{t_{\text{end}}} I(t) dt = \sum_{i=\frac{t_1}{\Delta t}+1}^{\frac{t_{\text{end}}}{\Delta t}} I_i \quad (3.14)$$

In principle, the interval boundaries can be chosen freely. The following math will still work if we define overlapping or very short intervals. But the restriction we applied when setting  $t_1$  as interval divider is necessary for error calculation and SNR optimization as we will see later. With the signal bins  $b_1$  and  $b_2$  defined, we can now build a simple equation system:

$$\begin{aligned} b_1 &= n_F P_{F1} + n_S P_{S1} \\ b_2 &= n_F P_{F2} + n_S P_{S2} \end{aligned} \quad (3.15)$$

The decay probabilities  $P$  are constants and are calculated by:

$$\begin{aligned} P_{F1} &= 1 - e^{-\lambda_F t_1} & P_{S1} &= 1 - e^{-\lambda_S t_1} \\ P_{F2} &= e^{-\lambda_F t_1} - e^{-\lambda_F t_{\text{end}}} & P_{S2} &= e^{-\lambda_S t_1} - e^{-\lambda_S t_{\text{end}}} \end{aligned} \quad (3.16)$$

We choose Cramer's rule [76], [85] to solve equation (3.15). We build the matrices  $A$ ,  $A_{k=1}$  and  $A_{k=2}$  according to Cramer's rule from the constants of the equation system:

$$\mathbf{A} = \begin{pmatrix} P_{F1} & P_{S1} \\ P_{F2} & P_{S2} \end{pmatrix} \quad \mathbf{A}_F = \begin{pmatrix} b_1 & P_{S1} \\ b_2 & P_{S2} \end{pmatrix} \quad \mathbf{A}_S = \begin{pmatrix} P_{F1} & b_1 \\ P_{F2} & b_2 \end{pmatrix} \quad (3.17)$$

Then, the signal intensities  $n_k$  are given from the ratios of the determinants:

$$n_F = \frac{\det \mathbf{A}_F}{\det \mathbf{A}} \qquad n_S = \frac{\det \mathbf{A}_S}{\det \mathbf{A}} \qquad (3.18)$$

We can solve the determinant ratios with the help of the Laplace expansion [85]:

$$n_F = \frac{b_1 P_{S2} - b_2 P_{S1}}{P_{F1} P_{S2} - P_{F2} P_{S1}} \qquad n_S = \frac{b_2 P_{F1} - b_1 P_{F2}}{P_{F1} P_{S2} - P_{F2} P_{S1}} \qquad (3.19)$$

The introduced procedure can be applied to any number of components, as the source code of `decompose_OSLcurve()` demonstrates (appendix A.2). Figure 3.4 displays the same procedure for the 3-component case as flow chart.

The disadvantage of using Cramer's rule is that with increasing number of components, the necessary computing time increases strongly [86]. So why not using a more efficient way of solving equation systems, like for example Gaussian elimination? First, most quartz OSL samples are described sufficiently with 3 to 5 components, as we will see later in chapter 5. So, computational costs remain small. Second and more important: As (3.19) demonstrates is the equation system solved purely analytical. This allows us to develop an error estimation approach, which is also solely analytical.

## Error calculation

We will use the method of propagation of uncertainty in indirect measurements. See for example chapter 8 of Fornasini [87] or the GUM guideline [88] for a detailed introduction into this method. Under the assumption of statistically independent measurements  $X, Y, \dots$ , can the uncertainty  $\sigma_Z$  of an indirectly achieved measurement  $Z$  be estimated by:

$$Z = f(X, Y, \dots) \qquad \sigma_Z = \sqrt{\left(\frac{\partial f(X, Y, \dots)}{\partial X}\right)^2 \sigma_X^2 + \left(\frac{\partial f(X, Y, \dots)}{\partial Y}\right)^2 \sigma_Y^2 + \dots} \qquad (3.20)$$

This equation is also known as Gaussian error propagation.

We will continue with the 2-component case for simplicity. If we replace  $Z$  in (3.20) with  $n_F$  and  $f(X, Y, \dots)$  with equation (3.18), then we get:

$$\sigma_F = \frac{1}{\det \mathbf{A}} \sqrt{\left(\frac{\partial \det \mathbf{A}_F}{\partial b_1}\right)^2 \sigma_1^2 + \left(\frac{\partial \det \mathbf{A}_F}{\partial b_2}\right)^2 \sigma_2^2} \qquad (3.21)$$

Here  $\sigma_1^2$  and  $\sigma_2^2$  are the uncertainty of the signal bin values  $b_1$  and  $b_2$  and will be discussed soon. If we apply the Laplace expansion onto (3.21) like we have done for (3.19), we get:

$$\sigma_F = \frac{\sqrt{P_{S2}^2 \sigma_1^2 + (-P_{S1})^2 \sigma_2^2}}{P_{F1}P_{S2} - P_{F2}P_{S1}} \quad (3.22)$$

But are we allowed to use the Gaussian error propagation (3.20) in the first place? The propagation of uncertainty method presumes an approximately linear behaviour of the investigated function in the statistical uncertainty of its input measurement values. As can be seen in (3.19) and can be proved with the Leibniz formula for any determinant, the values of  $\det \mathbf{A}$  and  $\det \mathbf{A}_k$  do change linearly with the change of any single matrix element. The linearity-requirement is fulfilled because every signal bin value  $b_j$  ( $j$  = bin index) appears just once in a matrix  $\mathbf{A}_k$ . Another requirement behind the equations (3.20) and (3.21) is that all signal bin values  $b_j$  are statistically independent. In other words, they are not allowed to be correlated to each other regarding their uncertainty caused by instrumental or statistical noise. We ensured this by our definition of non-overlapping intervals in equation (3.14). The math presented here would still work in case of overlapping intervals, but we would have to add covariance terms to (3.20). These covariance terms need correlation coefficients as input parameters which we would have to obtain somehow. We avoid this additional layer of complexity with the requirement of non-overlapping integration intervals.

The signal bins  $b_i$  are uncorrelated regarding statistical errors, but they are not uncorrelated regarding systematic errors. Systematic errors could be unexpected OSL curve shapes due incorrect or incomplete global curve fitting or the occurrence of a significant signal offset due not corrected background. Even if systematic errors are somehow correctly incorporated into the uncertainty  $\sigma_i$ , equation (3.20) would not support their propagation into  $\sigma_k$  due to the independence-requirement.

However, to calculate the error  $\sigma_k$  of a component's intensity value, we need values for the signal bins uncertainty  $\sigma_j$  in the first place. One approach is to develop a noise model for the measurement system used. A noise model would allow us to calculate  $\sigma_j$  from the signal intensity and the detection settings. This is a reasonable approach if a signal bin consists of just one data point or if the data points in a signal bin are not ordered by time but by some other property, like spatial or spectral location. One example of this are spatially resolved CW-OSL measurements with a CCD camera, where Greilich *et al.* [89] proposed a noise model.

We can also evaluate a noise model for PMT measurements, like various authors have already discussed in detail [70]–[72], [90], [91]. In the simplest case, we assume Poisson-distributed errors [92]. But that would lead to error underestimations, because we would ignore the detector noise at least partly [70], [91]. We can also apply other models which either need separate background measurements or exact knowledge about the instrumental noise function

[93]. But neither of both might be available if we analyse a data-set from an archive or another workgroup. We will surpass this problem by using a statistical approach which doesn't need input parameters or noise model assumptions.

The idea is to calculate the signal bin errors from the residual curve we get if we subtract the fitting model expected OSL curve from the actually measured OSL curve. We calculate the expected OSL curve by inserting the decay constants  $\lambda_k$  we found in step 1 and the component amplitudes  $n_k$  from equation (3.18) into equation (3.2). For the 2-component case, the expected measurement value  $I_i^*$  for any channel  $i$  with the channel width  $\Delta t$  is given by:

$$I_i^* = n_F(e^{-\lambda_F(i-1)\Delta t} - e^{-\lambda_F i \Delta t}) + n_S(e^{-\lambda_S(i-1)\Delta t} - e^{-\lambda_S i \Delta t}) \quad i = 1, 2, 3, \dots, N \quad (3.23)$$

The residual between  $I_i$  and  $I_i^*$  allows us to calculate the corrected sample variance for the data points inside the measurement interval of a signal bin. Because a signal bin value is the sum of its data point values, the signal bin variance is also the sum of its data point variances (see rule of Bienaymé). Thus, the standard deviation  $\sigma_j$  of a signal bin  $b_j$  containing  $N_j$  data points is given by:

$$\sigma_j = \sqrt{\frac{N_j}{N_j - 1} \sum_{i=\frac{t_{j-1}}{\Delta t}+1}^{\frac{t_j}{\Delta t}} (I_i - I_i^*)^2} \quad i = 1, 2, 3, \dots, N \quad N = \sum N_j \quad (3.24)$$

$$N_j = \frac{t_j - t_{j-1}}{\Delta t}$$

Applied to our 2-component example, we get:

$$\sigma_1 = \sqrt{\frac{N_1}{N_1 - 1} \sum_{i=1}^{\frac{t_1}{\Delta t}} (I_i - I_i^*)^2} \quad \sigma_2 = \sqrt{\frac{N_2}{N_2 - 1} \sum_{i=\frac{t_1}{\Delta t}+1}^{\frac{t_{\text{end}}}{\Delta t}} (I_i - I_i^*)^2} \quad i = 1, 2, 3, \dots, N \quad (4.25)$$

$$N = N_1 + N_2$$

Inserting the uncertainties  $\sigma_1$  and  $\sigma_2$  into equation (3.21) allows us to calculate the component error  $\sigma_F$  without any a priori knowledge of the instrumental noise.

Equation (3.24) has two constraints: First, at least two data points per signal bin are needed to calculate the sample variance. To solve this issue, a side-condition was programmed into `calc_OSLcurve()`: If a bin  $b_j$  consists just of one data point  $I_i$ , Poisson-statistics is assumed and the bins signal value is used as variance value ( $\sigma_j^2 = b_j = I_i$ ). Second, if a bin  $b_j$  consists of just a few data points, then the random scattering of these few data points have a large effect on



the particular value of  $\sigma_j$ . Depending on the pre-factor of  $\sigma_j$  in equation (3.20), this effect might lead to a significant over- or under-estimation of the component error  $\sigma_k$  in some cases. Thus, the precision (not the accuracy) of determining  $\sigma_k$  can be expected to be lower than from other error estimation approaches like Monte Carlo simulation or  $\chi^2$  evaluation.

The exact outcome of the presented error estimation procedure, however, relies on the chosen time intervals  $t_j$  when defining the signal bins. The uncertainty values  $\sigma_k$  are also estimates of the precision in calculating the component amplitudes  $n_k$ . Thus, finding the optimal interval boundaries is vitally important for the performance of the method.

## Interval determination

While setting up an equation system and applying Cramer's rule allows us to set the integration intervals arbitrarily, the error estimation procedure is in need of independent intervals. The requirement of signal-to-noise ratio optimization demands the use of all data points of a measurement. These constraints lead to the following rules: The intervals shall cover the whole OSL curve and shall be divided by boundaries given by discrete time stamps  $t_j$ . Therefore, for decomposing an OSL curve with  $K$  components,  $K - 1$  time parameters  $t_j = t_1, \dots, t_{K-1}$  have to be set, with  $t_0$  and  $t_K$  are already set by the start and the end of the measurement.

Again, we can consider a variety of approaches. We can minimize  $\sigma_k$  in the error propagation equation (3.20) for every single CW-OSL curve. All input parameters in (3.20) are functions of at least one  $t_j$ . So  $\sigma_k$  is a function of all  $t_j$ . Because this minimization problem is hard to solve in case of more than two components, a numerical approach might be considered. But this would not just add significant computing time; also would every OSL curve create its own set of interval parameters. The exact interval parameters of each OSL curve would rely on the exact distribution of signal intensity in each particular curve, including deviations due to random and systematic errors. Errors of second order would be induced, creating additional sources of uncertainty not covered by our error estimation approach. Alternatively, we could apply the same minimization approach to the global OSL curve, created in step 1. Thus, every OSL curve of a data set would use the same integration intervals and curve-to-curve variations would not change any parameters, besides the signal bin values  $b_j$ . Still, we would reach an approximately near-optimum SNR for each curve. If signal sensitivity is the most important feature, this approach is recommended.

Here, we will use another approach instead. We formulate the requirement to determine the interval parameters independently from the component intensities. Two related data sets with the same detection settings and the same set of signal components shall use the same set of intervals. This way, we can compare and adopt methodical findings from one data set to another.

We also set the requirement to maximize the mathematical independence between the components. In some data sets, we may experience over- or under-fitting or changing decay kinetics over the measurement duration or some other unexpected component behaviour. We

want to minimize the impact of occurring systematic errors in a components calculation path onto the decomposition results for the other components.

The idea is to maximize the value of  $\det \mathbf{A}$  for a given set of decay constants and channel settings. We formulate two arguments for doing this. Both arguments are based upon hypotheses and have yet to be proven for mathematical validity, which will not be done in this thesis. Nonetheless, the simulation results in chapter 4.2 and the experience gathered in the analyses of actual data sets show that this approach works reasonably well for the vast majority of CW-OSL measurements.

The first argument is based on equation (3.21). There, the component intensity error  $\sigma_k$  (respectively  $\sigma_F$  in that example) is inversely proportional to the value of  $\det \mathbf{A}$ . Without considering the terms inside the square root and their alteration, we can assume that maximizing  $\det \mathbf{A}$  decreases the error value  $\sigma_k$  and therefore increases the SNR of the intensity value  $n_k$ . When we take the square root term also in consideration, the lowest error  $\sigma_k$  probably does not correspond exactly to the maximum of  $\det \mathbf{A}$  for most OSL curves. Nonetheless, we formulate the hypothesis that the maximum of  $\det \mathbf{A}$  corresponds to component intensity uncertainty values  $\sigma_k$  and with it to a SNR value which is sufficiently close to the best achievable SNR values for the majority of CW-OSL curves.

The second argument is based on geometric considerations: We build matrix  $\mathbf{A}$  from a set of linearly independent vectors  $\vec{v}_k$ . Each vector is the combination of a series of  $j = 1, \dots, K$  de-trapping probabilities  $P_j$  of one particular signal component  $k$ . The exact values of  $P_j$  depend not just on the interval boundaries  $t_j$  but also on the decay constant  $\lambda_k$ . If we change  $\lambda_k$ , we change also the values of the elements  $P_j$  and with it the direction of the vector  $\vec{v}_k$ . We conclude that every uncertainty of  $\lambda_k$  leads to an uncertainty in the direction of  $\vec{v}_k$ . When maximizing the value of the determinant, then we maximize also the angles between the vectors  $\vec{v}_k$  (see the geometrical meaning of determinants in chapter 16 in Arens *et al.* [94]). A maximum in the sum of angles between vectors leads to a minimum of propagation of uncertainty from the vectors into the determinant value. We can formulate the following hypothesis: A maximum in the value of  $\det \mathbf{A}$  corresponds to a minimum of uncertainty in the value of  $\det \mathbf{A}$ , caused by the unknown statistical and systematic errors from the deployed decay constants  $\lambda_k$ .

The challenge is to find the maximum of  $\det \mathbf{A}$  in dependence of its interval boundaries  $t_j$ . In case of a 2-component system were we have to calculate just the value of  $t_1$ , we can solve this problem analytically:

$$t_1 = \frac{\ln \left( (1 - e^{-t_{\text{end}} \lambda_S}) \lambda_F \right) - \ln \left( (1 - e^{-t_{\text{end}} \lambda_F}) \lambda_S \right)}{\lambda_F - \lambda_S} \quad (3.26)$$

To meet some earlier requirements, the value of  $t_1$  will be rounded up to the next higher multiple of the channel time. Note that if we set  $t_{\text{end}} = \infty$ ,  $t_1$  becomes the inverse of the logarithmic mean

between  $\lambda_F$  and  $\lambda_S$ .

Calculating the whole set of  $K - 1$  interval boundaries for data sets with  $K > 2$  components is more complex. An analytical solution for the 3-component solution was tried but not solved successfully. Instead the problem will be solved numerically by varying all  $t_j$  until the largest value for  $\det \mathbf{A}$  is found. This is realized in the function `calc_OSIntervals()` which is executed directly after the global decay constants were calculated. Accordingly, `calc_OSIntervals()` is executed just once per data set. To calculate the maximum determinant, the following algorithm is applied:

- 1) Define  $20 \cdot 2^K$  random sets of  $K - 1$  interval boundaries  $t_j = t_1, \dots, t_{K-1}$ . Replace interval sets which contain  $t_j$  duplicates.
- 2) Build the matrix  $\mathbf{A}$  and calculate its determinant for each set of interval boundaries.
- 3) Sort the  $\det \mathbf{A}$  values and create a subset from the highest 10% of determinants
- 4) Extract the minimum and the maximum time mark from each interval boundary. Redefine the allowed value range with the minimum/maximum time marks and go back to step 1.
- 5) If all determinants in the 10% subset have the same value, return the first interval set in the subset as final result
- 6) For usual cases with between 3 and 5 components, this algorithm needs in the order of  $10^3$  determinant calculations to return an optimized set of interval boundaries. Unfortunately, the algorithm results are not reproducible, although just varying slightly. Repeated runs may lead to different interval sets, which is an indication that rather local maxima than global maxima are found. The missing reproducibility leads to the conclusion, that the algorithm needs further improvement or should be replaced entirely. Nonetheless, as an easy-to-implement and practical solution it proved itself sufficient.

The source code of `calc_OSIntervals()` can be found in appendix A.3.

### 3.3 Step 3 – Component-wise dose calculation

So far, we discussed the identification and separation of signal components in a set of CW-OSL measurements. Now we focus back to the application of retrospective dose determination. We want to calculate the dose information hidden in the decomposition results and estimate the age of the sample. The task of step 3 is to find a historical or palaeolithic dose or ‘paleodose’ in short. If an environmental dose rate is given for a sample, this paleodose can be converted into an age. The chosen methods and their parameters depend on the sample mineral type, its geomorphologic history, the quality of the data set and the laboratories preferences. But it is not task of this thesis to investigate and discuss the variety of methods. We will go strictly with the ‘default’ approach described by Murray, Wintle and Galbraith in their publications [19], [35], [71], [95]. Note that all data sets we will discuss in chapter 5, were analysed with that approach, even if other approaches would be better suiting.

#### L/T table

**Table 3.2:** L/T table example; Fastest decaying component of the first aliquot for the  $K = 4$  case in sample BT594. Test dose for generating all  $T_i$  is:  $D_T = 19.4$  Gy

Cycle $i$	Dose (Gy)	$L_i/T_i$	$\sigma_{L_i/T_i}$	$L_i$	$\sigma_{L_i}$	$T_i$	$\sigma_{T_i}$
0	natural	3.13	0.16	5638	99	1801	86
1	19.4	1.08	0.05	1984	46	1831	70
2	48.3	2.32	0.13	4444	116	1914	93
3	83.9	3.63	0.11	7192	187	1979	34
4	103.2	3.96	0.17	8527	271	2154	65
5	19.4	1.15	0.05	2625	92	2289	64
6	0	0.00	0.02	-26	49	2311	72

First, we have to structure the OSL decomposition results and set them into relation with the regenerated doses. We assume the data set is sequenced in accordance to the standard SAR protocol defined by Murray and Wintle [19]. Then every OSL measurement returns a value  $L_i$  and is followed by the regeneration of a fixed test-dose and the measurement of the OSL signal  $T_i$  related to this test-dose. The normalized OSL signal is therefore given by  $L_i/T_i$ .

A L/T table provides a structure for the signal values and dose regeneration points we need to build dose-signal curves and to test for signal behaviour criteria. One L/T table per signal component and aliquot is built. To avoid some potential issues, we apply the following conditions when assigning the signal values to the table:

- The decomposition process returns also a residuum value  $r_k$  for each component. This residuum value indicates the part of the signal component intensity  $n_k$  which could not be measured because the stimulation ended. We assume that this residuum signal would be

carried into the signal of the next OSL measurement. Therefore, we subtract the residuum values  $r_k$  from the  $n_k$  values of the subsequent OSL curve. This enables reasonable L/T table estimates for slow decaying components.

- In case of long OSL measurement times, it is useful to shorten the OSL curves to prevent over-fitting in step 1 and declining fast component precision in step 2 (See chapter 4). In case of a shortened OSL curve, we use  $r_k$  as rejection criterion for the whole L/T table. Is the value of  $r_k$  larger than 1% of  $n_k$ , the we discard the table. The component can't be further evaluated and misleading conclusions are avoided.
- Negative values of  $L_i/T_i$  will be set to  $L_i/T_i = 0$  to avoid runtime exceptions in the later used **R** functions. In addition: Although negative values are mathematically reasonable, it is discussable if they are also physically reasonable.

The L/T table is created by `decompose_SARdata()`. This function does also call the function `decompose_OSLcurve()` to decompose all CW-OSL curves in a SAR-compatible data set. It does also perform the rejection tests and hand over the L/T tables to `Luminescence::plot_GrowthCurve()`.

## Growth curve

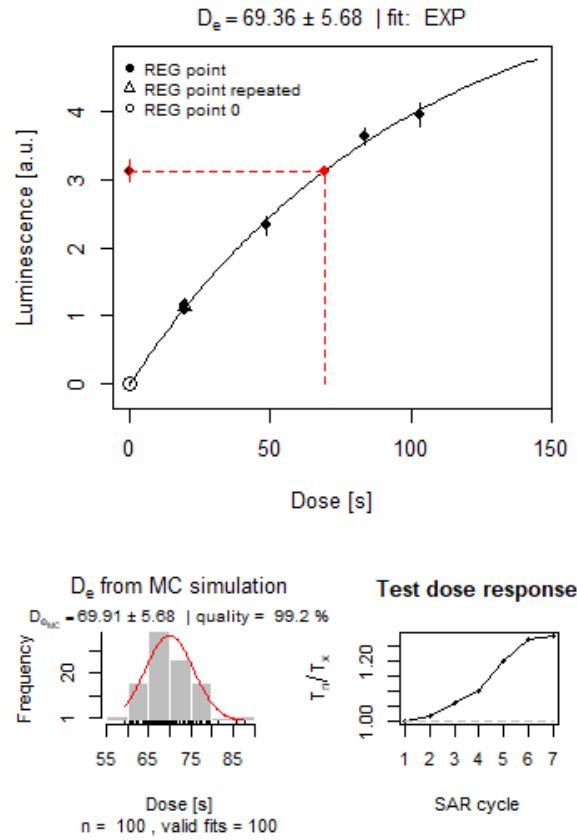


**Figure 3.4:** Signal-dose curve example; Fastest decaying component of the first aliquot of sample BT594, plotted by `Luminescence::plot_GrowthCurve()`.  
*Lower left:* Distribution of Monte Carlo simulated  $D_e$  values, used to calculate the  $D_e$  error value. *Lower right:* Variation of the normalized test-dose signal over the measurement sequence, useful to display luminescence sensitivity changes.

From the L/T table, we create a signal-dose curve or ‘growth curve’ by calling the function `Luminescence::plot_GrowthCurve()` programmed by Kreutzer and Dietze [96]. The function plots the luminescence signal values  $y = L_i/T_i$  against the regeneration doses  $x = D_i$ . Several fitting models are selectable. We will use the default model:

$$y(x) = a(1 - e^{-(x+c)/b}) \quad (3.27)$$

Here  $a$ ,  $b$  and  $c$  are fitting factors. The natural or ‘equivalent’ dose  $D_e$  related to the natural luminescence signal is calculated by solving  $y(D_e) = L_0/T_0$ . The uncertainty of the equivalent dose  $D_e$  is calculated by a Monte Carlo simulation assuming normal distributed  $L_i/T_i$  values with a standard deviation equal to  $\sigma_{L_i/T_i}$ .

## Rejection criteria

The equivalent dose values calculated so far, are not necessarily physical meaningful. Murray and Wintle [19] introduced two tests to detect and reject not trustworthy  $D_e$  values: the recycling ratio and the recuperation rate. We use their range of acceptance proposals to keep or discard equivalent dose values.

**Table 3.3:** Rejection criteria for equivalent dose values  $D_e$ , measured and calculated according to the SAR protocol by Murray and Wintle [19].

Criterion	Formula	Range of acceptance
Recycling ratio	$r_{recycling} = \frac{L_1/T_1}{L_{D_i=D_1}/T_i}$	$0.9 < r_{recycling} < 1.1$
Recuperation rate	$r_{recuperation} = \frac{L_{D_i=0}/T_i}{L_0/T_0}$	$r_{recuperation} < 0.05$

### Recycling ratio test

In the SAR protocol, the first and usually the last dose regeneration cycle apply the same dose  $D_1$  (=recycled dose). The corresponding normalized luminescence signals  $L_1/T_1$  and  $L_{D_i=D_1}/T_i$  should be about equal. If the ratio between both differs significantly from one, it implicates that the applied doses cannot be monitored precisely and the resulting equivalent dose should be discarded. But the recycling ratio calculation is quite noise-sensitive, especially if small test doses are chosen. For low-SNR data sets, false positive as well as false negative aliquot rejections are likely.

### Recuperation test

In the regeneration cycle after the cycle with the largest applied dose, usually no dose is applied before measuring  $L_i$ . If no dose is applied, the corresponding normalized luminescence signal  $L_i/T_i$  should be about zero. The occurrence of significant luminescence signal hints towards the appearance of charge transfer into the observed OSL traps unrelated to dose regeneration.

## Paleodose and age estimation

We will use two statistical models to calculate the sample age from a distribution of equivalent dose values. Both models are common in the geo-scientific community: The central age model and the minimum age model. Both models were introduced by Galbraith *et al.* [95] and are comprehensibly recapitulated and summarized in Galbraith and Roberts [71].

### Central age model

The central age model (short: 'CAM') assumes that the logarithmic values of the equivalent doses  $\log(D_e)$  are approximately normal distributed. It is assumed that this normal distribution arises not just from statistical errors but also from unknown geologic or physical uncertainties. The CAM algorithm calculates a variance-weighted arithmetic mean from the values but includes an uncertainty parameter in the weighting term, called 'overdispersion'. The overdispersion  $\sigma_b$  is used as second fitting parameter besides the paleodose. If the scattering in the  $D_e$ -distribution is just caused by instrumental errors, then the overdispersion should be around zero. We will calculate the CAM paleodoses and overdispersion values using `Luminescence::calc_CentralDose()` programmed by Burow [97].

### Minimum age model

The central age model does not take into account that the sample might be bleached incompletely before the burial event. In that case, a stretched  $D_e$ -distribution towards higher doses is assumed. The central age model would lead to over-estimated paleodoses, so Galbraith *et al.* added an additional fitting parameter to the CAM approach to compensate for the spreading. If the paleodose from this minimum age model (short: 'MAM') is significantly lower than the CAM paleodose, incomplete bleaching before burial is likely. We will calculate the MAM paleodoses using `Luminescence::calc_MinDose()` also programmed by Burow [98].

The decision which age model to apply is done by considering the likely geomorphologic sediment accumulation event. Did the sediment accumulate slowly and all sample grains can be considered well bleached? Or did the sediment accumulate in one single event? Then many grains may never be exposed to sunlight long enough to be fully bleached.



## 4 Method verification: Simulated OSL curves

The methods introduced in chapter 3.1 and 3.2 need to be tested for reliability and accuracy. We will do this by simulating a large number of OSL curves with varying parameters. As parameters we will chose OSL properties like the number of components and their amplitudes and detection parameters like channel width and signal background. We will vary each parameter by two to four steps inside reasonable margins. As reasonable margins, we will consider typical values obtained from 470 nm stimulated CW-OSL measurements of quartz. The correlation between input parameters and output values gives us not only a measure for the methodical accuracy and precision but will also help us to identify systematic errors and methodical limits. In addition, we get the opportunity to test algorithm options like the  $\chi^2$ -weighting (see equation (3.6) and (3.7)) and the choice between determinant-based or regression-based decomposition.

For the OSL curve creation, the function `simulate_OSLcurve()` was programmed. It builds CW-OSL curves according to equation (3.2). All component parameters and also the detection settings can be chosen freely. The simulated signal values are scattered randomly in accordance to the Poisson distribution with `stats::rpois()`. This emulates photon shot noise. In most of the simulations, a signal background is added. The background signals are also Poisson-scattered to emulate dark current noise.

The definition of the parameter spaces and the data evaluation are handled by `Rmarkdown` scripts. For the step 1 and step 2 simulation data sets, correlation matrices were calculated, using `stats::cor()`. As measure of association, Kendall's  $\tau$  [80], [99] was chosen. Simplified spoken, Kendall's  $\tau$  measures whether the values of two variables will be ranked in the same order if they are sorted as pairs or if they are sorted separately. The values of  $\tau$  will always lie in between  $-1 \geq \tau \geq 1$ . If  $\tau \rightarrow 1$  then the variables are correlated (ranking the value lists as pair or as single lists leads to about the same order); if  $\tau \approx 0$  then the variables are uncorrelated; if  $\tau \rightarrow -1$  then the variables are anti-correlated (the single-list-order vs. pair-order is inverted). For table 4.4 Spearman's  $\rho$  [80] was tested as alternative correlation measure. The results were qualitatively the same. Kendall's  $\tau$  was chosen because of its better robustness against outliers.

## 4.1 Step 1 reliability

Does the method described in chapter 3.1 find the number of components and their corresponding decay constants with sufficient certainty? Which particular threshold value of  $F$  will return the best possible results? How does the method depend on the detection settings? These questions are evaluated by the script `Test_Step1.Rmd`. Nine parameters are defined, summarized in table 4.1. The parameter variants lead to a total of 10368 combinations. For each parameter combination, one global CW-OSL curve was simulated. Each curve was analysed by `fit_OSLcurve()`. Four of the nine parameters are intensity value of CW-OSL components. Curves with less than four components are created by setting one or more components to an intensity of  $n = 0$ . The decay constants are set to constant values which correspond roughly to the known major quartz OSL components at standard blue CW-OSL SAR measurement conditions (see chapter 2.3).

**Table 4.4:** Input parameters for the step 1 simulations

	<b>Parameter</b>	<b>Input variants</b>
<b>OSL components</b>	Fast ( $\lambda = 2 \text{ s}^{-1}$ )	$n = 0, 1000, 3000, 10000$
	Medium ( $\lambda = 0.5 \text{ s}^{-1}$ )	$n = 0, 1000, 3000, 10000$
	Slow1 ( $\lambda = 0.1 \text{ s}^{-1}$ )	$n = 0, 3000, 10000$
	Slow2 ( $\lambda = 0.02 \text{ s}^{-1}$ )	$n = 10000, 30000, 100000$
<b>Detection settings</b>	Channel width	$\Delta t = 0.1, 0.2, 0.5 \text{ s}$
	Number of channels	$N = 100, 400$
	Background signal	$b = 0, 20, 40 \text{ cts s}^{-1}$
	Curve additions	$M = 100, 400$
<b>Method options</b>	$\chi^2$ weighting	$\sigma^2 = 1, I_i$

The simulation and fitting process of all 10368 curves took 2 days and 6 hours on a desktop PC with Intel core2 duo E7500 CPU. Most of the CPU time was used by the fitting function `fit_OSLcurve()`. This leads to a mean time consumption of about 20 seconds per run on this rather old PC.

## Determining the best threshold value for the $F$ -test

The true number of components in a data set is determined by a statistical test, the  $F$ -test. The  $F$  value measures the fit quality improvement after adding another component to the fitting model. But which particular threshold value for  $F$  is the best-suited for our method? We know from the discussion in chapter 3.1 and the case studies in chapter 5 that the literature-proposed threshold of  $F \approx 3$  is too low for our purposes. We will use the distribution of  $F$ -values in our simulation results to estimate a higher but still sufficient threshold value.

To achieve this, we have to narrow the data set to sufficiently fitted curves:

- 1) Set those  $F$ -table lines as correct fit, where the number of input components  $K_{\text{in}}$  equals the number of found components  $K_{\text{out}}$ . Curves where the maximum number of found components is smaller than the number of input components are excluded (724 of 10368 curves).
- 2) Exclude curves simulated with  $[N = 400, \Delta t = 0.5, b = 20 \text{ or } 40]$  or  $[N = 400, \Delta t = 0.2, b = 40]$ . Thus we eliminate curves which are background-dominated and therefore fitted insufficiently with a high likelihood (1728 of 9644 curves).
- 3) Exclude curves where the calculated decay constant of any component differs more than 10 % from the expected value to ensure just sufficiently fitted curves remain (2336 of 7916 curves). Component slow2 shall be excluded from this rule, because slow2 might be influenced by the background signal.

We split the remaining 5580 curves into weighted and not weighted  $\chi^2$  calculations, see equation (3.6) and (3.7). Figure 4.1 shows the distribution plots of  $F_K$  and  $F_{K+1}$ . A threshold value close to the  $F_{K+1}$  peak (blue curve) would lead to too many over-fitted results. A threshold value close to the  $F_K$  peak (red curve) would lead to too many under-fitted results.

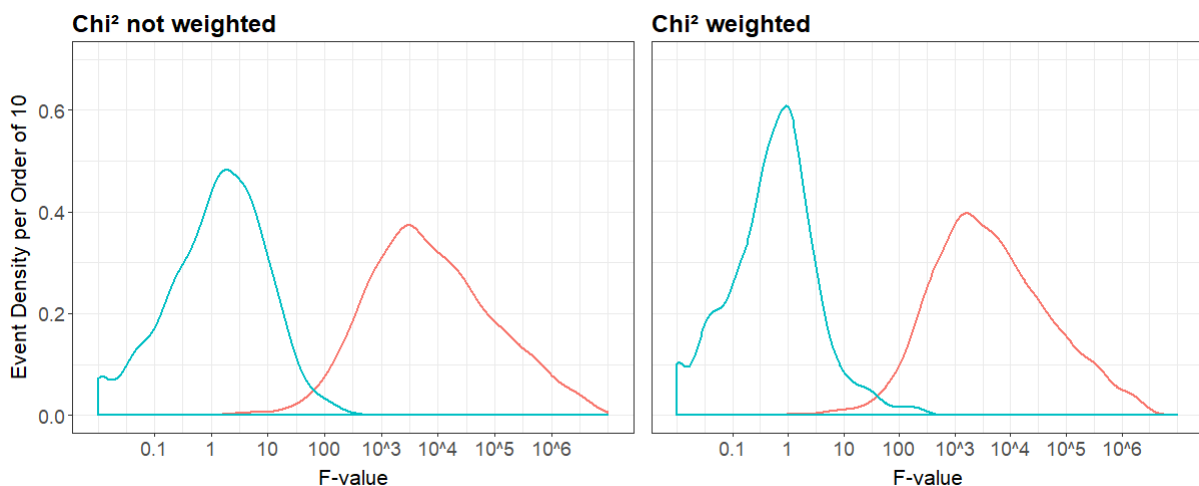


**Figure 4.1:** Distribution of  $F$  values for reduced simulated data set.

**Red:**  $F_K$  values comparing the correct  $K_{\text{out}} = K_{\text{in}}$  fit with the previous  $K_{\text{out}} = K_{\text{in}} - 1$  fit  
**Blue:**  $F_{K+1}$  values comparing the over-fitted  $K_{\text{out}} = K_{\text{in}} + 1$  fit with the  $K_{\text{out}} = K_{\text{in}}$  fit

Both  $\chi^2$ -weighting approaches lead to similar  $F$ -distributions, as expected from the discussion in chapter 3.1. The  $\chi^2$ -weighted approach lead to a slightly more narrow  $F_{K+1}$  distribution. There is an overlap between  $F_K$  distribution and  $F_{K+1}$  distribution, so no particular threshold value assures certainty in detecting the right number of components  $K$ . But a good trade-off with a low likelihood of under-fitting and over-fitting for both  $\chi^2$ -cases represents:

$$F_{\text{threshold}} = 50 \quad (4.1)$$

We will apply this particular value in all further data analyses in this thesis.

### Performance test summary and $\chi^2$ approach comparison

With a calibrated threshold value for  $F$  defined, we are able to fully analyse the data set with the step 1 method presented in chapter 3.1. But how can we decide, that the method did find the right number of components and the correct decay constants, without manually analysing every of the 10386 fitting outcomes? To do this, we define for the decay constants an input-output-ratio attribute  $R_\lambda$  and a deviation-from-perfect-match attribute  $D_\lambda$ . We define also a discrepancy attribute  $\Delta K$  for the component numbers:

$$\begin{aligned} R_\lambda &= \frac{\lambda_{\text{out}}}{\lambda_{\text{in}}} \\ D_\lambda &= \left| 1 - \frac{\lambda_{\text{out}}}{\lambda_{\text{in}}} \right| \\ \Delta K &= K_{\text{out}} - K_{\text{in}} \end{aligned} \quad (4.2)$$

$\Delta K$  gives us a measure of over- and under-fitting;  $R_\lambda$  gives us a measure of decay constant over- and under-estimation, which we will call ‘accuracy’;  $D_\lambda$  gives us a measure of decay constant scattering, which we will call ‘precision’. Note, that  $D_\lambda$  still inherits systematic errors in  $\lambda_{\text{out}}$  and is intrinsically correlated to  $R_\lambda$ . With the test approach as described in this chapter, we cannot calculate an accuracy-independent measure of the precision. Nonetheless, if some other parameter is just weakly correlated with  $R_\lambda$  but strongly correlated with  $D_\lambda$ , it is evident, that this parameter influences the precision of the fitting. The association, which output component  $\lambda_{\text{out}}$  belongs to which input component  $\lambda_{\text{in}}$  was performed by comparing all possible sets of  $D_\lambda$  values and taking the set with the smallest sum. In case of a fake component caused by over-fitting, the component with the largest deviation value  $D_\lambda$  was ignored in the further analysis.

The first issue we will look at, is the likelihood of over- and under-fitting and its dependence on the  $\chi^2$ -weighting approach.

**Table 4.5:** Simulation statistics of component number  $K$  in dependence of  $\chi^2$ -weighting approach.  
**Green cells:** Fraction of  $\Delta K = 0$  cases; **Grey cells:** Sample sizes

		Number of components $K_{in}$									
		$\chi^2$ not weighted					$\chi^2$ weighted				
		$K =$	1	2	3	4	Fittings	1	2	3	4
Output $K_{out}$	1	87%	4.1%	<i>Under-fitting</i>		129	90%	3.8%	<i>Under-fitting</i>		130
	2	13%	86%	15%	0.4%	1115	10%	88%	15%	0.4%	1113
	3		10%	79%	36%	2572		8%	79%	37%	2582
	4			6.1%	58%	1266			6%	59%	1280
	5	<i>Over-fitting</i>				5.2%	102	<i>Over-fitting</i>			4.1%
Curves		108	864	2268	1944	=5184	108	864	2268	1944	=5184

As table 4.2 shows, the performance in finding the right number of components for both  $\chi^2$ -approaches is about the same. Independent of the used  $\chi^2$ -approach, 73% of all curves were fitted with the correct number of components. In 6% of all cases, more than the expected components were found. In 21% of all cases, less than the expected components were found.  $\chi^2$ -weighted curves had slightly less over-fitting events (5.7%, compared with 6.5%). Under-fitting was mostly caused by not detecting the slow1 component (75% of all under-fittings). In 38% of all cases,  $K_{out}$  was not selected by the  $F$  criteria but because the  $K + 1$  fit failed.

The second issue we will look at, is the accuracy, precision and likelihood of finding the correct decay constants, also in dependence on the  $\chi^2$ -weighting approach.

**Table 4.6:** Accuracy  $R_\lambda$ , precision  $D_\lambda$  and success rate in determining the decay constants. The full data set is displayed, including under- and over-fittings.  $Q_{0.05} \dots Q_{0.95}$ : Accuracy values for selected quantiles. **Blue cells:** Decay constant underestimation; **Red cells:** Decay constant overestimation. Green cells: High likelihood of accurate component determination.

		Components							
		Fast		Medium		Slow1		Slow2	
$\chi^2$ weighted?		No	Yes	No	Yes	No	Yes	No	Yes
$R_\lambda$	$Q_{0.05}$	0.943	0.910	0.785	0.777	0.691	0.705	0.631	0.655
	$Q_{0.25}$	0.988	0.987	0.953	0.952	0.909	0.920	0.897	0.909
	<b>Median</b>	<b>0.998</b>	<b>0.997</b>	<b>0.991</b>	<b>0.991</b>	<b>0.981</b>	<b>0.986</b>	<b>0.995</b>	<b>0.998</b>
	$Q_{0.75}$	1.003	1.001	1.004	1.003	1.013	1.018	1.042	1.066
	$Q_{0.95}$	1.021	1.018	1.065	1.059	1.507	1.725	2.266	2.205
$D_\lambda < 0.1$		97.4%	95.3%	83.7%	82.7%	65.5%	66.1%	52.8%	52.7%
<b>Component found?</b>		99.95%	99.0%	95.8%	94.2%	73.8%	72.8%	96.6%	97.0%

As Table 4.3 shows, the vast majority of all calculated decay constants lay within a  $\pm 10\%$  range. Slow decaying components however, tend towards lower accuracy and higher probability of being not found or producing outlier values. Both  $\chi^2$ -approaches produce very similar outputs. But the  $\chi^2$ -not-weighted approach proves itself as slightly more robust and accurate in detecting the fast component. We conclude that the selection of the  $\chi^2$ -weighting approach is in most cases not relevant for the result of the method. We select the  $\chi^2$ -not-weighted approach as default for all further calculations in this thesis because of the dominant relevance of the fast component in quartz dating applications (see chapter 2). See equation (3.5) for details on this approach.

## Correlation matrix

We will classify parameter dependencies and identify further methodical issues with the help of correlation matrices. Table 4.4 displays a reduced version of the input-output correlation matrix and the output-output cross-correlation matrix which can be found in appendix B.1. The matrices cover all 5184 cases of  $\chi^2$ -not-weighted curve fittings. The calculation was performed by:

```
stats::cor(... , use = "pairwise.complete.obs", method = "kendall")
```

**Table 4.7:** Step 1 simulation correlation table displaying Kendall's  $\tau$  between input values and selected output values. Values  $< 0.1$  are considered as not significantly correlated and were deleted to improve clarity. Notation equals table 4.1 and equation set (4.2); the measurement length is given by  $L = \Delta t * N$ ; **Blue cells:** positive correlation: increased input values lead to increased output values; **Red cells:** anti-correlation: increased input values lead to decreased output values

Shift/deviation of $\lambda_{out}$		Component numbers		Signal amplitudes $n_{in}$				Detection parameters		
		$\Delta K$	$K_{in}$	Fast	Medium	Slow1	Slow2	$L$	$b$	$M$
$R_\lambda$	Fast	0.23		0.13				0.58		
	Medium	0.36	-0.13		0.10	-0.12		0.11	-0.10	
	Slow1	0.21					0.12		-0.15	
	Slow2	-0.33	0.12				0.16	-0.20	-0.22	
$D_\lambda$	Fast	-0.16	0.22	-0.41	0.21					-0.20
	Medium	-0.30	0.29	0.17	-0.35	0.20		-0.12		-0.13
	Slow1	-0.37	0.14			-0.11		-0.25	0.19	-0.13
	Slow2	-0.44	0.20			0.21	-0.23	-0.32	0.32	
Fit properties	$\chi^2$	0.21					0.33	0.38	0.11	-0.47
	$F_K$	0.44	-0.52			-0.34		0.30		0.16

All values inside the cells of table 4.4 are measures of correlation or anti-correlation. If two variables are most likely to be independent from each other than their correlation-cell remains blank.

Table 4.4 and appendix B.1 allow the following statements about parameter dependencies:

- $\Delta K$  is anti-correlated to  $K_{in}$ : Cases with many components tend to under-fitting, cases with few components tend to over-fitting
- In case of over-fitting ( $\Delta K > 1$ ), additional components appear mostly between Medium and Slow2. This leads to an overestimation of  $\lambda_{Fast}$  and  $\lambda_{Medium}$  and an underestimation of  $\lambda_{Slow2}$ .  $\lambda_{Slow1}$  becomes uncertain
- In case of under-fitting ( $\Delta K < 1$ ), the missing component is mostly Slow1. This might lead

to an underestimation of  $\lambda_{\text{Fast}}$  and  $\lambda_{\text{Medium}}$  and an overestimation of  $\lambda_{\text{Slow2}}$ , but the correlation is much weaker as in the over-fitting case

- $n_{\text{in}}$  is anti-correlated to  $D_\lambda$  and (weakly) correlated to  $R_\lambda$ : With increasing component signal, the precision and accuracy in finding the correct decay constant increases
- But  $n_{\text{in}}$  and  $R_\lambda$  of nearby components are correlated: With increasing component signal, the precision in finding the correct decay constant decreases for the neighbour components
- The detection background  $b$  has little to no effect on the fitting besides an underestimation of the slow decaying components, especially  $\lambda_{\text{Slow2}}$
- Increasing curve additions  $M$  lead to higher precision in determining fast decaying components
- Large channel widths  $\Delta t$  and a high number of channels  $N$ , equal with long measurement times  $L$ , lead to over-fitting; Short measurement times  $L$  lead to under-fitting
- Short measurement times  $L$  decrease the precision  $D_\lambda$  of slow decaying components
- $F_K$  statistics are shifted towards higher  $F$  values with increasing measurement time  $L$  and in case of over-fitting and vice versa
- But the fit-deciding  $F_{K+1}$  attribute has no significant correlation to any input parameter

The biggest apparent problem is the dependency of  $\Delta K$  on the measurement length  $L$ . Wrong channel settings lead to over- or under-fitting. Over- and under-fitting lead to shifted decay constants  $\lambda_{\text{out}}$ . This effect is probably the major constraint of the presented step 1 method. It might be worth a consideration to define the  $F$  threshold value as function of the measurement time  $L$ . Alternatively, the method could be allowed just for a pre-defined bandwidth of channel settings.



## 4.2 Step 2 reliability

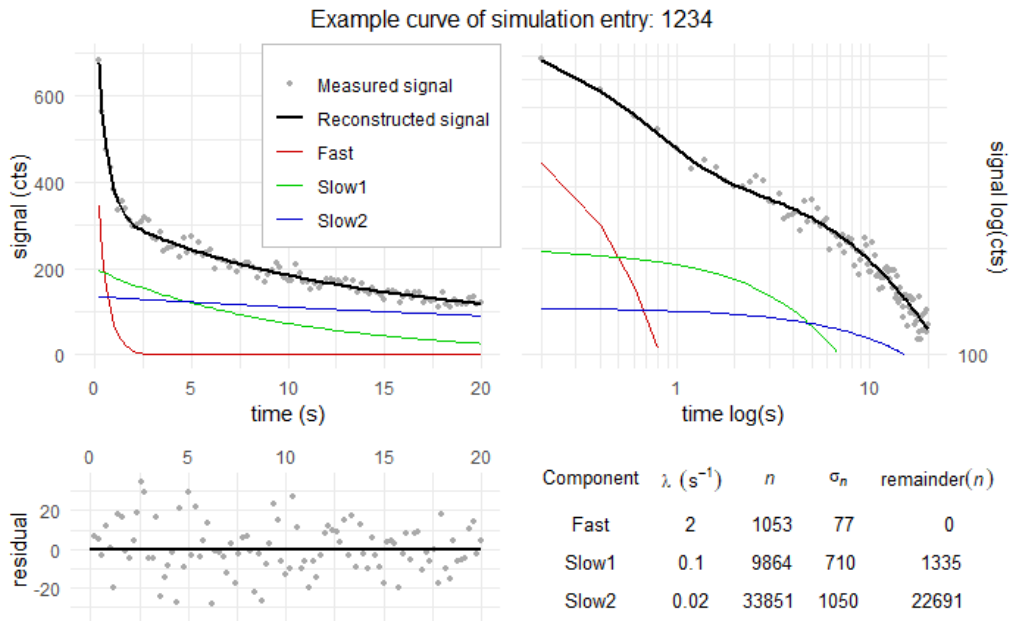


**Figure 4.2:** Decomposition of arbitrary simulated CW-OSL curve; Upper-left: Simulated signal and component curves; Upper-right: The same curves but with logarithmic x- and y-axis; Lower-left: Residual curve with drawn-in signal bin intervals; Lower-right: Result table

We test the accuracy and precision of the Step 2 algorithms by simulating various scenarios, similar to the approach used in the chapter 4.1. The input set of parameters is the same as for the step 1 simulations. But we remove the parameters  $\chi^2$  weighting and curve additions (see table 5.1) and deploy the new parameters *determine signal offset* and *decomposition algorithm* instead. We give the determinant based algebraic decomposition approach the token `det` named after the **R** function to calculate determinants: `base::det()`. We give the alternative nonlinear regression approach the token `nls` named after the **R** wrapper for nonlinear least square methods: `stats::nls()`. We test also the algorithm `det+nls`. In this case, the `det`-results are refined by `nls` fitting. For error calculation, the `det`-procedure is applied but the `nls`-results serve as input parameters for the OSL curve model.

**Table 4.8:** Input parameters for the step 2 simulations

	Parameter	Input variants
<b>OSL components</b>	Fast ( $\lambda = 2 s^{-1}$ )	$n = 0, 1000, 3000, 10000$
	Medium ( $\lambda = 0.5 s^{-1}$ )	$n = 0, 1000, 3000, 10000$
	Slow1 ( $\lambda = 0.1 s^{-1}$ )	$n = 0, 3000, 10000$
	Slow2 ( $\lambda = 0.02 s^{-1}$ )	$n = 10000, 30000, 100000$
<b>Detection settings</b>	Channel width	$\Delta t = 0.1, 0.2, 0.5 s$
	Number of channels	$N = 100, 400$
	Background signal	$b = 0, 20, 40 \text{ cts } s^{-1}$
<b>Method options</b>	Determine signal offset	TRUE, FALSE
	Decomposition algorithm	det, nls, det+nls

Table 4.5 gives 15552 variations of parameters. Unlike the step 1 simulations, where the signal noise was averaged by the curve additions, show the OSL curves significant noise this time. All 15552 different OSL scenarios were simulated and decomposed 1000 times to account for the noise-caused randomization of the decomposition results.

## Performance & Robustness

The simulation was performed on the same year 2011 PC as step 1, with an Intel core2 duo E7500 CPU (2 cores at 2.9 GHz). Simulating and decomposing each of the 15.6 million OSL curves took 3.5 days. A simulation subset was also executed at a year 2019 PC with AMD Ryzen 3 2200G CPU (4 cores at 3.5 GHz). The modern PC needed about 60% of the time for the same calculations as the older PC. The average calculation times in dependence of the selected algorithm and the number of components  $K$ , are displayed in table 4.6.

**Table 4.9:** Computing time and failure rates of the decomposition algorithms. `det` = determinant based decomposition; `nls` = nonlinear regression with fixed  $\lambda_k$ 's; `det+nls` = `det` but with `nls` -refinement of the  $n_k$  values. (\*) in case of `nls` -failures, the `det+nls` returns the `det` determined values

		$K =$	Decomposition method		
			<code>det</code>	<code>nls</code>	<code>det+nls</code>
<b>average computing time</b>		<b>1</b>	2.4 ms	2.9 ms	4.9 ms
		<b>2</b>	3.6 ms	3.4 ms	6.6 ms
		<b>3</b>	4.9 ms	4 ms	8.5 ms
		<b>4</b>	6.2 ms	4.8 ms	10.7 ms
<b>Failure rate</b>	without offset determination		0%	0.03%	0% (0.03%)*
	with offset determination		0%	0.65%	0% (0.7%)*

Although the `det` algorithm is not optimized and neither `det` nor `nls` are parallelized, are the necessary computing times of decomposing PMT-measured standard SAR data sets a matter of seconds. We can conclude that in case of much more data intensive measurement approaches, like spatial resolved EM-CCD measurements, computing times might be within acceptable margins.

In none of the 5.2 million `det`-simulations, did the function `decompose_OSLcurve()` throw an exception returned none-finite values. For the 2.6 million `nls`-simulations without offset determination, 773 exceptions were counted. The `nls` -algorithm produced also 755 exceptions when performing `det+nls` decomposition without offset determination. But here the `det` -results could still be given back. Adding an offset variable (see chapter 5.3) to the `nls` input model increased the number of failed fittings to about 16800 respectively 18100 (`det+nls`).

For now, we exclude all data set entries with a simulated background signal and/or activated offset determination. We will investigate these background-related issues separately in chapter 4.3. Thus, the following conclusions are just valid for measurements with no or accurately corrected signal background.

## Accuracy

To investigate the accuracy of calculating the component intensity  $n_k$ , we define a measure of accuracy  $R_n$ . Unlike the accuracy measure  $R_\lambda$  used for Step 1,  $R_n$  is calculated from all 1000 simulation runs performed for one set of parameters. This way, we can remove almost entirely the statistical influence of the simulated signal noise onto  $R_n$ . The accuracy  $R_n$  is defined by the ratio of the mean component intensity outcome of  $n_{\text{out}}$  to the simulation input component intensity  $n_{\text{in}}$ .

$$R_n = \frac{\bar{n}_{\text{out}}}{n_{\text{in}}} \quad \bar{n}_{\text{out}} = \sum_{i=1}^{1000} \frac{n_{i,\text{out}}}{1000} \quad (4.3)$$

Looking at the distribution of  $R_n$  values from all 2592 parameter settings which don't include the simulation or estimation of a signal background, we see none or only small deviations from the 'perfect-accuracy' value  $R_n = 1$ :

**Table 4.10:** Accuracy in the decomposition of simulated OSL curves without background signals.

**Blue cells:** Signal component amplitude  $n_k$  underestimation; **Red cells:**  $n_k$  overestimation

Ratio $R_n$ between real and decomposed signal amplitude $n$												
	Fast			Medium			Slow1			Slow2		
Method	det	nls	det+nls	det	nls	det+nls	det	nls	det+nls	det	nls	det+nls
Minimum	0.942	0.991	0.986	0.949	0.971	0.962	0.902	0.908	0.924	0.967	0.959	0.965
Q <sub>0.05</sub>	0.996	0.997	0.997	0.991	0.992	0.993	0.988	0.990	0.991	0.998	0.998	0.997
Q <sub>0.25</sub>	0.999	0.999	0.999	0.999	0.998	0.998	0.998	0.998	0.998	1.000	1.000	1.000
<b>Median</b>	<b>1.000</b>	<b>1.000</b>	<b>1.000</b>	<b>1.000</b>	<b>1.000</b>	<b>1.000</b>	<b>1.000</b>	<b>1.000</b>	<b>1.000</b>	<b>1.000</b>	<b>1.000</b>	<b>1.000</b>
Q <sub>0.75</sub>	1.001	1.001	1.001	1.002	1.001	1.001	1.002	1.002	1.002	1.000	1.000	1.000
Q <sub>0.95</sub>	1.004	1.004	1.003	1.011	1.008	1.008	1.009	1.011	1.011	1.003	1.003	1.002
Maximum	1.121	1.009	1.012	1.166	1.050	1.029	1.059	1.061	1.105	1.038	1.060	1.047

Significant inaccuracies can be observed just in a few extreme cases. For the nls and the det+nls algorithms show these extreme cases less deviation as for the det algorithm.

## Precision

Repeated simulation runs for every set of parameters allows us to measure the decomposition precision. As measure of precision, we define  $\sigma_{\text{dec}}$ :

$$\sigma_{\text{dec}} = \frac{\sqrt{\sum_{i=1}^{1000} (\bar{n}_{\text{out}} - n_{i,\text{out}})^2}}{n_{\text{in}}} - \frac{\sqrt{n_{\text{in}}}}{n_{\text{in}}} \quad (4.4)$$

The first term is the relative standard deviation of the signal component intensity outcome. The second term accounts for the signal value scattering arising from Poisson-distributed noise simulation. Thus,  $\sigma_{\text{dec}}$  measures the relative uncertainty, corrected for the fundamental uncertainty. Note, the inverse of  $\sigma_{\text{dec}}$  would be the shot noise corrected signal-noise-ratio.

**Table 4.11:** Distribution of the decomposition-caused uncertainty  $\sigma_{\text{dec}}$  for simulated CW-OSL curves without background signals and background estimation.

Method	Algorithm-induced relative uncertainty $\sigma_{\text{dec}}$											
	Fast			Medium			Slow1			Slow2		
	det	nls	det+nls	det	nls	det+nls	det	nls	det+nls	det	nls	det+nls
Minimum	0.00	0.00	0.00	0.00	0.00	0.00	0.00	0.01	0.01	0.00	0.00	0.00
Q <sub>0.05</sub>	0.00	0.00	0.00	0.01	0.01	0.01	0.01	0.02	0.02	0.00	0.00	0.00
Q <sub>0.25</sub>	0.01	0.01	0.01	0.02	0.02	0.02	0.03	0.03	0.03	0.00	0.00	0.00
<b>Median</b>	<b>0.02</b>	<b>0.02</b>	<b>0.02</b>	<b>0.06</b>	<b>0.06</b>	<b>0.06</b>	<b>0.07</b>	<b>0.08</b>	<b>0.08</b>	<b>0.01</b>	<b>0.01</b>	<b>0.01</b>
Q <sub>0.75</sub>	0.05	0.04	0.04	0.15	0.14	0.14	0.17	0.16	0.15	0.02	0.02	0.02
Q <sub>0.95</sub>	0.14	0.11	0.11	0.36	0.33	0.33	0.67	0.64	0.67	0.23	0.23	0.22
Maximum	0.54	0.17	0.16	0.99	0.86	0.88	1.56	1.52	1.51	0.85	1.00	0.99

For a large part of OSL curve scenarios, the decomposition precision is equal or close to the theoretical maximum, allowed by the noise-based signal scattering. For a fraction of OSL curves, however, an additional uncertainty caused by the decomposition method is added. This is especially the case for some of the medium and slow1 components. But there is no significant difference in precision between the methods.

## Error estimation accuracy

When reviewing the step 3 approach in chapter 3.3, the age calculation with the CAM and the MAM algorithm use the error values of the equivalent doses  $D_e$  to weight the  $D_e$ -distribution. The  $D_e$ -determination algorithm itself, uses a Monte Carlo approach to estimate these errors [96]. This Monte Carlo approach relies on the reliability of the component errors  $\sigma_k$ , because these are used to randomize the  $L_x/T_x$  points. In conclusion, a high accuracy in estimating the component errors is an important quality criterion for a decomposition algorithm.

We test this criterion by counting all cases, when the input value of the component intensity  $n_{in}$  is located inside the  $1-\sigma$ -error bar of the outcome value  $n_{out} \pm \sigma_{out}$ . Because the simulated uncertainty is based on the Poisson-distribution, it is reasonable to assume also a Poisson-distributed signal error  $\sigma_{in}$ . The Poisson-distribution converges with the normal distribution with increasing statistical sample size. Therefore, we can conclude that according to the normal distribution, in around 68% of the cases  $n_{in}$  lies within the decomposition results error ranges.

**Table 4.9:** Distribution of the error estimation accuracy depending of on the component and the decomposition method. Perfect accuracy is given at values around 68%. Higher values indicate error overestimation. Lower values indicate error underestimation.

		How often is the real value inside the 1- $\sigma$ error bar?											
		Fast			Medium			Slow1			Slow2		
Method		det	nls	det+nls	det	nls	det+nls	det	nls	det+nls	det	nls	det+nls
Minimum		51%	6%	39%	62%	12%	43%	64%	23%	43%	62%	41%	41%
	Q <sub>0.05</sub>	60%	12%	51%	65%	19%	53%	66%	32%	53%	66%	48%	52%
	Q <sub>0.25</sub>	65%	19%	59%	67%	30%	63%	67%	47%	63%	67%	65%	62%
	<b>Median</b>	<b>67%</b>	<b>27%</b>	<b>65%</b>	<b>68%</b>	<b>40%</b>	<b>69%</b>	<b>68%</b>	<b>57%</b>	<b>70%</b>	<b>68%</b>	<b>69%</b>	<b>66%</b>
	Q <sub>0.75</sub>	68%	36%	71%	69%	49%	75%	69%	63%	74%	69%	72%	70%
	Q <sub>0.95</sub>	73%	48%	98%	71%	59%	99%	71%	67%	90%	71%	76%	75%
Maximum		77%	59%	100%	73%	68%	100%	73%	71%	100%	73%	81%	81%

The results in table 4.9 show nearly perfect error estimation accuracies for the `det` algorithm. The statistical scattering in the results should be  $68.3\% \pm 2.6\%$  ( $1-\sigma$ ) which is matched by the medium, slow1 and slow2 component error estimation accuracies distribution quite well. Only for the fast component, small case-dependent inaccuracies can be observed. The `nls` method on the other hand, does systematically underestimated component intensity errors. Only for the slow2 component does `nls` work acceptably. The results of the `det+nls` method are centred at the correct error estimation values but show a significant case-dependency, which leads to sometimes over- and sometimes under-estimated errors. It is apparent that the `nls`-refining weakens the reliability of the `det`-error estimation algorithm.

## Correlation matrix

Again, we use a correlation tables to detect further dependencies. We omit all background-related parameters and to avoid background-dominated correlations restrain the correlation table to det-decomposition method. In appendix B.2 can be found the resulting input-output and output-cross-correlation. Table 4.10 displays a reduced variant of the input-output correlation table.

**Table 4.10:** Step 2 correlation table displaying Kendall's  $\tau$  between input values and selected output values. Values  $< 0.1$  are considered as not significantly correlated and were deleted to improve clarity. Notation equals table 4.5; measurement length  $L = \Delta t * N$

**Blue cells:** positive correlation: increased input values lead to increased output values

**Red cells:** anti-correlation: increased input values lead to decreased output values

		$K_{in}$	Component intensity $n_{in}$				Detection settings		
			Fast	Medium	Slow1	Slow2	$N$	$\Delta t$	$L$
<b>Decomposition uncertainty</b> $\sigma_d$	Fast	0.30	-0.68	0.32	0.12	0.18			
	Medium	0.35	0.20	-0.65	0.24	0.21			
	Slow1	0.18		0.16	-0.43	0.29	-0.37	-0.31	-0.47
	Slow2	0.28			0.34	-0.28	-0.46	-0.39	-0.60
<b>Error over-/under-estimation</b>	Fast	0.18	-0.33	0.16		0.26	0.13	-0.23	
	Medium			-0.12		0.16		-0.13	
	Slow1								
	Slow2								

Table 4.10 and the tables in appendix B.2 allow the following statements about parameter dependencies:

- There is no significant inaccuracy caused by any input parameter
- The decomposition-caused error  $\sigma_{dec}$  increases with the number components  $K_{in}$ . Therefore, the precision decreases with increasing  $K_{in}$ .
- The decomposition-caused error  $\sigma_{dec}$  decreases with the component intensity but the relative error of other components increases
- The overestimation of one component intensity  $n_k$  due statistical uncertainty, leads likely to an underestimation of the intensity values of the neighbouring components, and vice versa. (see correlation between  $\sigma_{dec}$  in appendix B.2)
- Increasing measurement lengths decreases the method-caused relative error for the slow1 and slow2 component. Their precision is increased.
- The error estimation accuracy of the fast component shows some dependencies to the component intensities and the detection settings. The cause is not clear.

### 4.3 Signal background dependence

The results in chapter 4.2 showed sufficient accuracy, precision and robustness of all tested decomposition methods. Especially the determinant-based method introduced in chapter 3.2 revealed no significant problems. But how are the results affected if the OSL measurements contain an offset in their values due an uncorrected signal background?

Background signals can be induced for example by the dark current of the detector, stimulation light leakages or steady photoluminescence emissions of the sample. To test the influence on the component intensity results, we add Poisson-distributed background signals to the CW-OSL simulations discussed in the previous chapter.

**Table 4.11:** Background-dependent accuracy in the decomposition of simulated OSL curves in dependence of offset level and the decomposition method. **Blue cells:** Signal component intensity  $n_k$  underestimation; **Red cells:**  $n_k$  overestimation

		Ratio $R_n$ between real and decomposed signal amplitude $n$											
		Fast			Medium			Slow1			Slow2		
Method		det	nls	det+nls	det	nls	det+nls	det	nls	det+nls	det	nls	det+nls
		<b>Background = 0 cts / s</b>											
Q <sub>0.05</sub>		1.00	1.00	1.00	0.99	0.99	0.99	0.99	0.99	0.99	1.00	1.00	1.00
Median		1.00	1.00	1.00	1.00	1.00	1.00	1.00	1.00	1.00	1.00	1.00	1.00
Q <sub>0.95</sub>		1.00	1.00	1.00	1.01	1.01	1.01	1.01	1.01	1.01	1.00	1.00	1.00
		<b>Background = 20 cts / s</b>											
Q <sub>0.05</sub>		0.54	0.98	0.98	0.65	0.94	0.94	-0.32	0.71	0.71	1.01	1.01	1.01
Median		1.00	1.00	1.00	1.01	1.00	1.00	0.93	0.94	0.94	1.07	1.06	1.06
Q <sub>0.95</sub>		1.21	1.01	1.01	2.81	1.11	1.11	0.99	0.99	0.99	1.49	1.25	1.25
		<b>Background = 40 cts / s</b>											
Q <sub>0.05</sub>		-0.25	0.96	0.96	0.26	0.89	0.89	-1.93	0.43	0.43	1.03	1.03	1.03
Median		1.00	1.00	1.00	1.01	1.01	1.01	0.88	0.89	0.89	1.14	1.12	1.12
Q <sub>0.95</sub>		1.37	1.03	1.03	4.21	1.23	1.23	0.98	0.98	0.98	1.91	1.50	1.50

As table 4.11 demonstrates, is the influence of a signal background on the fast component signal value insignificant, especially if the nls or det+nls are used as decomposition methods. The slow1 and slow2 component intensities, on the other hand, are shifted towards smaller (Slow1) or higher (Slow2) values.

This background dependency of the slow decaying components underlines the importance of a sufficient background correction prior the data analysis. But the needed background measurements or instrumental properties may not be available for a given data set. Then the offset value has to be determined as part of the signal processing in step 1 or step 2.

The straight-forward approach is to include the offset as fitting parameter in step 1. This approach was tested for the data sets used in chapter 5.2 but resulted in some cases in offset values which were larger than expected from the deployed PMT detectors. Subtracting these too-large offsets from the single OSL curves resulted in some weak-signal cases in curves which progress into negative values. Accordingly, this approach was rejected. The alternative approach is to determine the offset value as part of the step 2 single CW-OSL curve decomposition. In case of the `nls` algorithm, we have just to add an additional fitting parameter 'offset' to the regression model. In case of the `det` and the `det+nls` algorithm, we have to extend the decomposition approach for another component 'offset'. This additional component with an intensity  $n_{\text{offset}}$  is incorporated the same way as the decaying components are. We define one additional signal bin  $b_{K+1} = b_{\text{offset}}$ , build one additional linear equation, build also one additional matrix  $A_{K+1} = A_{\text{offset}}$  and extend the matrices for solving the equation system by one dimension. Only the definition of the probabilities  $P_{j,\text{offset}}$  differs:

$$P_{j,\text{offset}} = t_j - t_{j-1} \quad j = 1, \dots, K + 1 \quad (4.5)$$

Here,  $t_j$  is the upper boundary of the signal bin interval with the index  $j$  and  $t_{j-1}$  is its lower boundary. We expect a lower precision when applying the additional offset component because as the correlation table in chapter 4.2 revealed, increases the method-caused error with an increase in the number of components.

For comparison, table 4.12 summarizes the reliability of the `det+nls` method with and without a background signal:

**Table 4.12:** Background-dependent reliability in the decomposition of simulated CW-OSL curves. Chosen algorithm: `det+nls` without offset determination. For the encodings, see the table descriptions in chapter 4.2.

Find offset? <b>FALSE</b>	Accuracy $R_n$				Method error $\sigma_{\text{dec}}$				$n_{\text{in}}$ inside $n_{\text{out}} \pm \sigma_{\text{out}}$ ?			
	Fast	Medium	Slow1	Slow2	Fast	Medium	Slow1	Slow2	Fast	Medium	Slow1	Slow2
<b>Background = 0 cts / s</b>												
$Q_{0.05}$	1.00	0.99	0.99	1.00	0.00	0.01	0.02	0.00	51%	53%	53%	52%
Median	1.00	1.00	1.00	1.00	0.02	0.06	0.08	0.01	65%	69%	70%	66%
$Q_{0.95}$	1.00	1.01	1.01	1.00	0.11	0.33	0.67	0.22	98%	99%	90%	75%
<b>Background = 40 cts / s</b>												
$Q_{0.05}$	0.96	0.89	0.43	1.03	0.00	0.01	0.02	0.00	51%	39%	0%	0%
Median	1.00	1.01	0.89	1.12	0.02	0.06	0.08	0.01	65%	64%	31%	0%
$Q_{0.95}$	1.03	1.23	0.98	1.50	0.18	0.89	1.49	0.97	99%	99%	75%	66%



We reconstruct the same table from the same subsets of OSL curves. But this time, we incorporate the additional offset-component in the decomposition process:

**Table 4.13:** Background-dependent reliability in the decomposition of simulated CW-OSL curves. Chosen algorithm: `det+nls` with offset determination. For the encodings, see the table descriptions in chapter 4.2.

Find offset? <b>TRUE</b>	Accuracy $R_n$				Method error $\sigma_{dec}$				$n_{in}$ inside $n_{out} \pm \sigma_{out}$ ?			
	Fast	Medium	Slow1	Slow2	Fast	Medium	Slow1	Slow2	Fast	Medium	Slow1	Slow2
	<b>Background = 0 cts / s</b>											
$Q_{0.05}$	1.00	0.99	0.92	0.90	0.00	0.01	0.03	0.00	48%	52%	53%	53%
Median	1.00	1.00	1.00	1.00	0.02	0.08	0.16	0.08	63%	68%	71%	70%
$Q_{0.95}$	1.00	1.01	1.07	1.08	0.12	0.67	<b>8.5</b>	<b>13.5</b>	75%	78%	78%	78%
	<b>Background = 40 cts / s</b>											
$Q_{0.05}$	1.00	0.99	0.91	0.95	0.00	0.01	0.03	0.00	49%	53%	55%	57%
Median	1.00	1.00	1.00	1.00	0.02	0.08	0.16	0.09	63%	69%	71%	71%
$Q_{0.95}$	1.00	1.01	1.05	1.09	0.12	0.67	<b>8.5</b>	<b>13.2</b>	75%	78%	79%	78%

The accuracy in determining the component intensity and its uncertainty is improved significantly for all OSL curves which contain background signals. The decomposition accuracy for the slow1 and slow2 component in none-background OSL curves is slightly decreased however. At the same time is the error estimation accuracy improved, which indicates smaller value shifting in the `nls`-refining process.

But the apparent problem is the massive decreased precision for the slow1 and slow2 component intensities for significant subset of OSL curves whether they include a signal background or not. In at least 5% of the simulated OSL curve scenarios, the scattering of the slow1 and slow2 component intensity values is at least one order of magnitude larger than the true component intensity values itself. This means, the slow1 and slow2 component outcomes for such scenarios are not usable at all. A closer examination of the affected OSL scenarios implies that this issue occurs when the measurement length is short and the slow2 component is bright. In that case the decomposition algorithms (`det` and `nls` are affected about equally) are not able to resolve between a large offset value and a large Slow2 intensity. For example, the algorithm might overestimate the offset and underestimate the Slow2 intensity. The underestimated Slow2 intensity leads to a negative residual in the earlier parts of the OSL curve, which then is compensated by an overestimated Slow1 intensity. Although the result might be far off the true values, the algorithms might nonetheless hit a local or even global minimum of the residual square sum.

We can conclude that the offset-including-decomposition is not suited for all kinds of OSL decay curve shapes and that we have to check the compatibility prior the decomposition. This counteracts our easy-to-use requirement on the method unless we find an improved algorithm to determine the offset.

## 5 Application: Automated sample analysis

One goal of this thesis is to provide an automated analysis of OSL dating data sets. To fulfil this goal, the Rmarkdown script `EvaluateDataSet.Rmd` was programmed. The script processes BIN files measured with either Risø OSL/TL readers [100] or Freiberg Instruments lexsyg systems [82], [101]. The measurement sequences in each data set entry (one entry = one aliquot) has to be structured according to the SAR protocol (see table 3.1 in chapter 3.3). The user can define laboratory and environmental dose rates to get back paleodose and age results, otherwise the results are returned in time units of artificial irradiation. The user can also select data set entries as background measurements. Then the average OSL curve of these measurements will be subtracted from all other OSL curves. The user can also change the method parameters, like the  $F$ -threshold value or the selected decomposition algorithm. But all these settings are optional; the script will run successfully by using the default settings and just selecting a BIN file for analysis. Depending on the data set and the used PC, the computation will need a few minutes and return the data analysis report as Microsoft Word document. The document is about 20 pages long, an example can be found in the appendix C. Currently, an **R** environment is needed to execute the script. For the future, an interactive online version of the analysis, including a PDF export function, is planned. Some preliminary tests to do so were performed and showed the feasibility of this idea.

To test the script and also to test the reliability of the Step 1, Step 2 and Step 3 algorithms on actual data sets, several dating-relevant data sets were re-evaluated:

- Six standard SAR data sets from six samples of different origin were analysed: Batagai, BK8, BT594, BT1214, BT1240 and Oy7. BT1240 was discarded afterwards because Step 3 of the analysis failed due a SAR-incompatible measurement sequence. The analysis results of the other five are summarized and discussed in the following.
- Two single-grain laser-stimulated OSL [102] data sets were analysed: C-SAL1 and SUV3. In both cases Step 1 found three components. Step 2 decomposed successfully all OSL records although the OSL curves in SUV3 have very low SNR values and the SUV3 as well as C-SAL1 contain many data set entries without OSL signals and just noise. Yet, no paleodoses could be calculated. `Luminescence::plot_GrowthCurve()` produced diverging  $D_e$  values and  $D_e$  error values for some data set entries. The rejection criteria did not reject all of these erroneous dose values. Instead they caused diverging CAM and MAM results. We can conclude: The Step 3 approach has to be adapted for this kind of data set, which will not be part of this thesis.

- To test a new SAR-like protocol, four experimental data sets of two samples were analysed: FB and BT1713. Two data sets were measured under not-SAR-conditions. All computing were successful and produced reasonable outcomes. The experimental protocol itself, worked for sample FB but not for sample BT1713. The protocol and the experimental results are discussed in chapter 5.3.

All data sets, their automatically created reports and the corresponding Rmarkdown files can be found on the CD provided with this thesis.

## 5.1 Example analysis

We chose sample BT594 as example to have a closer look at the workflow and the analysis results of the Rmarkdown script. We chose BT594 for the following reasons:

- The same sample was used as example in my bachelor thesis [36]. This thesis already proposed to use an equation system and Cramer's rule to decompose OSL measurements. Although the bachelor thesis evaluated just on aliquot (the first one) of the data set, the findings there can be compared with the findings here
- The OSL signals of the sample are rather dim compared to other published OSL measurements. The OSL records show also significant Medium component intensities. The sample had been successfully dated before but the age results are suspected to be underestimated. We conclude that the sample is well suited to test the precision and reliability of the method.

### Sample origin

Sample BT594 is a coarse grain quartz from Seilitz near Meißen in Saxony. It is part of a larger stratigraphic sequence, evaluating the accumulation of loess soils during the last glacial era. Meszner *et al.* [103] dated this sample to an age of  $22.2 \pm 3.5$  ka. Sediment layers above the sample layer were dated to about 25 - 27 ka. The sediment layer below BT594 was dated to about 31 ka. Corresponding samples from another sample site were also dated to about  $\sim 26$  ka. Although the published age of BT594 as well as the ages of related samples is given with significant error bars, one can argue that the estimated age of BT594 should also be between 25 and 30 ka. It might be that the layers above BT594 were not fully bleached or contaminated with unbleached sediments at the burial event [103]. Or the effect described in Li and Li [50] and Steffen *et al.* [51] took place: A thermally unstable and/or recuperating Medium component caused age underestimation.

## Step 1 results

First, we calculate the global average OSL curve from all 24 aliquots. For each aliquot 14 OSL curves were measured, leading to 336 OSL curves overall.

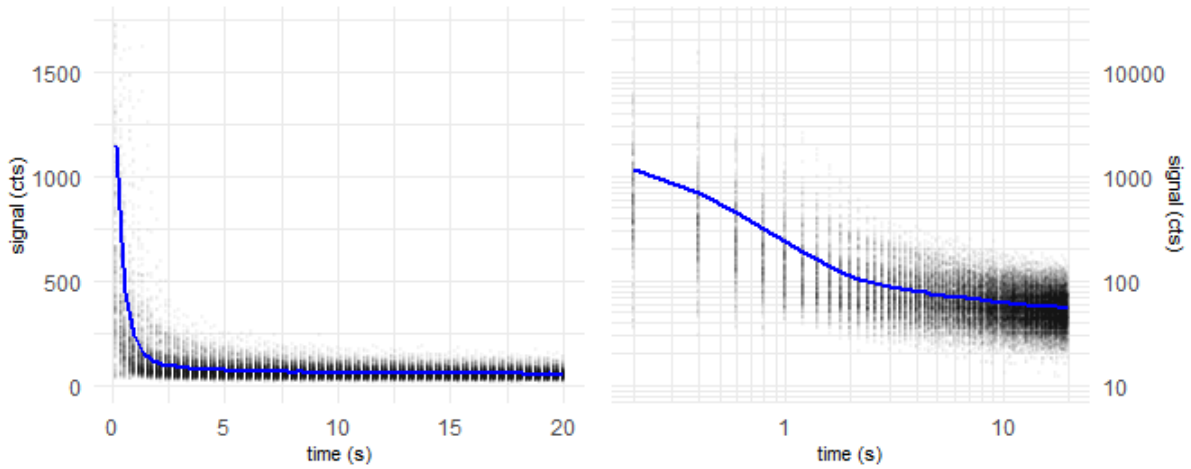


**Figure 5.1:** Average OSL curve of BT594; **Blue:** Average OSL curve. **Grey:** Data points of all 336 OSL records of sample BT594. Left: linear axes; Right: double-logarithmic axes.

In Step 1, the average OSL curve is fitted with an increasing number of components  $K$ . The algorithm generates the following  $F$ -test table:

**Table 5.1:**  $F$ -table: Decay constants  $\lambda$  and fit quality parameters as a function of number components  $K$ . **Red square:** Fitting selected as true because  $F < 50$

$K$	$\lambda_1$ (s <sup>-1</sup> )	$\lambda_2$ (s <sup>-1</sup> )	$\lambda_3$ (s <sup>-1</sup> )	$\lambda_4$ (s <sup>-1</sup> )	$\lambda_5$ (s <sup>-1</sup> )	$\chi^2$ (RSS)	$F_K$
1	1.76					3.99e+05	
2	2.54	0.0333				4.84e+03	3.91e+03
3	3.17	0.796	0.0164			216	1.01e+03
4	4.34	2.03	0.353	0.00885		27.1	320
5	5.66	2.65	1.08	0.249	0.00576	24	5.79

Comparing the 5-component fit with the 4-component fit gives us an  $F$ -value of 5.79 which is below our pre-set threshold value of  $F_{\text{thr}} = 50$ . This implies that the  $K = 5$  fitting does not significantly improve the fit quality.

We assume a stimulation wavelength of 470 nm with an intensity of 50 mW cm<sup>-2</sup> and calculate expected decay constants from literature photo-ionisation cross-sections [30], [47], [48]. This is done by `plot_PhotoCrosssections()`, which returns figure 5.2. The function renames the components to the common quartz OSL component names, if their decay constant lies within the averaged 2- $\sigma$ -interval of the literature values.

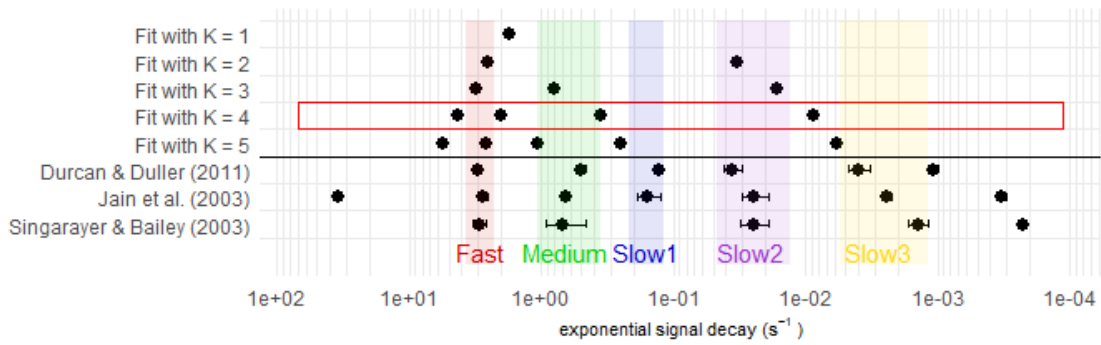


**Figure 5.2:** BT594: Comparison of obtained decay constants with literature values, see [30], [47], [48]. **Red square:** Fitting model selected by  $F$ -test.

The  $F$ -test declares four components as correct number of components but looking at the fitting diagrams and the decay constant comparison shows that the 3-component fit is already adequate ( $< 3\%$  deviation at any point) and matches the literature values better. Because of this discrepancy, we will not only evaluate the  $K = 4$  case but also all  $K < 4$  cases.

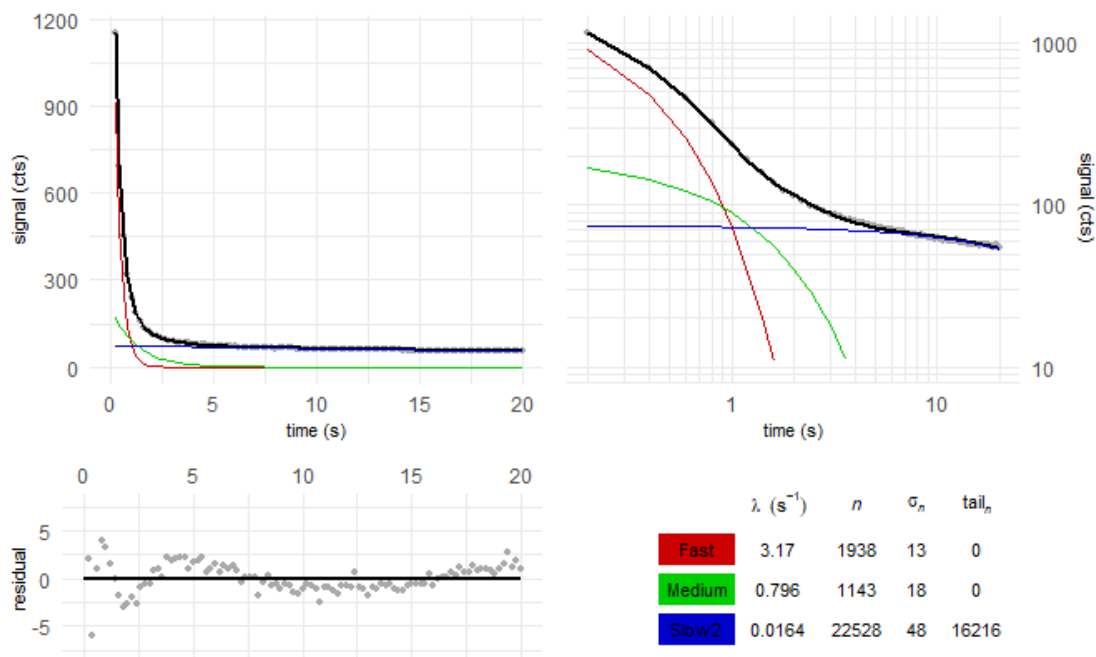


**Figure 5.3:** Average OSL curve of BT594 fitted with  $K = 3$  components

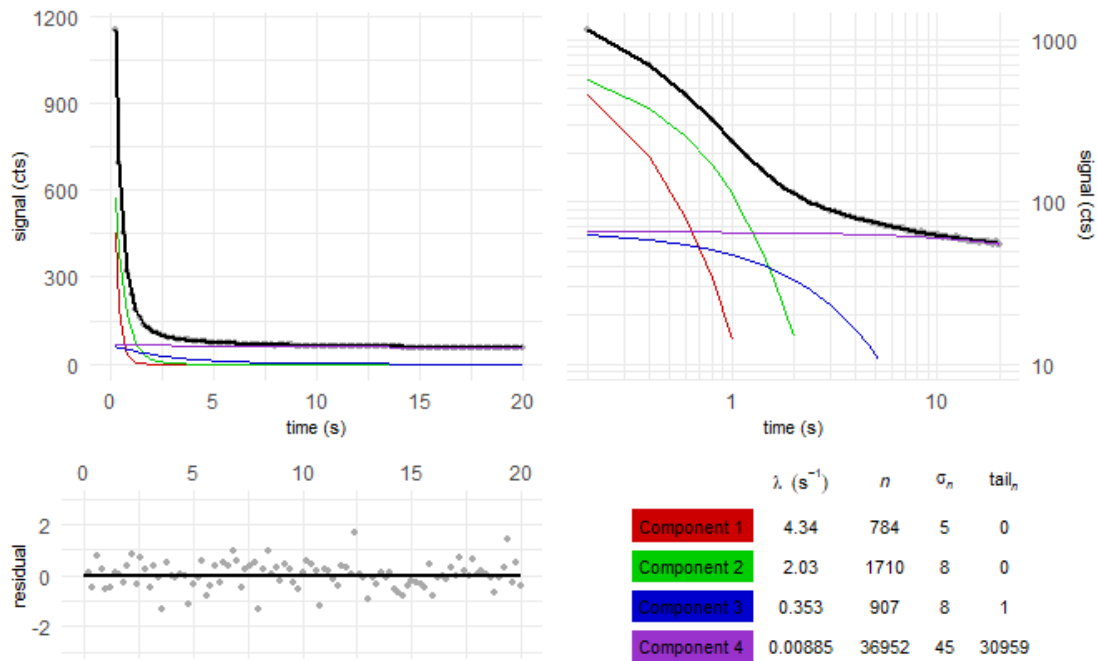


**Figure 5.4:** Average OSL curve of BT594 fitted with  $K = 4$  components

### Step 3 results

The function `decompose_SARdata()` builds L/T tables for all components in all  $K = 1, \dots, 4$  cases. It also creates L/T tables for late light background subtracted (=late b.) luminescence values, which are the default SAR approach. In addition, L/T tables for early light background subtracted (=early b.) luminescence values are generated for comparison (see chapter 2.3). For the component-separated L/T tables, a few fittings failed because of an incoherent growth of L/T values with increasing dose.

The equivalent doses  $D_e$  calculated from the growth curves have similarly distributed values for both background subtraction cases as well as for the fast components in all separation cases. The Medium components in the  $K = 3$  and the  $K = 4$  case show lower  $D_e$  values than the expected natural dose. Figure 5.5 displays this separation of  $D_e$  values with increasing number of components  $K$ .

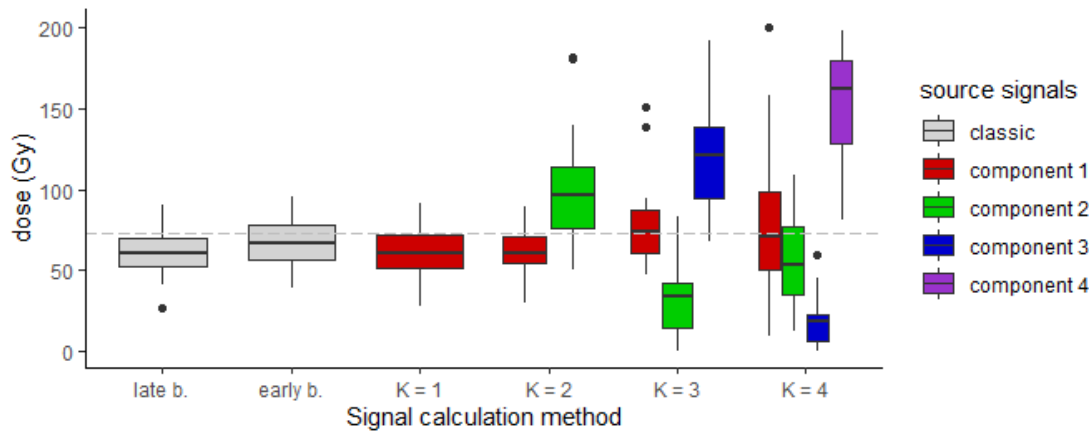


**Figure 5.5:** BT594: Box plots of the  $D_e$ -distributions from 24 aliquots from different signal calculation approaches. The dashed line shows the expected dose

**Box plot rules:** The whiskers enclose all four quartiles besides outlier. The rectangles enclose the second and third quartile. The middle line shows the median.

As next step, the rejection criteria are applied to all  $D_e$  subsets. This way, we sort out dose values with uncertain physical plausibility.

**Table 5.2:** BT594: Number of  $D_e$  values which passed rejection criteria successfully for various signal calculation approaches

component	late b.	early b.	$K = 1$	$K = 2$	$K = 3$	$K = 4$
1	13 of 24	14 of 24	2 of 24	11 of 24	9 of 22	1 of 20
2				1 of 24	3 of 23	4 of 20
3					1 of 22	1 of 23
4						9 of 20

Of the successfully calculated  $D_e$  values, about half passed the rejection criteria in both background subtraction cases as well as component 1 in the  $K = 2$  and the  $K = 3$  case. All other components did not pass the rejection criteria for most of their  $D_e$  values. The only exception is the background-dominated component 4 of the  $K = 4$  case. A closer look to the result data reveals that the majority of all rejections are caused by insufficient recycling ratios. In contrast, the recuperation for most of the  $D_e$  values remained low. Only component 2 in the  $K = 2$  case and component 4 in the  $K = 4$  case show increased average recuperation values (see table 6 in appendix C).

Applying the test criteria should reject the majority of inaccurate  $D_e$  measurements. Figure 5.6 shows the distribution of the remaining  $D_e$  values.

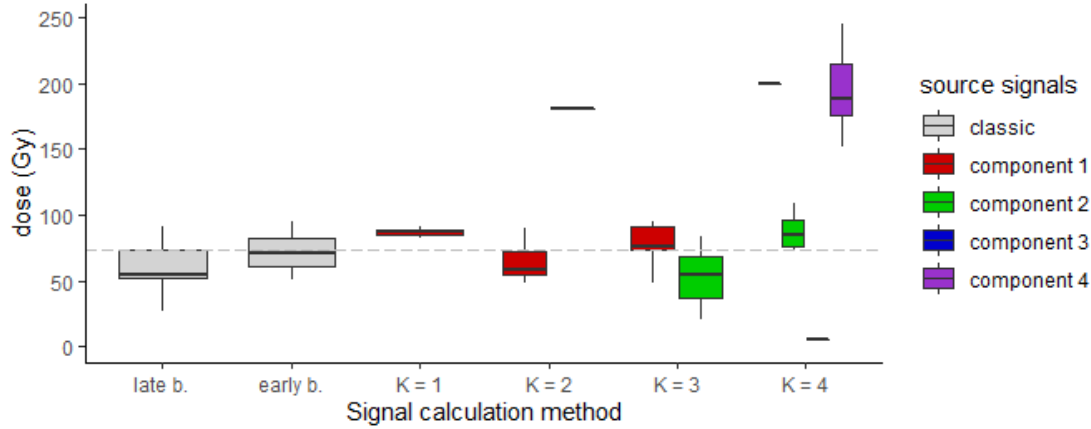


**Figure 5.6:** Box plots of the  $D_e$ -distributions from those aliquots which passed the rejection criteria

We apply the central age model and the minimum age model to all remaining equivalent doses. Then we convert the returned paleodoses into age value by applying the environmental dose rate of  $2.92 \text{ Gy ka}^{-1}$  given by Meszner *et al.* [103].

**Table 5.3:** BT594 analysis results, automatically calculated by `EvaluateDataSet.Rmd`. Components are named after literature values if their decay constant lies within  $2\text{-}\sigma$ -range of the average literature value. For the minimum age model, the overdispersion argument was set to  $\sigma_b = 0.2$ .

Method	Component name	Decay constant [ $\text{s}^{-1}$ ]	Mean intensity	Passed aliquots	Central age model [ka]	Over-dispersion	Minimum age model [ka]
late b.				13 of 24	$20 \pm 1.7$	30%	$15.7 \pm 2.7$
early b.				14 of 24	$24.1 \pm 1.5$	17%	$24 \pm 2.6$
<b>K = 1</b>	Component 1	1.76	$3.6\text{e}+03$	2 of 24	$30.6 \pm 6.6$	0%	$30.5 \pm 11.2$
<b>K = 2</b>	Fast	2.54	$2.6\text{e}+03$	11 of 24	$22.2 \pm 1.4$	17%	$22.1 \pm 2.5$
	Slow2	0.033	$1.4\text{e}+04$	1 of 24			$62 \pm 21.3$
<b>K = 3</b>	Fast	3.2	$1.9\text{e}+03$	9 of 22	$28.9 \pm 1.3$	4%	$26.8 \pm 3.5$
	Medium	0.8	$1.1\text{e}+03$	3 of 23	$19.6 \pm 3.3$	0%	$19.6 \pm 6.5$
<b>K = 4</b>	Slow2	0.016	$2.3\text{e}+04$	1 of 22			$312.6 \pm 138$
	Component 1	4.3	$7.8\text{e}+02$	1 of 20			
	Component 2	2	$1.7\text{e}+03$	4 of 20	$32.1 \pm 5.4$	0%	$31.3 \pm 8.5$
	Component 3	0.35	$9.1\text{e}+02$	1 of 23			
	Component 4	0.0088	$3.7\text{e}+04$	9 of 20	$72.7 \pm 5.4$	15%	$73.2 \pm 10.4$

The results in table 5.3 show significant differences between the signal calculation approaches. The sample age calculated by the late light background subtraction method is  $20 \pm 1.7 \text{ ka}$  for the CAM model and clearly underestimates the true sample age of between 25 and 30 ka. The



difference to the age value of  $22.2 \pm 3.5$  ka given in literature arises probably from differences in the signal integration intervals and/or rejection thresholds which are not given provided by Meszner *et al.* [103]. The overdispersion of the CAM age indicates that the distribution of  $D_e$  values is larger than expected from statistical errors. An unstable medium component with low natural dose might be the reason for age underestimation and overdispersion. This theory is underpinned by the older age and lower overdispersion returned by the early light background method. Of the decomposition analyses, the  $K = 3$  case returned the most reasonable results in terms of expected decay constants, rejection test values and expected sample age. This indicates that Step 1 of our method overestimates the actual OSL component number, at least with the chosen threshold value of  $F$ . The age results as well as the raw  $D_e$  results (see figure 5.5) of the  $K = 3$  case validate the theory of low natural dose values of the medium component. The CAM age as well as the MAM age determined from the fast component of the  $K = 3$  case lies within the expected age range and shows just small overdispersion. Thus we can conclude that these age values are more accurate than the default-SAR determined age values. Whether the MAM age or the CAM age is more accurate does not arise from the decomposition results but is also not in the scope of this thesis.

## 5.2 Re-evaluation of some standard SAR data sets

Besides BT594, four other samples measured with the standard SAR protocol were also analysed. All samples were measured with Risø TL/OSL readers [97] with 470 nm LED stimulation and an estimated stimulation intensity of about 35 mW cm<sup>-2</sup>. The data set of sample BT1214 was provided by C. Schmidt (Lehrstuhl Geomorphologie, Universität Bayreuth). The data sets of sample Oy7, Batagai and BK8 were provided by M. C. Fuchs (Helmholtz-Institut für Ressourcentechnologie, Freiberg).

**BT1214:** This sample is a fine grain (~4–11 μm) quartz originating from an archaeological site at the Toplița river in northern Romania. The sample is regarded as well suited for luminescence dating with bright average initial signals of about 10<sup>6</sup> counts s<sup>-1</sup>, dominant fast component and homogeneous luminescence properties across all aliquots due to averaging effects of in the order of 10<sup>6</sup> grains per aliquot. C. Schmidt evaluated an age of 53 ± 7 ka which is considered as reasonable [unpublished].

**BK8:** Sample BK-8\_1295-1280 is a 40–63 μm grain diameter quartz extraction from a drill-core taken at Buor-Khaya at the Siberian north coast [101]. M. C. Fuchs evaluated an age of 27 ± 3 ka which is considered as under-estimated. For the feldspar fraction, an IRSL age of about 45 ka was found. For the organic material, a radiocarbon date of about 51 ka was found [101]. The OSL measurements feature average initial signals of about 10<sup>5</sup> counts s<sup>-1</sup>, a bright medium component and inhomogeneous luminescence properties due large inter-aliquot scatter. Because the chosen test dose was small, a high uncertainty in the  $T_i$  signals is induced.

**Oy7:** Sample Oy7-01-14 is a 63–100 μm grain diameter quartz extract from an ice wedge taken at Oyagos-Yar, also at the Siberian north coast [102]. The feldspar extract was dated to about 120 ka. Dating attempts of the quartz sample were rejected so far because they were considered as under-estimated. The luminescence properties are similar to BK8 but with a less bright Medium component.

**Batagai:** Sample Batagai\_2-7\_B-2-47 is a 63–100 μm grain diameter quartz extract from a stratigraphic sequence opened by a mega-slump near the town Batagai in interior Siberia [103]. The Batagai mega-slump is an on-going more than 1.2 km wide and 150 m deep ground-collapsing event due to permafrost melting caused by deforestation and global warming. The feldspar extract was dated to about 210 ka.

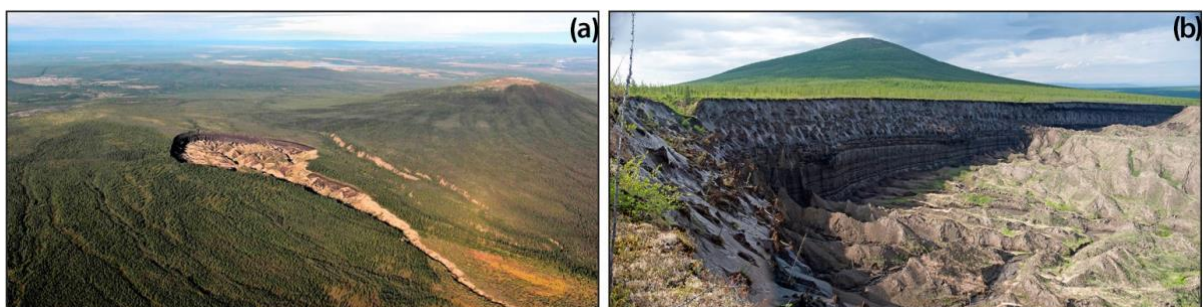


**Figure 5.7:** Batagai mega-slump: (a) view from aircraft in 2011, (b) view from southern edge in 2014. Photos taken from Ashastina *et al.* [103]

All samples were analysed with the Rmarkdown script `EvaluateDataSet.Rmd`. Report summaries can be found in appendix C. The full reports as well as the data files and the particular script files can be found on the accompanying CD.

## Results

Table 5.4 summarizes some measurement characteristics and the outcome of the  $F$ -test. The measurement duration of sample BK8, Oy7 and Batagai were reduced to 40 s to avoid over-fitting. For all samples, besides BT1214, four components were found. The large  $F$ -values in the model comparisons for BT1214 are related to the excellent SNR of this sample. A good SNR leads to a small noise-contribution to  $\chi^2$ . The fitting of even very weak signal components lead then to a significantly decreased  $\chi^2$  which results in large  $F$ -values.

**Table 5.4:** Summary of  $F$ -tests to find correct number of components  $K$  for five dating data sets.

**Red cells:** Clearly improved fit quality by the additional component.

**Green cells:** No improvement in the fit quality, thus the previous model is sufficient.

sample	aliquots	channel width (s)	meas. length (s)	$F$ value (fit improvement)				$K_{\text{selected}}$ @ $F_{\text{threshold}} = 50$
				$\rightarrow K=2$	$\rightarrow K=3$	$\rightarrow K=4$	$\rightarrow K=5$	
BT594	24	0.2	20	3910	1010	320	6	4
BT1214	30	0.1	40	2080	10400	8080	158	5
BK8	20	0.2	40*	5390	5240	502	6	4
Oy7	20	0.2	40*	46400	1110	1000	28	4
Batagai	20	0.4	40*	5020	1900	251	17	4

To account for possible over-fitting, all component number cases  $K = 1, \dots, K_{\text{select}}$  were analysed. The age determinations for the two fastest decaying components of the  $K = 3$  and  $K = 4$  case are shown in table 5.5.

**Table 5.5:** Component-resolved age determination results for 3-component and 4-component model

sample	expected age (ka)	late background		$K = 3$ decomposition				$K = 4$ decomposition			
				Fast		Medium		Component 1		Component 2	
		$N_{De}$	CAM (ka)	$N_{De}$	CAM (ka)	$N_{De}$	CAM (ka)	$N_{De}$	CAM (ka)	$N_{De}$	CAM (ka)
BT594	~ 25	13	20 ± 2	9	29 ± 1	3	20 ± 3	1	-	4	32 ± 5
BT1214	~ 50	29	51 ± 1	24	51 ± 1	26	39 ± 1	8	46 ± 3	22	49 ± 1
BK8	~ 50	16	31 ± 2	10	31 ± 2	7	26 ± 2	4	27 ± 7	8	65 ± 16
Oy7	~ 120	15	97 ± 10	8	128 ± 21	4	59 ± 20	6	99 ± 29	4	107 ± 22
Batagai	~ 200	14	155 ± 25	8	157 ± 31	6	62 ± 15	4	317 ± 96	2	57 ± 27

For all five data sets, the fast component of the  $K = 3$  case returned the most reasonable age results, while the medium component of the  $K = 3$  case underestimated the sample ages. The inconsistent age results for the  $K = 4$  case need further investigation, which shall not be

discussed here. We assume the  $K = 3$  case as physically true.

For three samples (BT594, BT1214, Oy7) the fast component returned the assumed correct age. For two samples (BT594 and Oy7) the fast component ages are of higher accuracy than the ages calculated based on the late background subtraction approach. Nevertheless, for two samples (BK8 and Batagai) OSL decomposition could not solve the problem of underestimated ages.

Sample BK8 showed evidence of high pressure events caused by several kilometre thick glaciers above the sample. Experiments showed that pressures of about 2 MPa are sufficient to fully discharge the traps accounted for the fast component [104][Fuchs, pers. comm.]. It is likely that the fast component of BK8 was partly or fully erased by this effect during the maximum of glacial impact.

The underestimated age of the sample Batagai is probably due to the maximum age limit of quartz OSL dating. For the rejected  $D_e$  values, a closer look at the data reveals saturated dose-signal curves with saturation levels below the actual natural doses. It is likely that the age underestimation arises from 'overcharged' signal-dose curves of the accepted  $D_e$  values. Overcharged means here, that the artificial high-dose signal points exceed the natural signal values related to the irradiation-charging/thermally-discharging equilibrium under environmental conditions.

But why did the algorithm of Step 1 find four respectively five components although three components are sufficient for all tested samples? The  $F$ -values in table 5.4 indicate large improvements in the fit qualities by an additional fourth component. Thus, we can consider the 4-component model as mathematically true. In contrast, the results in table 5.5 indicate that the 3-component model is physically true. Multiple hypotheses for this discrepancy are at hand:

- 1) Not all components might decay obeying first order kinetics. One or more components can be affected by retrapping or other types of charge carrier transfers. This would change the curve shape of this component, in case of retrapping towards a stretched exponential shape.
- 2) Decay constants might not be constant over the whole measurement sequence. For example, bleaching and heating can alter the transmittance of sample grains and with it the effective photon-flux at the OSL-contributing traps.
- 3) Inhomogeneities in the sample or the sample preparation between aliquots in combination with an inhomogeneous stimulation intensity can cause varying decay constants. This uncertainty in the decay constants might favour over-fitting

Further investigations are necessary to prove or dismiss these hypotheses, which shall not be part of this thesis. However, the mathematical overestimation of the number of components as well as the SNR-dependent and sometimes erratic  $F$ -values (see  $K = 1$  to  $K = 2$  in BT1214) in table 5.4 demonstrate the need for re-evaluating the statistical test to find the true number of components.

### 5.3 Omit thermal treatment in measurement protocol

In 2006, Ankerjaard *et al.* [108] and more recently Roberts *et al.* [109] proposed quartz OSL dating without thermal treatment during the measurement sequence. This would simplify instrumental demands and could enable accurate in-field dating. It could also prevent effects arising from thermally transferred charge carriers. At room temperature, however, contributes a thermally unstable shallow trap to the CW-OSL signal. This additional OSL component has a high intensity and is related to the 110°C thermoluminescence peak. Ankerjaard *et al.* [108] concluded that OSL signal decomposition is necessary to calculate reasonable doses. In addition, Roberts *et al.* [109] point out that these shallow traps compete with luminescing recombination centres about the charge carriers deployed from the thermally stable traps. Thus, they propose to apply a pre-dose of 10 Gy before the natural OSL signal is measured to fill the shallow traps. The results for the few aliquots they tested were promising. But they described their CW-OSL curve fitting procedure as ‘cumbersome’ and not practical. They also pointed out the uncertain correlation between room temperature signal components and 125°C OSL signal components.

The method presented in this thesis might provide the fast and reliable data analysis method needed to further investigate and develop the approach of Roberts *et al.* [109]. To test that, a series of measurements were performed at a Freiberg Instruments lexsyg research system [101] in the luminescence lab of the institute of geography at the university Bayreuth. The samples were prepared and the measurements supervised by C. Schmidt.

#### Experimental details

Two samples were selected: The coarse grain quartz ‘Les sables de Fontainebleau’, or short ‘FB’, is a well characterized reference quartz with high purity and very bright OSL signals [110]. The fine grain sample BT1713 has rather dim OSL signals and was chosen to test a more ordinary sample. 20 aliquots for each sample were prepared. Also one empty aliquot was prepared to perform background measurements. All 41 aliquots were first bleached for 30 min with the Freiberg Instruments solar simulator [101]. A blue/green wide band width spectrum of about ~ 200 mW/cm<sup>2</sup> intensity was chosen to erase any natural OSL signal. Then the samples were heated to 250°C to deplete light-insensitive traps. After the heating, all aliquots were irradiated for 200 s with a  $\beta$ -irradiation ring source [111] which lead to an accumulated dose of 10.5 Gy for FB and 11.3 Gy for BT1713. The dose difference arises from the different sample grain sizes. All irradiations were performed at 125°C to keep shallow traps depleted and simulate environmental defect state conditions.

10 aliquots of each sample were measured with the usual measurement sequence of the SAR protocol [19] but with 525 nm stimulation instead of the usual 470 nm stimulation and longer stimulation time to account for the lower decay constants, see table 5.6. The wavelength change is not intended but originates from the available stimulation wavelengths.

**Table 5.6:** Measurement sequence based on SAR protocol from Murray and Wintle [19] but with 525 nm stimulation. The regeneration doses are:  $D_i = 0, 100, 200, 400, 600, 0, 100$  s.

Step	Treatment	Details	Comment
1	Reg. Dose	Give dose $D_i$	Irradiate at room temperature $D_i = 0$ Gy at first cycle (natural dose)
2	Preheat	Heat at 5 °C /s to 250°C, hold 10 s	Cool to 60°C before proceeding
3	OSL	525 nm stimulation at 125°C	with LEDs for 100 s at 80 mW/cm <sup>2</sup>
4	Test dose	Give dose $D_T$	$D_T = 100$ s
5	Preheat	Heat at 5 °C /s to 250°C, hold 10 s	
6	OSL	525 nm stimulation at 125°C	with LEDs for 100 s at 80 mW/cm <sup>2</sup>
		Return to step 1	

The other 10 aliquots of each sample were measured with the sequence proposed by Roberts *et al.* [109], see table 5.7. The device time needed to process the sequences was just about 2/3 of the time needed for the standard SAR sequence.

**Table 5.7:** Measurement sequence based on protocol from Roberts *et al.* [109] but with 525 nm stimulation. The regeneration doses are:  $D_i = 200, 100, 200, 400, 600, 0, 100$  s.

Step	Treatment	Details	Comment
1	Reg. Dose	Give dose $D_i$	$D_i = 200$ s at first cycle (pre-dose)
2	OSL	525 nm stimulation for 100 s	at room temperature
3	Test dose	Give dose $D_T$	$D_T = 100$ s
4	OSL	525 nm stimulation for 100 s	at room temperature
		Return to step 1	

The four measured data sets were successful analysed with `EvaluateDataSet.Rmd`. The analysis summaries can be found in appendix D. The full reports as well as the data sets and the sequence files can be found at the accompanying CD.

## Results

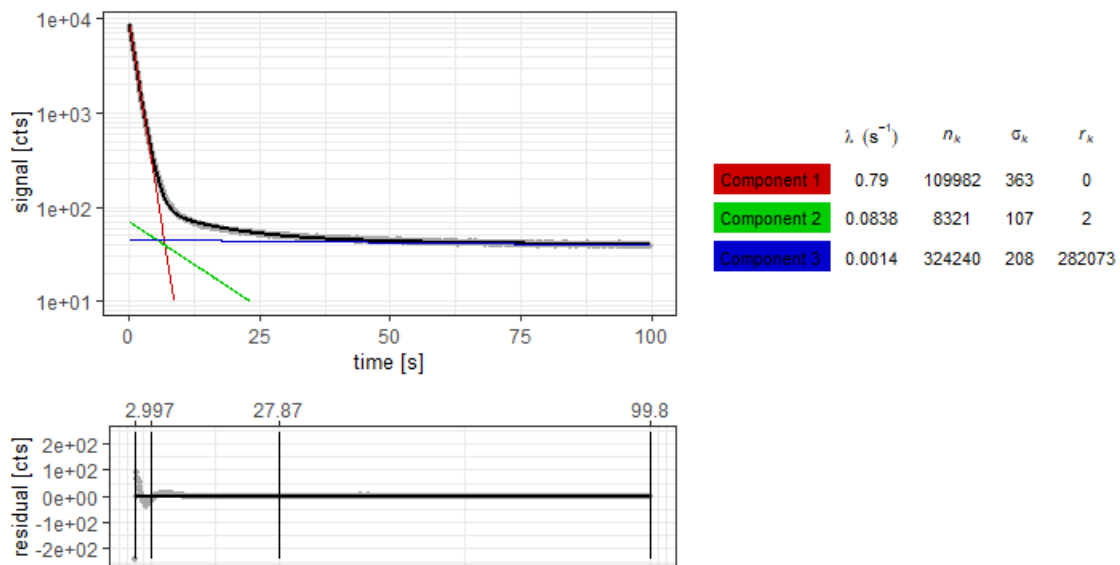


**Figure 5.8:** Average CW-OSL curve of sample FB measured with the SAR protocol from Murray and Wintle [19]; Upper-left: logarithmic y-scale, linear x-scale; Lower-left: Residual curve with drawn-in signal bin intervals

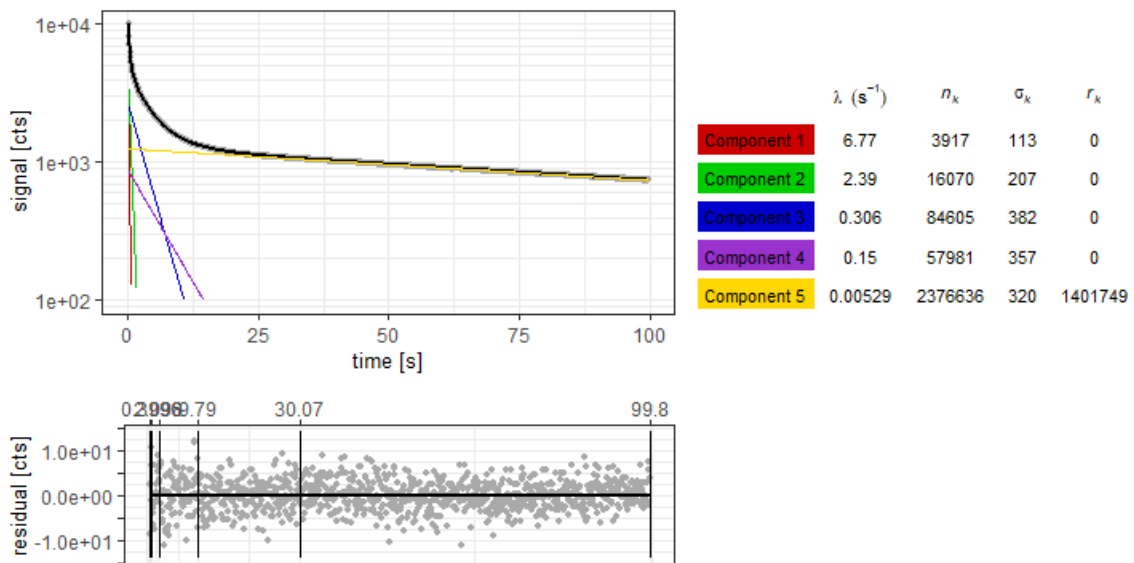


**Figure 5.9:** Average CW-OSL curve of sample FB measured with the protocol from Roberts *et al.* [109]; Upper-left: logarithmic y-scale, linear x-scale; Lower-left: Residual curve with drawn-in signal bin intervals

In case of sample FB, the fitting of the global average OSL curve found three components for the standard SAR protocol measurement (figure 5.8). Component 1 is likely identical with the fast component in 470 nm CW-OSL measurements. The dose calculation for component 1 returned an underestimated dose value, see table 5.8. That is not unusual for dose recovery experiments

with quartz and can be further investigated by pre-heat plateau tests. Global curve fitting at the Roberts *et al.* protocol measurements revealed five components (figure 5.9). A closer look at the data implies that the fast component in the 125°C CW-OSL curves is related to component 3 in the Roberts *et al.* protocol. The dose calculation for component 3 returned an accurate dose, see table 5.8. Therefore, the protocol seems to return accurate dose estimations, at least for this particular sample and this particular dose recovery test.

**Table 5.8:** Recovery dose determination results for sample FB. *SAR*: Fast component parameters and dose values measured at 125°C and 525 nm stimulation with the Murray and Wintle [19] protocol. *Roberts et al.*: Component 3 parameters and dose values measured at ~25°C and 525 nm stimulation with the Roberts *et al.* [109] protocol.

Protocol	decay constant [s <sup>-1</sup> ]	Signal amplitude	Passed rejection crit.	expected dose [Gy]	CAM [Gy]	Over-dispersion
<b>SAR</b>	0.79	1.20E+05	10 of 10	10.5	8.7 ± 0.1	1%
<b>Roberts <i>et al.</i></b>	0.31	8.46E+04	7 of 10		10.2 ± 0.5	0%

In case of sample BT1713, the global curve fittings found very similar OSL characteristics. The CW-OSL signals are nearly two orders of magnitude weaker and the signal decays are slightly faster than of sample FB, but the curve shapes are very similar. This applies for both, the standard SAR protocol measurements as well as the Roberts *et al.* protocol measurements. The dose calculation returned an accurate dose estimation for the standard SAR protocol, but a heavily dose overestimation for the Roberts *et al.* protocol, see table 5.9. Note that this overestimation is represented by just one  $D_e$  value in table 5.9, because that calculation was the only one to pass the rejection criteria. A closer look at the data reveals that all  $D_e$  values overestimate the true dose more or less.

**Table 5.9:** Recovery dose determination results for sample BT1713. *SAR*: Fast component parameters and dose values measured at 125°C and 525 nm stimulation with the Murray and Wintle [19] protocol. *Roberts et al.*: Component 3 parameters and dose values measured at ~25°C and 525 nm stimulation with the Roberts *et al.* [109] protocol.

Protocol	decay constant [s <sup>-1</sup> ]	Signal amplitude	Passed rejection crit.	expected dose [Gy]	CAM [Gy]	Over-dispersion
<b>SAR</b>	0.98	2.00E+03	6 of 10	11.3	12.3 ± 1.7	33%
<b>Roberts <i>et al.</i></b>	0.35	2.80E+03	1 of 10		31.8	-

Further investigations are necessary to explain this outcome. When looking at the full analysis reports, one will find more details which need further discussion. But that shall not be the scope of this thesis. The added benefit of the applied method is the rapid data analysis. Roberts *et al.* [109] mentioned their struggle to calculate the wanted dose information. We demonstrated an automated and reliable way to do this.



## 6 Conclusion and Outlook

This work introduced a new approach towards separating the signal components in CW-OSL measurements of quartz. The proposed method can be divided into three major steps:

- 1) Identify CW-OSL components
- 2) Decompose all CW-OSL measurements
- 3) Determine retrospective dose information resolved by individual components

### Step 1 summary

In the first step, an average CW-OSL curve from all records of a data set is calculated. The resulting global curve is fitted according to the approach suggested by Bluszcz & Adamiec [54]. The fitting model consists of a sum of exponential decays. The correct number of components is chosen based on a statistical  $F$ -test. The best-suited threshold value for the  $F$ -test was determined in a simulation with about 10,000 global OSL curves, each simulated by an individual set of parameters. The same simulation data set was used to evaluate the accuracy and precision of the algorithm. While over-fitting and under-fitting can occur and is strongly correlated to the length of the measurement, in most cases the correct number of components was found. The most important component for dating applications is the 'fast' decaying component, which was found in 99.95% of all simulated cases. The determined decay constants lay in 97.4% of all cases inside a  $\pm 10\%$  margin of the true decay constant. The accuracy and reliability in finding and parameterizing a component decreases for slower decaying components but remained sufficient for most of the simulated OSL curves. The simulations therefore demonstrated the feasibility of that approach in identifying CW-OSL signal components. In the application tests on standard SAR data sets, however, four components were identified in most cases. However, three component models lead to more reliable and reasonable results. Thus, for practical use in automated analysis scripts, the component identification process has to be improved.

The following improvements are suggested for consideration in later works:

- The use of a fitting model with a fixed number of three components should be considered. It is suggested to test the introduction of a stretching parameter at the exponent of the slowest decaying component. Roberts *et al.* [106] apply this model and it is also in accordance with at least some of the kinetic models of quartz [38], [40]. However, the implications for the decomposition algorithm are unclear and this model would also undermine the variability of the method presented in this thesis.
- Instead of a global OSL curve, a subset could be used for component identification. This

might avoid uncertainties in the decay constants, which lead to over-fitting. For example, using just test-dose CW-OSL measurements would erase dose dependencies and would also allow the monitoring of shifts and deviations in the decay constants.

- A less SNR-sensitive statistical test as substitute for the  $F$ -test should be considered. Bluszcz [pers. comm.] proposes the use of Student's  $t$ -test or the sign test.

## Step 2 summary

In the second step, each single CW-OSL measurement is decomposed analytically. First, multiple signal bins are defined. Their number is equal to the number of components found in the first step. These signal bins have a largely improved SNR, compared to single data points. From the signal bin values and the decay constants from the first step, an equation system is built. This equation system is solved by linear algebra methods. These linear algebra methods allow for the use of the propagation of uncertainty method to return statistical error estimates. The error estimation approach was also used to develop a numerical procedure to find the optimal signal bin intervals. However, the interval determination outcome is not fully reproducible. It is recommended to improve the procedure in future research. The decomposition approach and its regression-alternative were tested in a simulation with over 15,000 parameter sets and 15 million OSL curves. The simulation demonstrates a sufficient accuracy, precision and error estimation for all OSL curves without a background offset. The precision could be further improved by an additional regression step. With the appearance of background signals, however, the accuracy in determining slowly decaying component intensities decreased. For most OSL curves, this problem could be solved with the introduction of an additional offset component. For some OSL curve scenarios though, this offset component destabilized the decomposition algorithm. In consequence, this approach was abandoned for the practical tests.

No problems could be observed in the automated analysis of several data sets. Although not shown and discussed in this thesis, some tests with simulated and actual noise-dominated and zero-signal measurements were performed. The decomposition algorithm proved its reliability by always returning reasonable intensity values and error estimations.

## Step 3 summary

For the third step, standard approaches [19], [92] provided by the **R** package 'Luminescence' [61] were used to recover dose information and estimate sample ages. These allowed the development of an automated analysis script. This script was tested successfully on five geomorphologic data sets. It was also applied successfully to investigate a new measurement protocol. However, the dose determination approach was neither specifically chosen nor optimized for analysing component-separated data sets. Therefore, there is a high potential for improving the SNR and accuracy of sample age calculations. The component-separated data sets may also contain valuable information about sample conditions like the completeness of the natural bleaching.

## Conclusion

At the end of chapter 2, we defined the following requirements:

- 1) Identify the number of components and their decay constants on a sample-to-sample basis
- 2) Allow component-resolved dose calculation, even for samples with low-SNR measurements
- 3) Allow automated component and dose evaluation, without inherent need for user interaction
- 4) Be applicable for a large variety of instrumental and measurement conditions

This thesis proved that the introduced method for quartz CW-OSL component separation fulfils points 1 – 3. Nonetheless, further tests and improvements for step 1 and step 3 of the method are recommended. One way to investigate and test the method further is to apply it to the kinetic models of quartz introduced in chapter 2.3. The **R** package published by Friedrich *et al.* [42] can simulate CW-OSL measurement sequences based on particular models and defect settings. This allows relations between signal components and theoretical defect concentrations and charge carrier movements to be revealed. Comparing these relations with experimental findings might allow methodological improvements in the age determination and might also improve our understanding of optically stimulated luminescence of quartz.

Point 4 in the list above was proven just partly in this thesis. We tested a variety of channel widths, measurement lengths and background offsets by simulations. It turned out that these parameters can compromise the accuracy of the method. The introduction of a test criterion should be considered. Tested with just one experiment was the methods feasibility for other stimulation and temperature conditions. Changes in these conditions can change the OSL characteristics significantly. While the method demonstrated its usefulness in decomposing the CW-OSL curves obtained with the no-thermal-treatment SAR protocol of Roberts *et al.* [106], it might lead to wrong conclusion if the underlying multi-exponential decay model is not suitable for certain conditions. Also not considered were detection modes other than photon-counting mode of a photomultiplier tube.

## Outlook

The experimental results in chapter 5.3 demonstrated that the introduced method can enable new protocols with simplified instrumental settings or shorter measurement sequences. The individual characteristics of the signal components in a particular sample might give new insights into the origin and history of the sample. In addition, if the signal components can be related to specific levels of thermal stability, then thermochronometry of quartz might become feasible [108].

The introduced method might also provide a new strategy of separating OSL components in spatially or spectrally resolved measurements. The cheapest and most common way to perform spatially or spectrally resolved OSL measurements is to deploy scientific CCD or CMOS cameras. Yet these cameras produce the most signal noise in the event of image read-out. Thus, long exposure times and low read-out frequencies are deployed to enable sufficient measurement SNRs. However, the lack of time resolution in such measurements prevents the use of traditional component fitting methods. Moreover, sensitive detectors with good time resolutions like EM-CDD or ICCD cameras are costly and complex to use. The introduced method enables a new strategy to solve this issue: First, we gather the component number and the decay constants by applying step 1 on common PMT measurements. Then we use an adapted version of step 2 to decompose the camera measurements. The signal bin intervals in step 2 can be adjusted to the exposure intervals of the camera. Only three exposures are necessary to decompose an image or spectrum with three signal components. Thus, CW-OSL component separation would be enabled for measurement series like those performed by Greilich *et al.* [109], [110] or Lomax *et al.* [111].

Furthermore, we only considered CW-OSL measurements of quartz. Beyond that, the introduced method might also be helpful for OSL measurements of other materials. For example, in  $\text{Al}_2\text{O}_3:\text{C}$  dosimetry, a similar issue is known [112]. And the mathematical problem of decomposing multi-exponential decay curve is also crucial in other scientific fields. Mentioned here shall be capacitor discharge curves and the multi-compartment model in pharmacological kinetics.

# Bibliography

- [1] I. K. Bailiff, S. Sholom, und S. W. S. McKeever, „Retrospective and emergency dosimetry in response to radiological incidents and nuclear mass-casualty events: A review“, *Radiat. Meas.*, Bd. 94, S. 83–139, Nov. 2016.
- [2] S. Sholom, R. DeWitt, S. L. Simon, A. Bouville, und S. W. S. McKeever, „Emergency optically stimulated luminescence dosimetry using different materials“, *Radiat. Meas.*, Bd. 46, Nr. 12, S. 1866–1869, Dez. 2011.
- [3] P. W. Reiners u. a., *Geochronology and thermochronology*. Washington, DC: American Geophysical Union, 2018.
- [4] M. J. Aitken, „Luminescence dating: A guide for non-specialists“, *Archaeometry*, Bd. 31, Nr. 2, S. 147–159, Aug. 1989.
- [5] G. A. T. Duller, *Luminescence Dating: Guidelines on using luminescence dating in archaeology*. Swindon: English Heritage, 2008.
- [6] H. Gray, S. Mahan, T. Rittenour, und M. Nelson, „GUIDE TO LUMINESCENCE DATING TECHNIQUES AND THEIR APPLICATION FOR PALEOSEISMIC RESEARCH“, *Proc. Vol. Basin Range Prov. Seism. Hazards Summit III Utah Geol. Surv. Misc. Publ. 15-5 Lund WR Ed.*, Bd. 2015, S. 5, Jan. 2015.
- [7] M. Ikeya, *New Applications of Electron Spin Resonance: Dating, Dosimetry and Microscopy*. WORLD SCIENTIFIC, 1993.
- [8] W. J. Rink, „Electron spin resonance (ESR) dating and ESR applications in quaternary science and archaeometry“, *Radiat. Meas.*, Bd. 27, Nr. 5, S. 975–1025, Dez. 1997.
- [9] M. J. Aitken, *Thermoluminescence dating*, U.S. ed. London ; Orlando: Academic Press, 1985.
- [10] G. Erfurt und M. R. Krbetschek, „Studies on the physics of the infrared radioluminescence of potassium feldspar and on the methodology of its application to sediment dating“, *Radiat. Meas.*, Bd. 37, Nr. 4, S. 505–510, Aug. 2003.
- [11] L. Bøtter-Jensen, S. W. S. McKeever, und A. G. Wintle, *Optically stimulated luminescence dosimetry*, 1st ed. Amsterdam ; Boston ; London: Elsevier, 2003.
- [12] E. G. Yukihara und S. W. S. McKeever, *Optically stimulated luminescence: fundamentals and applications*. Chichester, West Sussex: Wiley, 2011.
- [13] E. J. Rhodes, „Optically Stimulated Luminescence Dating of Sediments over the Past 200,000 Years“, *Annu. Rev. Earth Planet. Sci.*, Bd. 39, Nr. 1, S. 461–488, Mai 2011.
- [14] M. J. Aitken, *An introduction to optical dating: the dating of Quaternary sediments by the use of photon-stimulated luminescence*. Oxford ; New York: Oxford University Press, 1998.
- [15] K. Lepper, „In-Situ Geochronology for Martian Dunes: A Review of Optical Dating Concepts and Experiments with Analog Materials“, *Planet. Dunes Workshop Rec. Clim. Change*, 2008.
- [16] R. Sohbaty, M. Jain, und A. Murray, „Surface exposure dating of non-terrestrial bodies using optically stimulated luminescence: A new method“, *Icarus*, Bd. 221, Nr. 1, S. 160–166, Sep. 2012.
- [17] A. K. Singhvi und V. Mejdahl, „Thermoluminescence dating of sediments“, *Nucl. Tracks Radiat. Meas.* 1982, Bd. 10, Nr. 1, S. 137–161, Jan. 1985.
- [18] D. J. Huntley, D. I. Godfrey-Smith, und M. L. W. Thewalt, „Optical dating of sediments“, *Nature*, Bd. 313, Nr. 5998, S. 105–107, Jan. 1985.
- [19] A. S. Murray und A. G. Wintle, „Luminescence dating of quartz using an improved single-aliquot regenerative-dose protocol“, *Radiat. Meas.*, Bd. 32, Nr. 1, S. 57–73, Feb. 2000.
- [20] J. Wallinga, A. Murray, und A. Wintle, „The single-aliquot regenerative-dose (SAR) protocol applied to coarse-grain feldspar“, *Radiat. Meas.*, Bd. 32, Nr. 5, S. 529–533, Dez. 2000.
- [21] J. Götze und R. Möckel, Hrsg., *Quartz: deposits, mineralogy and analytics*. Berlin ; New York: Springer, 2012.

- [22] J. Götze, „Chemistry, textures and physical properties of quartz – geological interpretation and technical application“, *Mineral. Mag.*, Bd. 73, Nr. 4, S. 645–671, Aug. 2009.
- [23] F. Preusser u. a., „Quartz as a natural luminescence dosimeter“, *Earth-Sci. Rev.*, Bd. 97, Nr. 1–4, S. 184–214, Dez. 2009.
- [24] M. Martini, M. Fasoli, und A. Galli, „Quartz OSL emission spectra and the role of [AlO4]<sup>o</sup> recombination centres“, *Radiat. Meas.*, Bd. 44, Nr. 5–6, S. 458–461, Mai 2009.
- [25] M. Martini, M. Fasoli, und I. Villa, „Defect studies in quartz: Composite nature of the blue and UV emissions“, *Nucl. Instrum. Methods Phys. Res. Sect. B Beam Interact. Mater. At.*, Bd. 327, S. 15–21, Mai 2014.
- [26] R. Chen und V. Pagonis, *Advances in Physics and Applications of Optically and Thermally Stimulated Luminescence*. WORLD SCIENTIFIC (EUROPE), 2019.
- [27] N. Itoh, D. Stoneham, und A. M. Stoneham, „Ionic and electronic processes in quartz: Mechanisms of thermoluminescence and optically stimulated luminescence“, *J. Appl. Phys.*, Bd. 92, Nr. 9, S. 5036–5044, Nov. 2002.
- [28] R. Chen und S. W. S. McKeever, *Theory of thermoluminescence and related phenomena*. Singapore ; River Edge, N.J.: World Scientific, 1997.
- [29] R. Chen und V. Pagonis, *Thermally and optically stimulated luminescence: a simulation approach*. The Atrium, Southern Gate, Chichester, West Sussex, UK ; Hoboken, NJ: Wiley, 2011.
- [30] J. S. Singarayer und R. M. Bailey, „Further investigations of the quartz optically stimulated luminescence components using linear modulation“, *Radiat. Meas.*, Bd. 37, Nr. 4, S. 451–458, Aug. 2003.
- [31] J. S. Singarayer und R. M. Bailey, „Component-resolved bleaching spectra of quartz optically stimulated luminescence: preliminary results and implications for dating“, *Radiat. Meas.*, Bd. 38, Nr. 1, S. 111–118, Feb. 2004.
- [32] C. Schmidt, O. Simmank, und S. Kreutzer, „Time-resolved optically stimulated luminescence of quartz in the nanosecond time domain“, *J. Lumin.*, Bd. 213, S. 376–387, Mai 2019.
- [33] R. Chen und P. L. Leung, „The decay of OSL signals as stretched-exponential functions“, *Radiat. Meas.*, Bd. 37, Nr. 4–5, S. 519–526, Aug. 2003.
- [34] A. S. Murray und R. G. Roberts, „Measurement of the equivalent dose in quartz using a regenerative-dose single-aliquot protocol“, *Radiat. Meas.*, Bd. 29, Nr. 5, S. 503–515, Okt. 1998.
- [35] A. G. Wintle und A. S. Murray, „A review of quartz optically stimulated luminescence characteristics and their relevance in single-aliquot regeneration dating protocols“, *Radiat. Meas.*, Bd. 41, S. 369–391, 2006.
- [36] D. Mittelstraß, „Mathematische und physikalische Grundlagen der Lumineszenzmessung im Rahmen der retrospektiven Dosimetrie“, Bachelor thesis, TU Bergakademie Freiberg, Freiberg, 2013.
- [37] B. W. Smith und E. J. Rhodes, „Charge movements in quartz and their relevance to optical dating“, *Radiat. Meas.*, Bd. 23, Nr. 2, S. 329–333, Apr. 1994.
- [38] R. M. Bailey, B. W. Smith, und E. J. Rhodes, „Partial bleaching and the decay form characteristics of quartz OSL“, *Radiat. Meas.*, Bd. 27, Nr. 2, S. 123–136, Apr. 1997.
- [39] R. M. Bailey, „Towards a general kinetic model for optically and thermally stimulated luminescence of quartz“, *Radiat. Meas.*, Bd. 33, Nr. 1, S. 17–45, Feb. 2001.
- [40] R. M. Bailey, „Paper I—simulation of dose absorption in quartz over geological timescales and its implications for the precision and accuracy of optical dating“, *Radiat. Meas.*, Bd. 38, Nr. 3, S. 299–310, Juni 2004.
- [41] V. Pagonis, A. G. Wintle, R. Chen, und X. L. Wang, „A theoretical model for a new dating protocol for quartz based on thermally transferred OSL (TT-OSL)“, *Radiat. Meas.*, Bd. 43, Nr. 2, S. 704–708, Feb. 2008.
- [42] J. Friedrich, V. Pagonis, R. Chen, S. Kreutzer, und C. Schmidt, „Quartz radiofluorescence: a modelling approach“, *J. Lumin.*, Bd. 186, S. 318–325, Juni 2017.

- [43] J. Friedrich, S. Kreutzer, und C. Schmidt, „Solving ordinary differential equations to understand luminescence: ‘RLumModel’, an advanced research tool for simulating luminescence in quartz using R“, *Quat. Geochronol.*, Bd. 35, S. 88–100, Okt. 2016.
- [44] J. Peng und V. Pagonis, „Simulating comprehensive kinetic models for quartz luminescence using the R program KMS“, *Radiat. Meas.*, Bd. 86, S. 63–70, März 2016.
- [45] E. Bulur, „An alternative technique for optically stimulated luminescence (OSL) experiment“, *Radiat. Meas.*, Bd. 26, Nr. 5, S. 701–709, Sep. 1996.
- [46] E. Bulur, L. Bøtter-Jensen, und A. S. Murray, „Optically stimulated luminescence from quartz measured using the linear modulation technique“, *Radiat. Meas.*, Bd. 32, Nr. 5–6, S. 407–411, Dez. 2000.
- [47] M. Jain, A. S. Murray, und L. Bøtter-Jensen, „Characterisation of blue-light stimulated luminescence components in different quartz samples: implications for dose measurement“, *Radiat. Meas.*, Bd. 37, S. 441–449, 2003.
- [48] J. A. Durcan und G. A. T. Duller, „The fast ratio: A rapid measure for testing the dominance of the fast component in the initial OSL signal from quartz“, *Radiat. Meas.*, Bd. 46, Nr. 10, S. 1065–1072, Okt. 2011.
- [49] M. Jain, J. H. Choi, und P. J. Thomas, „The ultrafast OSL component in quartz: Origins and implications“, *Radiat. Meas.*, Bd. 43, Nr. 2, S. 709–714, Feb. 2008.
- [50] B. Li und S.-H. Li, „Comparison of De estimates using the fast component and the medium component of quartz OSL“, *Radiat. Meas.*, Bd. 41, Nr. 2, S. 125–136, Feb. 2006.
- [51] D. Steffen, F. Preusser, und F. Schlunegger, „OSL quartz age underestimation due to unstable signal components“, *Quat. Geochronol.*, Bd. 4, Nr. 5, S. 353–362, Okt. 2009.
- [52] B. Li und S.-H. Li, „Correcting for thermal transfer in OSL measurements of young sediment samples“, *Radiat. Meas.*, Bd. 41, Nr. 7–8, S. 855–861, Aug. 2006.
- [53] E. Bulur, „A simple transformation for converting CW-OSL curves to LM-OSL curves“, *Radiat. Meas.*, Bd. 32, Nr. 2, S. 141–145, Apr. 2000.
- [54] A. J. J. Bos und J. Wallinga, „How to visualize quartz OSL signal components“, *Radiat. Meas.*, Bd. 47, Nr. 9, S. 752–758, Sep. 2012.
- [55] A. Bluszcz und G. Adamiec, „Application of differential evolution to fitting OSL decay curves“, *Radiat. Meas.*, Bd. 41, Nr. 7–8, S. 886–891, Aug. 2006.
- [56] J. Peng, Z. Dong, F. Han, H. Long, und X. Liu, „R package numOSL: numeric routines for optically stimulated luminescence dating“, *Anc. TL*, Bd. 31, 2013.
- [57] R. M. Bailey, „The interpretation of quartz optically stimulated luminescence equivalent dose versus time plots“, *Radiat. Meas.*, Bd. 32, Nr. 2, S. 129–140, Apr. 2000.
- [58] R. M. Bailey, „Paper II: The interpretation of measurement-time-dependent single-aliquot equivalent-dose estimates using predictions from a simple empirical model“, *Radiat. Meas.*, Bd. 37, Nr. 6, S. 685–691, Dez. 2003.
- [59] R. M. Bailey, „Direct measurement of the fast component of quartz optically stimulated luminescence and implications for the accuracy of optical dating“, *Quat. Geochronol.*, Bd. 5, Nr. 5, S. 559–568, Okt. 2010.
- [60] M. Jain, A. S. Murray, L. Bøtter-Jensen, und A. G. Wintle, „A single-aliquot regenerative-dose method based on IR (1.49eV) bleaching of the fast OSL component in quartz“, *Radiat. Meas.*, Bd. 39, Nr. 3, S. 309–318, Juni 2005.
- [61] M. Ballarini, J. Wallinga, A. G. Wintle, und A. J. J. Bos, „A modified SAR protocol for optical dating of individual grains from young quartz samples“, *Radiat. Meas.*, Bd. 42, Nr. 3, S. 360–369, März 2007.
- [62] A. C. Cunningham und J. Wallinga, „Selection of integration time intervals for quartz OSL decay curves“, *Quat. Geochronol.*, Bd. 5, Nr. 6, S. 657–666, Dez. 2010.
- [63] Z. Shen und A. Lang, „Quartz fast component optically stimulated luminescence: Towards routine extraction for dating applications“, *Radiat. Meas.*, Bd. 89, S. 27–34, Juni 2016.

- [64] „R: The R Project for Statistical Computing“. [Online]. Verfügbar unter: <https://www.r-project.org/>. [Zugegriffen: 23-Juli-2019].
- [65] S. Kreutzer, C. Schmidt, M. C. Fuchs, M. Dietze, M. Fischer, und M. Fuchs, „Introducing an R package for luminescence dating analysis“, *Anc. TL*, Bd. 30, S. 1–8, Mai 2012.
- [66] S. Kreutzer, C. Burow, M. Fuchs, C. Schmidt, M. Fischer, und J. Friedrich, *Luminescence: Comprehensive Luminescence Dating Data Analysis*. R package, 2019.
- [67] W. Chang, *R graphics cookbook: practical recipes for visualizing data*, Second edition. Beijing Boston Farnham: O’Reilly, 2018.
- [68] Y. Xie, J. J. Allaire, und G. Golemund, *R Markdown: the definitive guide*. Boca Raton: Taylor & Francis, CRC Press, 2018.
- [69] *Photomultiplier tubes - Basics and Applications*, 3rd edition. Hamamatsu Photonics, 2006.
- [70] R. Galbraith, „A note on the variance of a background-corrected OSL“, *Anc. TL*, Bd. 20, Nr. 2, 2002.
- [71] R. F. Galbraith und R. G. Roberts, „Statistical aspects of equivalent dose and error calculation and display in OSL dating: An overview and some recommendations“, *Quat. Geochronol.*, Bd. 11, S. 1–27, Aug. 2012.
- [72] B. Li, „A note on estimating the error when subtracting background counts from weak OSL signals“, *Anc. TL*, Bd. 25, Nr. 1, 2007.
- [73] J. More, D. Sorenson, B. Garbow, und K. Hillstrom, „MINPACK - Least Squares Minimization of Vector Functions“, 1999. [Online]. Verfügbar unter: [http://people.sc.fsu.edu/~jburkardt/f\\_src/minpack/minpack.html](http://people.sc.fsu.edu/~jburkardt/f_src/minpack/minpack.html). [Zugegriffen: 09-Juli-2019].
- [74] C. T. Kelley, *Iterative methods for optimization*. Philadelphia: SIAM, 1999.
- [75] R. Storn und K. Price, „Differential Evolution – A Simple and Efficient Heuristic for global Optimization over Continuous Spaces“, *J. Glob. Optim.*, Bd. 11, Nr. 4, S. 341–359, Dez. 1997.
- [76] P. R. Bevington und D. K. Robinson, *Data reduction and error analysis for the physical sciences*, 2nd ed. New York: McGraw-Hill, 1992.
- [77] R. Waldi, *Statistische Datenanalyse: Grundlagen und Methoden für Physiker*. Berlin: Springer Spektrum, 2015.
- [78] J. R. Janesick, *Scientific charge-coupled devices*. Bellingham, Wash: SPIE Press, 2001.
- [79] C. Ritz und J. C. Streibig, *Nonlinear regression with R*. New York: Springer, 2008.
- [80] J. Hedderich und L. Sachs, *Angewandte Statistik - Methodensammlung mit R*, 16. Berlin, Heidelberg: Springer Berlin Heidelberg, 2018.
- [81] T. Lapp, M. Kook, A. S. Murray, K. J. Thomsen, J.-P. Buylaert, und M. Jain, „A new luminescence detection and stimulation head for the Risø TL/OSL reader“, *Radiat. Meas.*, Bd. 81, S. 178–184, Okt. 2015.
- [82] D. Richter, A. Richter, und K. Dornich, „Lexsyg smart — a luminescence detection system for dosimetry, material research and dating application“, *Geochronometria*, Bd. 42, Nr. 1, Dez. 2015.
- [83] O. M. Williams, N. A. Spooner, B. W. Smith, und J. E. Moffatt, „Extended duration optically stimulated luminescence in quartz“, *Radiat. Meas.*, Bd. 119, S. 42–51, Dez. 2018.
- [84] D. Mittelstraß, S. Kreutzer, und D. Richter, „An analytical method to separate signal components of CW-OSL measurements of quartz“, gehalten auf der gLED, Freiberg, 26-Okt-2013.
- [85] I. N. Bronštejn, K. A. Semendjaev, und G. Grosche, *Taschenbuch der Mathematik*, 24. Aufl. Moskau: Verl. Nauka, 1989.
- [86] W. Dahmen und A. Reusken, *Numerik für Ingenieure und Naturwissenschaftler: mit 59 Tabellen*. Berlin: Springer, 2006.
- [87] P. Fornasini, *The uncertainty in physical measurements: an introduction to data analysis in the physics laboratory*. New York, N.Y: Springer, 2008.
- [88] „BIPM - Guide to the Expression of Uncertainty in Measurement (GUM)“. [Online]. Verfügbar unter: <https://www.bipm.org/en/publications/guides/gum.html>. [Zugegriffen: 01-Okt-2019].



- [89] S. Greulich, H.-L. Harney, C. Woda, und G. A. Wagner, „AgesGalore—A software program for evaluating spatially resolved luminescence data“, *Radiat. Meas.*, Bd. 41, S. 726–735, Juli 2006.
- [90] B. Li, Z. Jacobs, R. G. Roberts, R. Galbraith, und J. Peng, „Variability in quartz OSL signals caused by measurement uncertainties: Problems and solutions“, *Quat. Geochronol.*, Bd. 41, S. 11–25, Aug. 2017.
- [91] A. Bluszcz, G. Adamiec, und A. J. Heer, „Estimation of equivalent dose and its uncertainty in the OSL SAR protocol when count numbers do not follow a Poisson distribution“, *Radiat. Meas.*, Bd. 81, S. 46–54, Okt. 2015.
- [92] D. Banerjee, L. Bøtter-Jensen, und A. S. Murray, „Retrospective dosimetry: estimation of the dose to quartz using the single-aliquot regenerative-dose protocol“, *Appl. Radiat. Isot.*, Bd. 52, Nr. 4, S. 831–844, Apr. 2000.
- [93] G. Adamiec, A. J. Heer, und A. Bluszcz, „Statistics of count numbers from a photomultiplier tube and its implications for error estimation“, *Radiat. Meas.*, Bd. 47, Nr. 9, S. 746–751, Sep. 2012.
- [94] T. Arens, F. Hettlich, C. Karpfinger, U. Kockelkorn, K. Lichtenegger, und H. Stachel, Hrsg., *Mathematik*, 2. Aufl., 1. korrigierter Nachdr. Heidelberg: Spektrum, Akad. Verl, 2013.
- [95] R. F. Galbraith, R. G. Roberts, G. M. Laslett, H. Yoshida, und J. M. Olley, „Optical dating of single and multiple grains of quartz from Jinmium rock shelter, northern australia: Part I, experimental design and statistical models“, *Archaeometry*, Bd. 41, Nr. 2, S. 339–364, Aug. 1999.
- [96] S. Kreutzer und M. Dietze, *plot\_GrowthCurve(): Fit and plot a growth curve for luminescence data (Lx/Tx against dose)*. 2019.
- [97] C. Burow, *calc\_CentralDose(): Apply the central age model (CAM) after Galbraith et al. (1999) to a given De distribution*. 2019.
- [98] C. Burow, *calc\_MinDose(): Apply the (un-)logged minimum age model (MAM) after Galbraith et al. (1999) to a given De distribution*. 2019.
- [99] M. G. Kendall, „A NEW MEASURE OF RANK CORRELATION“, *Biometrika*, Bd. 30, Nr. 1–2, S. 81–93, Juni 1938.
- [100] L. Bøtter-Jensen und G. A. T. Duller, „A new system for measuring optically stimulated luminescence from quartz samples“, *Int. J. Radiat. Appl. Instrum. Part Nucl. Tracks Radiat. Meas.*, Bd. 20, Nr. 4, S. 549–553, Okt. 1992.
- [101] D. Richter, A. Richter, und K. Dornich, „Lexsyg — A new system for luminescence research“, *Geochronometria*, Bd. 40, Nr. 4, S. 220–228, Dez. 2013.
- [102] G. A. T. Duller, L. Bøtter-Jensen, A. S. Murray, und A. J. Truscott, „Single grain laser luminescence (SGLL) measurements using a novel automated reader“, *Nucl. Instrum. Methods Phys. Res. Sect. B Beam Interact. Mater. At.*, Bd. 155, Nr. 4, S. 506–514, Sep. 1999.
- [103] S. Meszner, S. Kreutzer, M. Fuchs, und D. Faust, „Late Pleistocene landscape dynamics in Saxony, Germany: Paleoenvironmental reconstruction using loess-paleosol sequences“, *Quat. Int.*, Bd. 296, S. 94–107, Mai 2013.
- [104] L. Schirrmeister u. a., „Yedoma Ice Complex of the Buor Khaya Peninsula (southern Laptev Sea)“, *Biogeosciences*, Bd. 14, Nr. 5, S. 1261–1283, März 2017.
- [105] T. Opel, S. Wetterich, H. Meyer, A. Y. Dereviagin, M. C. Fuchs, und L. Schirrmeister, „Ground-ice stable isotopes and cryostratigraphy reflect late Quaternary palaeoclimate in the Northeast Siberian Arctic (Oyogos Yar coast, Dmitry Laptev Strait)“, *Clim. Past*, Bd. 13, Nr. 6, S. 587–611, Juni 2017.
- [106] K. Ashastina, L. Schirrmeister, M. Fuchs, und F. Kienast, „Palaeoclimate characteristics in interior Siberia of MIS 6–2: first insights from the Batagay permafrost mega-thaw slump in the Yana Highlands“, *Clim. Past*, Bd. 13, Nr. 7, S. 795–818, Juli 2017.
- [107] M. C. Fuchs, „Luminescence dating - some basics for sediment dating and some applications in geoscience -“, 2018.
- [108] C. Ankjærgaard, A. S. Murray, und P. M. Denby, „Thermal pre-treatment in the OSL dating of quartz: is it necessary?“, *Radiat. Prot. Dosimetry*, Bd. 119, Nr. 1–4, S. 470–473, Sep. 2006.

- [109] H. M. Roberts, G. A. T. Duller, M. Gunn, C. R. Cousins, R. E. Cross, und D. Langstaff, „Strategies for equivalent dose determination without heating, suitable for portable luminescence readers“, *Radiat. Meas.*, Apr. 2018.
- [110] S. Kreutzer *u. a.*, „Les sables de Fontainebleau: a natural quartz reference sample and its characterisation“, *Anc. TL*, Bd. 35, Nr. 2, S. 21–31, Dez. 2017.
- [111] D. Richter, R. Pintaske, K. Dornich, und M. R. Krbetschek, „A novel beta source design for uniform irradiation in dosimetric applications“, *Anc. TL*, Bd. 30, Nr. 2, S. 57–63, 2012.
- [112] B. Guralnik *u. a.*, „OSL-thermochronometry using bedrock quartz: A note of caution“, *Quat. Geochronol.*, Bd. 25, S. 37–48, Feb. 2015.
- [113] S. Greilich, U. A. Glasmacher, und G. A. Wagner, „Spatially resolved detection of luminescence: a unique tool for archaeochronometry“, *Naturwissenschaften*, Bd. 89, Nr. 8, S. 371–375, Aug. 2002.
- [114] S. Greilich, N. Gribenski, D. Mittelstraß, K. Dornich, S. Huot, und F. Preusser, „Single-grain dose-distribution measurements by optically stimulated luminescence using an integrated EMCCD-based system“, *Quat. Geochronol.*, Bd. 29, S. 70–79, Aug. 2015.
- [115] J. Lomax, D. Mittelstraß, S. Kreutzer, und M. Fuchs, „OSL, TL and IRSL emission spectra of sedimentary quartz and feldspar samples“, *Radiat. Meas.*, Feb. 2015.
- [116] R. H. Biswas, M. K. Murari, und A. K. Singhvi, „Dose-dependent change in the optically stimulated luminescence decay of Al<sub>2</sub>O<sub>3</sub>:C“, *Radiat. Meas.*, Bd. 44, Nr. 5–6, S. 543–547, Mai 2009.

# List of figures

<b>Figure 6.5:</b>	OTOR model: Irradiation events generate electron-hole pairs	4
<b>Figure 6.6:</b>	OTOR model: Optical stimulation	5
<b>Figure 6.1:</b>	General workflow of signal component-wise quartz OSL dose calculation	11
<b>Figure 6.2:</b>	Global arithmetic mean OSL curve	13
<b>Figure 6.3:</b>	Workflow of multi-component exponential decay fitting	15
<b>Figure 6.7:</b>	Workflow of OSL decomposition process for three components.	21
<b>Figure 6.8:</b>	Signal-dose curve example	32
<b>Figure 6.1:</b>	Distribution of $F$ values for reduced simulated data set	37
<b>Figure 4.2:</b>	Decomposition of arbitrary simulated CW-OSL curve	43
<b>Figure 5.1:</b>	Average OSL curve of BT594	54
<b>Figure 5.2:</b>	BT594: Comparison of obtained decay constants with literature values	55
<b>Figure 5.3:</b>	Average OSL curve of BT594 fitted with $K = 3$ components	55
<b>Figure 5.4:</b>	Average OSL curve of BT594 fitted with $K = 4$ components	56
<b>Figure 6.5:</b>	BT594: Box plots of the $D_e$ -distributions from 24 aliquots	57
<b>Figure 6.6:</b>	Box plots of the $D_e$ -distributions criteria	58
<b>Figure 5.7:</b>	Batagai mega-slump	60
<b>Figure 5.8:</b>	Average CW-OSL curve of sample FB measured with the SAR protocol	65
<b>Figure 5.9:</b>	Average CW-OSL curve of sample FB measured with Roberts <i>et al.</i>	65

# List of tables

<b>Table 6.12:</b>	Dominant irradiation and OSL defect mechanisms in quartz	3
<b>Table 6.13:</b>	L/T table example	30
<b>Table 6.14:</b>	Rejection criteria for equivalent dose values	33
<b>Table 6.15:</b>	Input parameters for the step 1 simulations	36
<b>Table 6.16:</b>	Simulation statistics of component number	39
<b>Table 4.17:</b>	Accuracy, precision and success rate in determining the decay constants	40
<b>Table 6.18:</b>	Step 1 simulation correlation table	41
<b>Table 6.19:</b>	Input parameters for the step 2 simulations	43
<b>Table 6.20:</b>	Computing time and failure rates of the decomposition algorithms	44
<b>Table 6.21:</b>	Accuracy in the decomposition of simulated OSL curves	45
<b>Table 6.22:</b>	Distribution of the decomposition-caused uncertainty	46
<b>Table 6.9:</b>	Distribution of the error estimation accuracy	47
<b>Table 6.10:</b>	Step 2 correlation table	48
<b>Table 6.11:</b>	Background-dependent accuracy in the decomposition	49
<b>Table 6.12:</b>	Background-dependent reliability in the decomposition	50
<b>Table 6.13:</b>	Background-dependent reliability in the decomposition	51
<b>Table 6.1:</b>	<i>F</i> -table: Decay constants $\lambda$ and fit quality parameters	54
<b>Table 6.2:</b>	BT594: Number of $D_e$ values which passed rejection	57
<b>Table 6.3:</b>	BT594 analysis results	58
<b>Table 6.4:</b>	Summary of <i>F</i> -tests	61
<b>Table 6.5:</b>	Component-resolved age determination results	61
<b>Table 6.6:</b>	Measurement sequence based on SAR protocol	64
<b>Table 6.7:</b>	Measurement sequence based on protocol from Roberts <i>et al.</i>	64
<b>Table 6.8:</b>	Recovery dose determination results for sample FB	66
<b>Table 6.9:</b>	Recovery dose determination results for sample BT1713	66

# Appendix



# Appendix contents

<b>A R-package: OSLdecomposition</b>	<b>3</b>
A.1 Scripting sequence.....	3
A.2 Source code decompose_OSLcurve().....	5
A.3 Source code calc_OSLintervals().....	11
<b>B Correlation tables</b>	<b>15</b>
B.1 Step 1 – Correlation tables .....	17
B.2 Step 2 – Correlation tables .....	18
<b>C Decomposition analysis reports</b>	<b>19</b>
C.1 Full BT594 analysis report.....	19
C.2 BT1214 analysis summary.....	35
C.3 BK8 analysis summary.....	36
C.4 Oy7 analysis summary .....	37
C.5 Batagai analysis summary .....	38
<b>D OSL dating without heating</b>	<b>39</b>
D.1 FB standard SAR protocol analysis summary .....	39
D.2 FB no-heating protocol analysis summary.....	40
D.3 BT1713 standard SAR protocol analysis summary .....	41
D.4 BT1713 no-heating protocol analysis summary.....	42





# A R-package: OSLdecomposition

## A.1 Scripting sequence

```
# load necessary packages
library(OSLdecomposition)
library(Luminescence)
library(numOSL)
library(knitr)
library(ggplot2)
library(gridExtra)
library(ggpubr)

# read BIN file. The prefix "Luminescence::" is not necessary and is
# displayed here just for documentation
lum_data <- Luminescence::read_BIN2R(file.choose(),
                                     fastForward = TRUE)

# cut records if they are longer than 40 s
lum_data <- prepare_OSLdata(lum_data,
                           record.type = "OSL",
                           cut.time = 40)

# calc arithmetic mean curve from all OSL curves
global_curve <- sum_OSLcurves(lum_data,
                              output.plot = TRUE)

# find components via nonlinear regression and F-statistics and return a
# list with all fitting results. fit_OSLcurve() calls numOSL::decomp() to
# perform nonlinear regressions and calls calc_OSLintervals() to define
# signal bin intervals
component_list <- fit_OSLcurve(global_curve,
                              K.max = 5,
                              F.threshold = 50,
                              stimulation.intensity = 35,
                              stimulation.wavelength = 470,
                              background.fitting = FALSE,
                              output.plot = TRUE)

# compare decay constants with literature values
plot_PhotoCrosssections(component_list,
                        stimulation.intensity = 35,
                        stimulation.wavelength = 470)
```

```

# scan through data set, decompose OSL curves, build L/T tables, fit growth
curves and apply rejection criteria. decompose_SARdata() calls
decompose_OSLcurve() and Luminescence::plot_growthCurve() to calculate
equivalent dose values from L/T tables
SAR_results <- decompose_SARdata(lum_data,
                                components = component_list$components,
                                recuperation_rate = 0.05,
                                recycling_ratio = 0.1)

# decompose and plot first OSL curve of data set as example
example_curve <- lum_data[[1]]@records[[SAR_results$index[1]]@data
example_result <- decompose_OSLcurve(example_curve,
                                    components=component_list$components,
                                    algorithm = "det+nls")
plot_OSLcurve(example_curve, example_components)

# display box plots of the De distributions and give a table with De
medians back
table_SARdata(SAR_results,
              data.type = "De",
              criterion = "median",
              unit = "s",
              output.plot = TRUE)

# further analyses can be performed with the function library Luminescence.
Each list entry of SAR_results is saved as "RLum.Results" class. For
example, the following function call gives a radial De plot of the fast
component back
Luminescence::plot_RadialPlot(SAR_results[[1]])

```

## A.2 Source code decompose\_OSLcurve()

### Description

The function calculates the CW-OSL component amplitudes by a determinant-based algorithm. It also estimates the standard deviation of the amplitudes by using the error propagation method.

### Arguments

<code>curve</code>	[ <code>RLum.Data.Curve</code> ] or [ <code>data.frame</code> ] ( <b>required</b> ): CW-OSL record. First column (x-axis) must contain time marks, Second column (y-axis) must contain signal values. Further columns will be ignored
<code>components</code>	[ <code>data.frame</code> ] ( <b>required</b> ): Template table containing the decay parameters of the OSL curve. One column must be named <code>\$lambda</code> . It is recommended to provide also the integration interval parameters (columns <code>t.start</code> , <code>t.end</code> , <code>ch.start</code> , <code>ch.end</code> ), which can be found by applying <code>calc_OSLintervals</code> on the global mean curve, calculated by <code>sum_OSLcurves</code> . If one or more column is missing, <code>calc_OSLintervals</code> is run automatically.
<code>error.calculation</code>	[ <code>string</code> ] ( <i>with default</i> ): integral error estimation approach, either "empiric" or "poisson" or a numerical value; Per default the data of <code>curve\$residual</code> provided by <code>simulate_OSLcurve</code> is used to calculate an empiric standard error for each integral which will be processed in the error propagation formula. Alternatively the integral standard error can be calculated by assuming a poisson distributed signal error, known as <i>Shot noise</i> . This is suitable if the lack of data points on the x-axis circumvent a empiric error estimation, like with spatial or spectral resolved CCD measurements. Also the parameter can be set to a numerical value which will be handled as standard deviation per channel and added to the Poisson distributed shot noise

### Return value

The input table `components` will be returned with added/overwritten columns: `$n`, `$n.error`, `$n.residual`, `$I`, `$I.error`

---

```
decompose_OSLcurve <- function(  
  curve,  
  components,  
  background.fitting = FALSE,  
  algorithm = "det+nls", # "det", "nls", "det+nls"  
  error.calculation = "empiric", # "poisson", "empiric", "nls", numeric  
  verbose = TRUE  
) {
```

```

##### Input checks #####

if(is(curve, "RLum.Data.Curve") == FALSE &
    is(curve, "data.frame") == FALSE & is(curve, "matrix") == FALSE){
  stop("[decompose_OSLcurve()] Error: Input object is not of type
      'RLum.Data.Curve' or 'data.frame' or 'matrix'!")
}

if(is(curve, "RLum.Data.Curve") == TRUE) curve <-
    as.data.frame(get_RLum(curve))

if (!("time" %in% colnames(curve)) ||
    !("signal" %in% colnames(curve))) {
  curve <- data.frame(time = curve[,1],
                      signal = curve[,2])
}

if ((algorithm == "nls") &! (error.calculation == "nls")) {
  if (verbose) warning("When algorithm 'nls' is chosen, error.calculation
      must be also 'nls'. Argument changed to error.calculation='nls'")
  error.calculation <- "nls"
}

channel.width <- curve$time[2] - curve$time[1]

# check if time begins with zero and add channel.width if the case
if (curve$time[1] == 0) curve$time <- curve$time + channel.width

components <- components

# are the integration intervals given?
if (!("t.start" %in% colnames(components)) ||
    !("t.end" %in% colnames(components)) ||
    !("ch.start" %in% colnames(components)) ||
    !("ch.end" %in% colnames(components))) {
  if (verbose) warning("Integration intervals not provided.
      calc_OSLintervals() executed")
}

components <- calc_OSLintervals(components,
                                curve,
                                background.fitting = background.fitting,
                                verbose = verbose)
}

# if background.fitting = FALSE (recommended), remove last row
# this removes also the last integration interval (which is good)
if (is.na(components$lambda[nrow(components)]) &&
    (background.fitting==FALSE)) {

  components <- components[1:(nrow(components)-1),]
}

##### Set parameters #####

K <- nrow(components)
X <- c(1:K)
signal <- curve$signal[1:components$ch.end[K]]
time <- curve$time[1:components$ch.end[K]]
components$n <- rep(NA, K)
components$n.error <- rep(NA, K)
components$n.residual <- rep(NA, K)

```

```

lambda <- components$lambda
t.start <- components$t.start
t.end <- components$t.end
ch.start <- components$ch.start
ch.end <- components$ch.end

### calculate integrals ###

I <- NULL
for (i in X) {
  I <- c(I, sum(signal[c(ch.start[i]:ch.end[i]) ]))
}
components$bin <- I
components$bin.error <- rep(NA, K)
n <- NULL

##### DET #####

if ((algorithm == "det") || (algorithm == "det+nls")) {

  ### define matrices ###

  # Build denominator matrix
  D <- matrix(0,K,K)
  for (i in X) {
    for (j in X) {

      if (is.na(lambda[j])) {

        D[i, j] <- t.end[i] - t.start[i]
      } else {

        D[i, j] <- exp(-t.start[i] * lambda[j]) - exp(- t.end[i] *
          lambda[j])
      }
    }
  }

  # Build enumerator matrices
  A <- list(NULL)
  for (j in X) {

    A.temp <- D
    A.temp[,j] <- I
    A[[j]] <- A.temp
  }

  ### Calculate component amplitudes ###
  for (i in X) {

    n.temp <- det(A[[i]])/det(D)
    n <- c(n, n.temp)
  }
  components$n <- n

} ##### end DET #####

```

```

##### NLS #####

if ((algorithm == "nls") || (algorithm == "det+nls")) {

  # use outcome from DET as start parameters. If not given, use integral
  # values
  if(is.null(n)) n <- I

  ### Create fit formula ###
  n.names <- paste0("n.",1:K)

  if (is.na(components$lambda[K])) {

    lambda <- components$lambda[1:(K - 1)]
    decays <- paste(n.names[1:(K - 1)],
                  " * (exp(-",lambda," * (time - ", channel.width,")) -
                  exp(-",lambda," * time))"
                  , collapse=" + ")
    decays <- paste0(decays, " + ", n.names[K], " * ",channel.width)

  } else {

    decays <- paste(n.names," * (exp(-",components$lambda," *
                  (time - ", channel.width,")) - exp(-",components$lambda," * time))"
                  , collapse=" + ")

  }

  fit.formula <- as.formula(paste0("signal ~ ", decays))
  names(n) <- n.names

  ### try Gauss-Newton fit ###
  fit <- try(nls(fit.formula,
                data = curve,
                start = c(n)),
            silent = TRUE)

  if (attr(fit,"class") == "try-error") {

    if (algorithm == "nls") {

      warning("nls-fit failed. Input component table returned")
      return(components)
    } else {

      if (verbose) warning("nls-fit failed. Falling back to det-results")
      algorithm <- "det-fallback"
    }

  } else {

    n <- coef(fit)
    components$n <- n

    # add error estimations of nls-fit as default
    components$n.error <- summary(fit)$parameters[, "Std. Error"][X]
  }
} ##### end NLS #####

```

```

##### ERROR CALC #####

if ((error.calculation == "empiric")
    || (error.calculation == "poisson")
    || is.numeric(error.calculation)) {

  ### Calculate signal bin variances ###
  I.err <- NULL
  if (error.calculation == "empiric") {

    # Calc reconstructed noise-free curve
    curve <- simulate_OSLcurve(components, curve, simulate.curve = FALSE)

    # Calc corrected sample variance
    for (i in X) {

      if (ch.start[i] == ch.end[i]) {

        # if signal bin consists just of one channel, assume Poisson
        # statistics:
        I.err <- I[i]^0.5
      } else {

        # in all other cases: Use the corrected sample variance formula
        korrektor <- length(ch.start[i]:ch.end[i]) /
          (length(ch.start[i]:ch.end[i]) - 1)
        I.err <- c(I.err,
          (korrektor *
            sum(curve$residual[ch.start[i]:ch.end[i]]^2))^0.5)
      }
    }
  } else {

    # Use poisson approach, add instrumental noise if defined
    if (!is.numeric(error.calculation)) error.calculation <- 0

    for (i in X) {

      I.err[i] <- (I[i] + length(ch.start[i]:ch.end[i]) *
        error.calculation^2 )^0.5
    }
  }
  components$bin.error <- I.err

  ### Propagation of uncertainty ###
  for (k in X) {
    sum.err <- 0

    for (i in X) {

      A.k <- A[[k]]

      # Differate the determinant term after I[j]
      A.k[i,] <- 0
      A.k[,k] <- 0
      A.k[i,k] <- 1

      sum.err <- sum.err + (det(A.k)*I.err[i])^2
    }

    components$n.error[k] <- sum.err^0.5 / det(D)
  }
}

```

```
    }  
  } ##### end ERROR CALC #####  
  
##### component residuals #####  
# set the end of the record as the end of stimulation. Need not to be the  
# same value as t.end  
stim.end <- curve$time[length(curve$time)]  
for (i in X) {  
  components$n.residual[i] <- round(n[i] * exp(- stim.end * lambda[i]))  
}  
  
if (verbose) print(components)  
  
return(components)  
}
```

---



## A.3 Source code calc\_OSLintervals()

### Description

The function provides the integration intervals for CW-OSL component separation with `decompose_OSLcomponents`

### Arguments

<code>components</code>	<code>data.frame</code> ( <b>required</b> ): Table containing the decay constants of the signal components
<code>curve</code>	<code>data.frame</code> ( <i>optional</i> ): OSL signal curve. The x-axis (time axis) will be used to define <code>channel.width</code> and <code>channel.number</code>
<code>channel.width</code>	numeric ( <i>optional</i> ): channel width in seconds. Necessary if <code>curve</code> is not given
<code>channel.number</code>	integer ( <i>optional</i> ): number of channels resp. data points. Necessary if <code>curve</code> is not given
<code>t.start</code>	numeric ( <i>with default</i> ): starting point of the first interval, per default the start of the measurement
<code>t.end</code>	numeric ( <i>optional</i> ): end point of the last interval, per default the end of the measurement

### Return value

The input table `components` `data.frame` will be returned with four additional columns: `$t.start`, `$t.end` defining the interval borders in time  
`$ch.start`, `$ch.end` defining the intervals as channels

---

```
calc_OSLintervals <- function(  
  components,  
  curve = NULL,  
  background.fitting = TRUE,  
  channel.width = NA,  
  channel.number = NA,  
  t.start = 0,  
  t.end = NA,  
  verbose = TRUE  
) {  
  
  ##### is a template curve given? #####  
  
  if (!is.null(curve)) {  
  
    dt <- curve$time[2] - curve$time[1]  
    n <- length(curve$time)
```

```

} else if ((!is.na(channel.width)) && (!is.na(channel.number))) {

  dt <- channel.width
  n <- channel.number

} else {
  warning("No template curve nor channel parameters given")
  return(components)
}

# round start and end point to full increments
t0 <- floor(t.start / dt) * dt

## set t.end if not preset
if (is.na(t.end) || (t.end > n*dt) || (t.end < 3*dt)) {
  t.end <- n*dt
} else {
  t.end <- floor(t.end / dt) * dt
}

# If the background also shall be fitted, add another component with
lambda = 0
if (background.fitting) {

  if (!is.na(components$lambda[nrow(components)])) {
    new.row <- components[nrow(components),]
    rownames(new.row) <- "Background"
    new.row[1:length(new.row)] <- NA
    new.row[1] <- "Background"
    components <- rbind(components, new.row)
  }
} else {

  if (is.na(components$lambda[nrow(components)])) {
    components <- components[1:(nrow(components) - 1),]
  }
}

component.number <- nrow(components)
lambdas <- components$lambda

##### is there just 1 components? #####

if (component.number == 1) {

  components$t.start <- t0
  components$t.end <- t.end
  components$ch.start <- 1 + floor(t0 / dt)
  components$ch.end <- ceiling(t.end / dt)

  return(components)
}

##### Create matrix #####

# channels: just the end of an interval. For example: 1:3 / 4:5 / 6:7
# becomes c(0,3,5,7)
calc_determinant <- function(lambdas, channels, component.number, dt) {

  M <- matrix(0, component.number, component.number)
  for (i in c(1:component.number)) {

```

```

for (j in c(1:component.number)) {

  #P <- exp(-t0 * f.fast) - exp(-t1 * f.fast)
  if (is.na(lambdas[j])) {

    M[i, j] <- channels[i + 1] * dt - channels[i] * dt

  } else {

    M[i, j] <- exp(- channels[i] * dt * lambdas[j]) -
      exp(- channels[i + 1] * dt * lambdas[j])

  }

}

}

# calc determinante
return(abs(det(M)))
}

##### Search for determinant maximum #####

max_found <- FALSE
max_iteration <- 50
iterations <- 0
iterations.stop <- 20 * 2^component.number
iterations.bests <- 2 * 2^component.number
min.ch <- NULL
max.ch <- NULL
A <- data.frame(NULL)

# start parameters for the choosable time intervals
for (i in c(1:component.number - 1)) {
  min.ch <- c(min.ch, i)
  max.ch <- c(max.ch, n - component.number + i)
}

while ((max_found == FALSE) && (iterations < max_iteration)) {

  # create random set of numbers
  interval_set <- c(1,1)
  while (any(duplicated(interval_set))) {
    interval_set <- NULL
    for (i in c(1:(component.number - 1))) {
      interval_set <- c(interval_set, round(runif(1, min = min.ch[i],
        max = max.ch[i])))
    }
  }

  # ... and sort it
  interval_set <- interval_set[order(interval_set)]

  # add start and end value
  #interval_set <- c(t0 / dt, interval_set, t.end / dt)

  # now calc the determinante
  det.value <- calc_determinant(lambdas,
    c(t0 / dt, interval_set, t.end / dt),
    component.number,
    dt)
}

```

```

# append the parameters to a data.frame
A <- rbind(A, c(det.value, interval_set))

if (nrow(A) == iterations.stop) {

  # order list elements by determinant value
  A <- A[order(A[,1]),]

  # reverse order to get large values first and reduce to the best 10
  rows
  A <- A[nrow(A):(iterations.stop - iterations.bests),]

  # check if all elements are the same, then
  if (all(A[,1] == A[1,1])) {

    interval_set <- A[1,2:component.number]
    max_found <- TRUE

    if (verbose) {
      writeLines(paste0("Maximum determinant = ", round(A[1,1],
        digits = component.number + 2),
        " with interval breaking channels [",
        paste0(interval_set, collapse = ", " ),
        "] found after ", iterations * iterations.stop,
        " iterations"))
    }
  } else {

    # redefine start parameters
    for (i in c(1:(component.number - 1))) {
      min.ch[i] <- min(A[,i + 1])
      max.ch[i] <- max(A[,i + 1])
    }
    iterations <- iterations + 1
    A <- data.frame(NULL)
  }
}

components$t.start <- unlist(c(t0, interval_set * dt))
components$t.end <- unlist(c(interval_set * dt, t.end))
components$ch.start <- unlist(c(1 + floor(t0 / dt), interval_set + 1))
components$ch.end <- unlist(c(interval_set, ceiling(t.end / dt)))

return(components)
}

```

# **B Correlation tables**



## B.1 Step 1 – Correlation tables

Calculated with: 2019-08-21\_Test\_Step1.Rmd

### Input-Output correlation:

	K_input	n_Fast	n_Medium	n_Slow1	n_Slow2	Background	Channels	Channelwidth	M.length	Additions
K_output	0.74	0.34	0.31	0.31	-0.02	0.04	0.30	0.23	0.35	0.04
K_out - K_in	-0.27	-0.03	-0.07	-0.25	-0.02	0.07	0.49	0.38	0.58	0.05
ratio Fast	-0.08	0.13	-0.04	-0.07	-0.04	-0.07	0.01	-0.01	0.01	0.05
deviation Fast	0.22	-0.41	0.21	0.09	0.06	0.05	0.00	0.03	0.01	-0.20
missed Fast	-0.41	-0.56	0.01	0.00	0.00	0.02	-0.02	-0.01	-0.02	0.01
ratio Medium	-0.13	-0.03	0.10	-0.12	-0.04	-0.10	0.11	0.04	0.11	0.02
deviation Medium	0.29	0.17	-0.35	0.20	0.05	0.08	-0.12	-0.05	-0.12	-0.13
missed Medium	-0.36	0.01	-0.57	0.03	0.01	0.05	0.02	0.03	0.03	-0.02
ratio Slow1	0.03	0.04	-0.06	0.00	0.12	-0.15	0.05	0.11	0.06	-0.01
deviation Slow1	0.14	0.05	0.07	-0.11	0.03	0.19	-0.14	-0.19	-0.25	-0.13
missed Slow1	-0.16	0.01	0.09	-0.33	0.02	0.05	-0.16	-0.04	-0.14	0.02
ratio Slow2	0.12	0.01	0.03	0.08	0.16	-0.22	-0.21	-0.11	-0.20	-0.01
deviation Slow2	0.20	0.02	0.05	0.21	-0.23	0.32	-0.26	-0.22	-0.32	-0.05
missed Slow2	0.07	0.00	0.01	0.20	-0.20	-0.03	-0.19	-0.14	-0.20	-0.01
Chosen by F criteria	-0.07	-0.06	-0.01	-0.02	0.04	-0.10	0.04	-0.20	-0.10	-0.05
Chi <sup>2</sup>	0.05	0.04	0.06	0.07	0.33	0.11	0.31	0.25	0.38	-0.47
F	-0.52	-0.08	-0.11	-0.34	-0.09	-0.02	0.23	0.19	0.30	0.16
F_K+1	0.06	0.06	-0.01	0.06	-0.01	0.08	-0.02	0.01	-0.01	0.03

### Output cross-correlation:

deviation Fast	-0.34																								
ratio Medium	0.51	-0.10	0.04																						
deviation Medium	-0.19	0.21	-0.17	-0.46																					
missed Medium	-0.04	-0.11	-0.03																						
ratio Slow1	0.23	0.01	-0.05	0.52	-0.13	0.11																			
deviation Slow1	-0.22	0.23	-0.02	-0.23	0.28	-0.02	-0.34																		
missed Slow1	-0.06	0.04	0.00	-0.10	0.03	-0.11																			
ratio Slow2	0.02	0.08	-0.01	0.03	0.12	-0.01	0.57	-0.10	0.15																
deviation Slow2	-0.20	0.14	-0.01	-0.30	0.28	0.00	-0.21	0.39	0.08	-0.09															
missed Slow2	-0.05	0.05	0.03	-0.10	0.12	-0.02	-0.34	0.29	-0.10																
K_output	0.08	0.09	-0.39	0.13	0.05	-0.33	0.11	-0.08	-0.23	-0.10	-0.06	-0.12													
K_out - K_in	0.23	-0.16	0.01	0.36	-0.30	0.03	0.21	-0.37	-0.13	-0.33	-0.44	-0.31	0.33												
Chosen by F criteria	0.12	-0.06	0.06	0.09	-0.08	0.00	0.06	-0.08	0.03	0.05	-0.08	0.00	-0.13	-0.12											
Chi <sup>2</sup>	-0.11	0.20	-0.02	-0.04	0.10	0.03	0.04	0.08	-0.05	0.03	-0.09	-0.08	0.16	0.21	-0.14										
F	0.09	-0.20	0.09	0.16	-0.36	0.19	0.02	-0.36	0.09	-0.19	-0.29	-0.18	-0.25	0.44	-0.09	-0.04									
F_K+1	0.00	0.05	-0.02	-0.03	0.09	0.05	0.07	0.12	0.06	0.09	0.13	0.06	-0.07	-0.22	-0.02	-0.02									
	ratio Fast	deviation Fast	missed Fast	ratio Medium	deviation Medium	missed Medium	ratio Slow1	deviation Slow1	missed Slow1	ratio Slow2	deviation Slow2	missed Slow2	K_output	K_out - K_in	Chosen by F criteria	Chi <sup>2</sup>	F								

## B.2 Step 2 – Correlation tables

Calculated with: 2019-11-15\_Test\_Step2.Rmd

No simulated background signal; no background determination; Method = det

### Input-Output correlation:

	K	n.Fast	n.Medium	n.Slow1	n.Slow2	Channels	Channel.width	M.length
Fast.R_n	-0.02	-0.04	-0.02	-0.01	-0.01	0.02	0.04	0.02
Fast.s_dec	0.30	-0.68	0.32	0.12	0.18	-0.01	0.00	-0.01
Fast.inside	0.18	-0.33	0.16	0.08	0.26	0.13	-0.23	-0.08
Medium.R_n	-0.01	0.02	0.05	-0.03	0.02	0.00	-0.04	-0.02
Medium.s_dec	0.35	0.20	-0.65	0.24	0.21	-0.08	-0.06	-0.09
Medium.inside	0.06	0.03	-0.12	0.02	0.16	0.08	-0.13	-0.05
Slow1.R_n	0.06	-0.02	0.04	0.00	0.02	-0.03	-0.01	-0.01
Slow1.s_dec	0.18	0.05	0.16	-0.43	0.29	-0.37	-0.31	-0.47
Slow1.inside	0.03	0.03	0.03	-0.04	0.02	0.02	-0.06	-0.02
Slow2.R_n	-0.02	0.02	-0.02	-0.01	-0.01	0.03	0.02	0.03
Slow2.s_dec	0.28	0.02	0.06	0.34	-0.28	-0.46	-0.39	-0.60
Slow2.inside	0.02	-0.03	0.04	0.01	0.00	0.05	-0.05	0.00

### Output cross-correlation:

Fast.s_dec	0.03										
Fast.inside	0.03	0.44									
Medium.R_n	-0.44	-0.02	-0.02								
Medium.s_dec	0.02	0.00	0.13	-0.04							
Medium.inside	0.04	0.05	0.28	-0.01	0.16						
Slow1.R_n	0.17	0.10	0.07	-0.49	0.03	0.02					
Slow1.s_dec	-0.02	0.14	0.19	0.03	0.18	0.12	0.04				
Slow1.inside	0.07	-0.01	0.06	-0.06	0.01	0.31	0.04	0.04			
Slow2.R_n	-0.06	-0.05	-0.05	0.19	-0.01	-0.01	-0.60	-0.03	-0.02		
Slow2.s_dec	-0.01	0.03	0.02	0.01	0.11	0.00	0.01	0.28	0.00	-0.02	
Slow2.inside	0.01	0.03	0.08	0.02	-0.01	0.13	-0.04	0.02	0.34	0.03	
	Fast.R_n	Fast.s_dec	Fast.inside	Medium.R_n	Medium.s_dec	Medium.inside	Slow1.R_n	Slow1.s_dec	Slow1.inside	Slow2.R_n	Slow2.s_dec



# C Decomposition analysis reports

## C.1 Full BT594 analysis report

### OSL decomposition report (*alpha version*)

#### Table of Contents

Basic idea.....	20
Script & data parameter .....	20
Data pre-treatment .....	21
Step 1 – Evaluation of component number and decay constants .....	22
Step 2 – Single curve decomposition .....	26
Step 3 – Equivalent dose calculation .....	28
Rejection criteria.....	30
Paleodose and age estimation .....	32
Summary .....	33
References .....	<b>Fehler! Textmarke nicht definiert.</b>

Data set                                    BT594\_607\_608\_612\_619.BIN  
Script executed at                        2019-10-29 15:02:24

#### **Preface**

This report was automatically generated using the **Rmarkdown** (see Xie *et al.* 2018) script **EvaluateDataSet.Rmd** in the **R** package **OSLdecomposition** written and maintained by Dirk Mittelstraß (dirk.mittelstrass@luminescence.de). The dose calculation deploys also functions of the R packages **numOSL** introduced by Jun Peng *et al.* (2013) and **Luminescence** introduced by Sebastian Kreuzer *et al.*(2012)

This report and the containing results can be used, shared and published by the data set maintainer at will. If the results are published, however, it is demanded to state the main **R** package **OSLdecomposition** including its version number (0.10.28). It is also recommended to add this report to the supplement of your publication.

## **Basic idea**

The method is based on the assumption, that every OSL curve can be described as sum of signal components (Bailey *et al.* 1997). It is further assumed, that each signal component can be described by an exponential decay following first order kinetics. The shape of every CW-OSL curve can then be modelled by:

$$I(t) = \sum_{i=1}^K n_i \lambda_i \exp(-\lambda_i t)$$

Here,  $I(t)$  represents the luminescence signal during continuous stimulation,  $K$  the number signal components,  $n_i$  the integrated signal intensities (or just 'signal values') of each signal component and  $\lambda_i$  their decay constants. We also assume, that the set of decay constants is the same for all OSL curves in a given data set. So we can apply the following data analysis approach:

- 
1. Determine the component number  $K$  and the decay parameters  $\lambda_1, \dots, \lambda_K$  globally by multi-exponential decay fitting at one representative superposition OSL curve
  2. Determine the signal values  $n_1, \dots, n_K$  for each OSL curve by a decomposition algorithm
  3. Determine the natural dose signal component-wise by building separate signal-dose growth curves for each set of  $n_i$  values
- 

## **Script & data parameter**

### **Script conditions**

---

Script version	2019-10-28
R version	3.6.1
Packages performing calculations	OSLdecomposition 0.10.28 Luminescence 0.9.5 numOSL 2.6

The data set is imported to **R** by the function **Luminescence::read\_BIN2R()** programmed by Kreutzer and Fuchs (2019). Files in the BIN and the BINX format produced by Risoe DA15, Risoe DA20, lexsyg research and lexsyg smart TL/OSL readers are supported.

### **Data set conditions**

---

Evaluated record types	OSL
Data set entries (aliquots)	48
Indices of dismissed aliquots	25 - 48
Indices of background measurements	none
Analyzed aliquots	24
OSL records per entry	14
Channels	$N = 100$
Channel width	$\Delta t = 0.2 \text{ s}$
Measurement time	$t_{end} = 20$

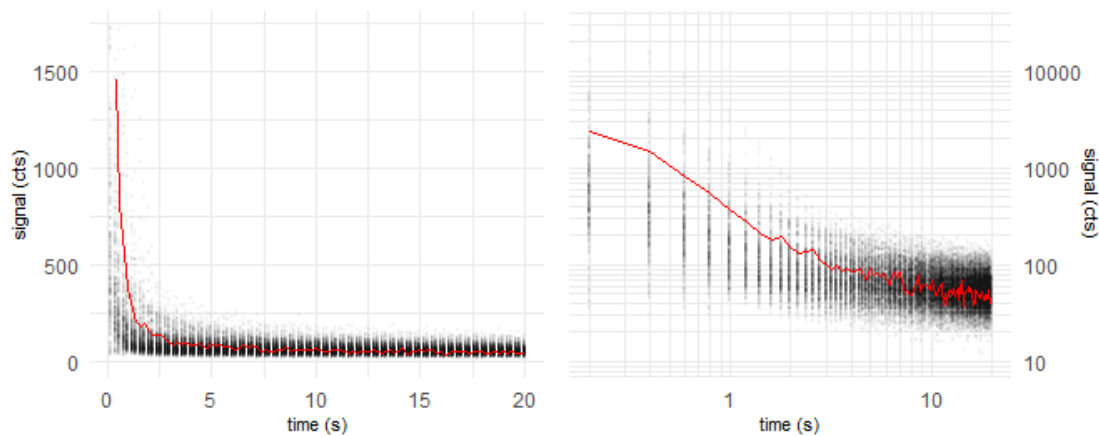


Figure 1: Raw data points of all OSL curves (grey opaque) and natural dose OSL curve of first aliquot (red)

### Sample conditions

Sample type	coarse grain quartz
Expected age	~ 25 ka
Environmental dose rate	2.92 Gy ka <sup>-1</sup>
Expected dose	~ 73 Gy
Laboratory dose rate	0.1373 Gy s <sup>-1</sup>
Stimulation wavelength	470 nm
Assumed stimulation intensity	50 mW cm <sup>-2</sup>

### Algorithm settings

Cut measurements if exceeding	$t_{max} = 40$ s
Maximum allowed components	$K_{max} = 5$
Threshold $F$ -value	$F_{threshold} = 50$
Decomposition algorithm	det+nls
Growth curve fitting algorithm	EXP
Allowed recuperation	5%
Allowed recycl. ratio deviation	10%

### Data pre-treatment

Prior data evaluation, the records will be corrected for signal background, measurement over-length, etc., depending on the script settings and the provided data. The following corrections were performed by applying the function `prepare_OSLdata()`:

**Step 1 – Evaluation of component number and decay constants**

For calculating the decay parameters, one representative OSL curve is needed. This is provided by combining all records to one global mean curve. Each data point of the global curve represents the arithmetic mean of all data point values of the same channel in all OSL curves. This increases the signal-to-noise ratio by about one to two orders of magnitude, but still maintains the decay parameter information.

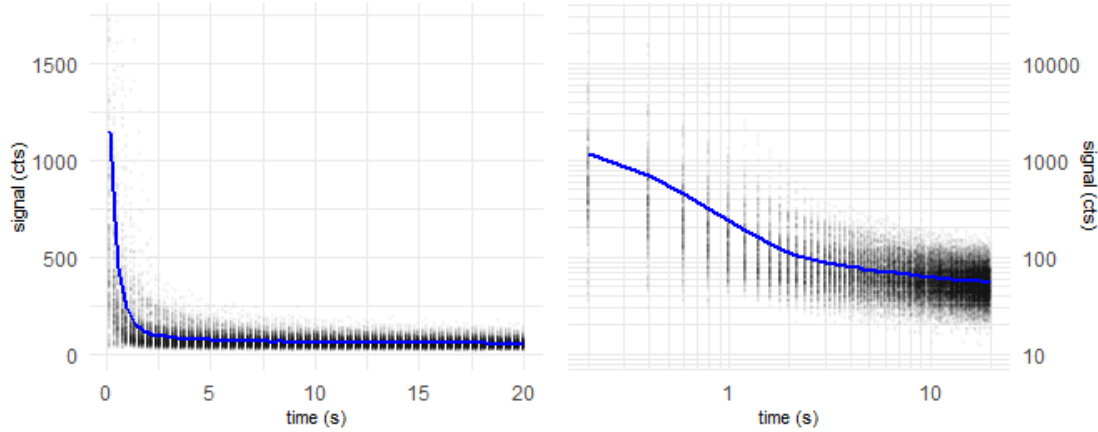


Figure 2: Global mean OSL curve (blue) and data points of all OSL records (grey opaque)

We take the global mean curve and perform a multiple cycles of multi-exponential nonlinear regression. In each cycle, the number of components  $K$  increases by one. With increasing number of components, decreases the signal deviation (residual curve) between the fitted model curve and the measured data and the fit gets better.

The underlying algorithm was proposed and described by Bluszcz & Adamiec (2006) and realized in R by the function `numOSL::decomp()` by Peng *et al.* (2013). Their function is used in `fit_OSLcurve()`, which calculated the following series of fittings, displayed with `plot_OSLcurve()`:

The subsequent diagrams are structured the following way:

- Upper left: Global mean curve (grey), fit model curve (black) and component signals
- Upper right: Same as log-log diagram
- Lower left: Residual curve between fit and global mean curve
- Lower right: Result table with estimated type of component names (colored)

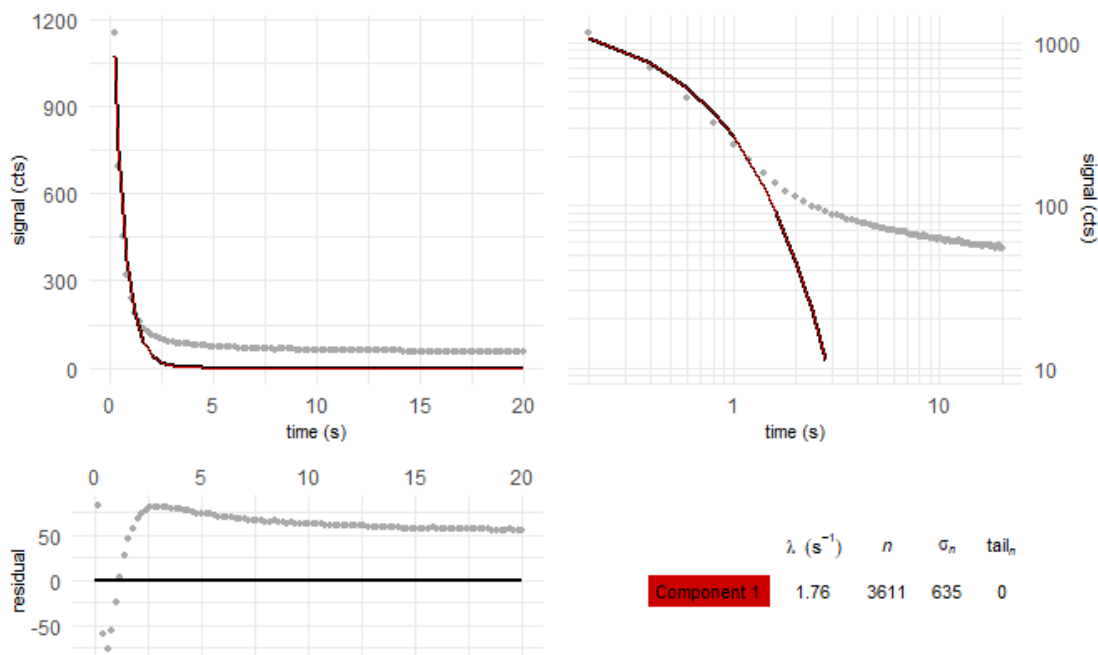


Figure 3: Global mean curve fit with  $K = 1$  components

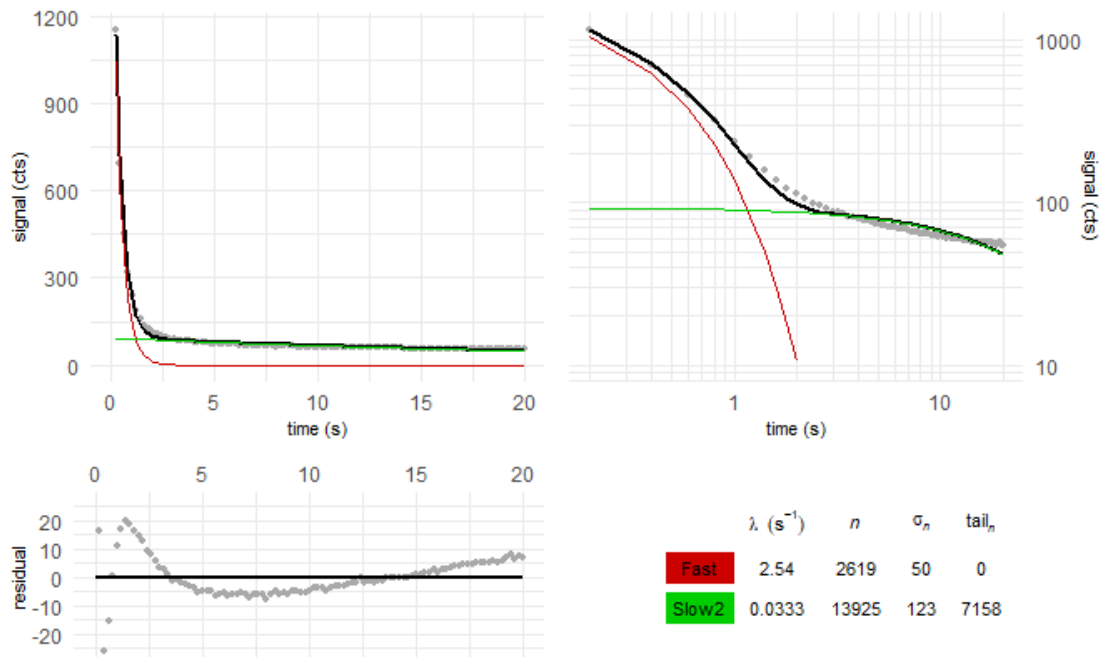


Figure 4: Global mean curve fit with  $K = 2$  components

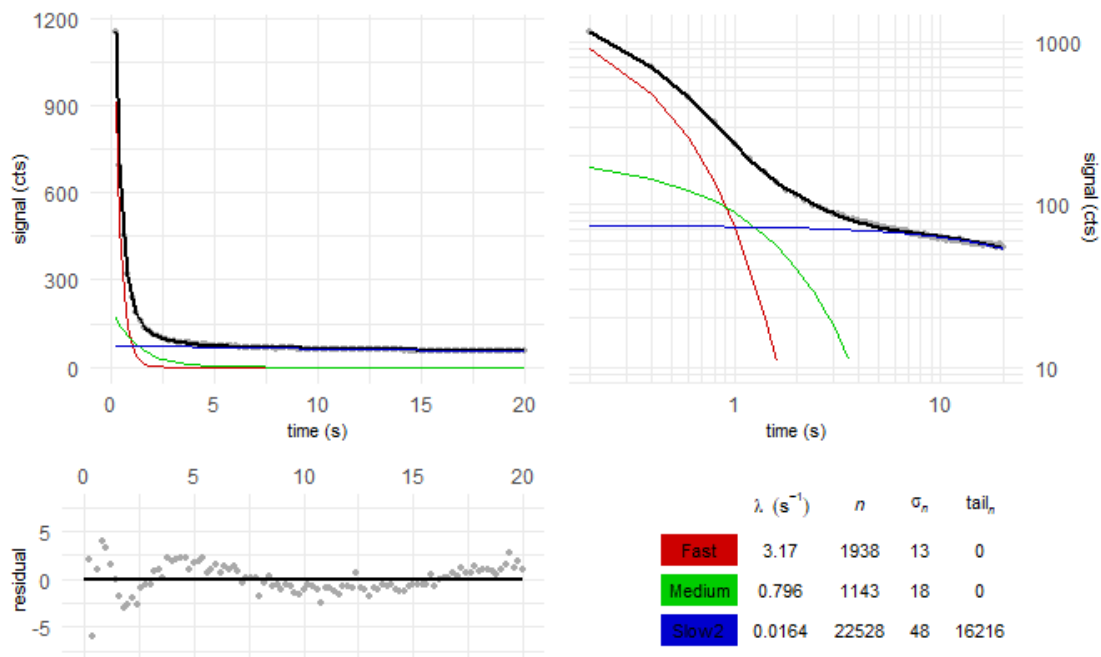


Figure 5: Global mean curve fit with  $K = 3$  components

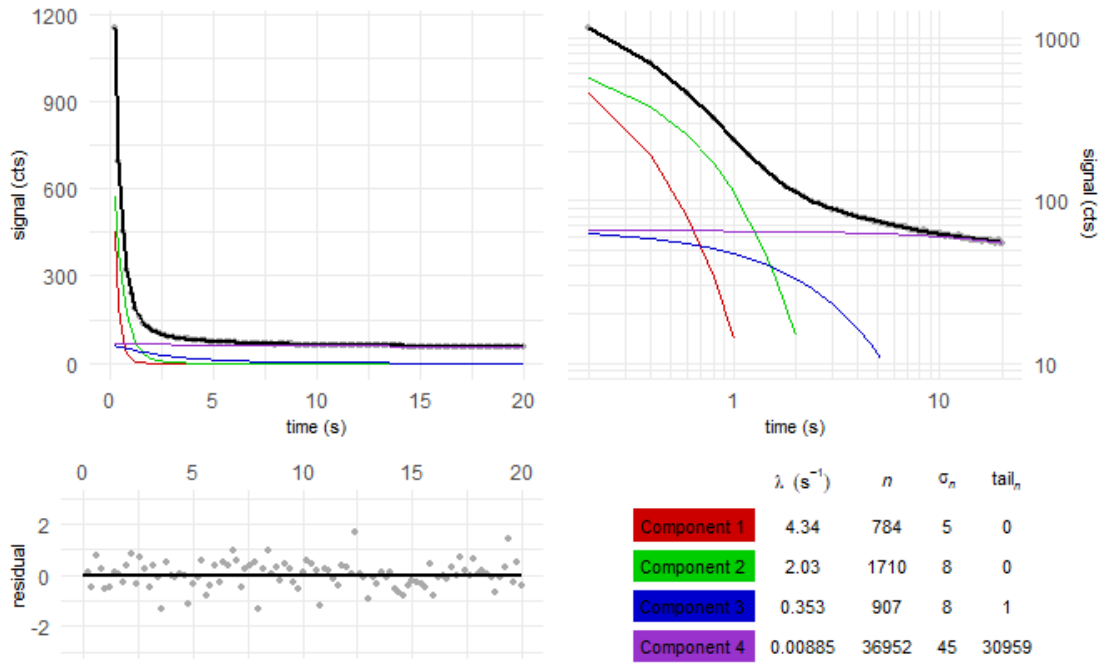


Figure 6: Global mean curve fit with  $K = 4$  components

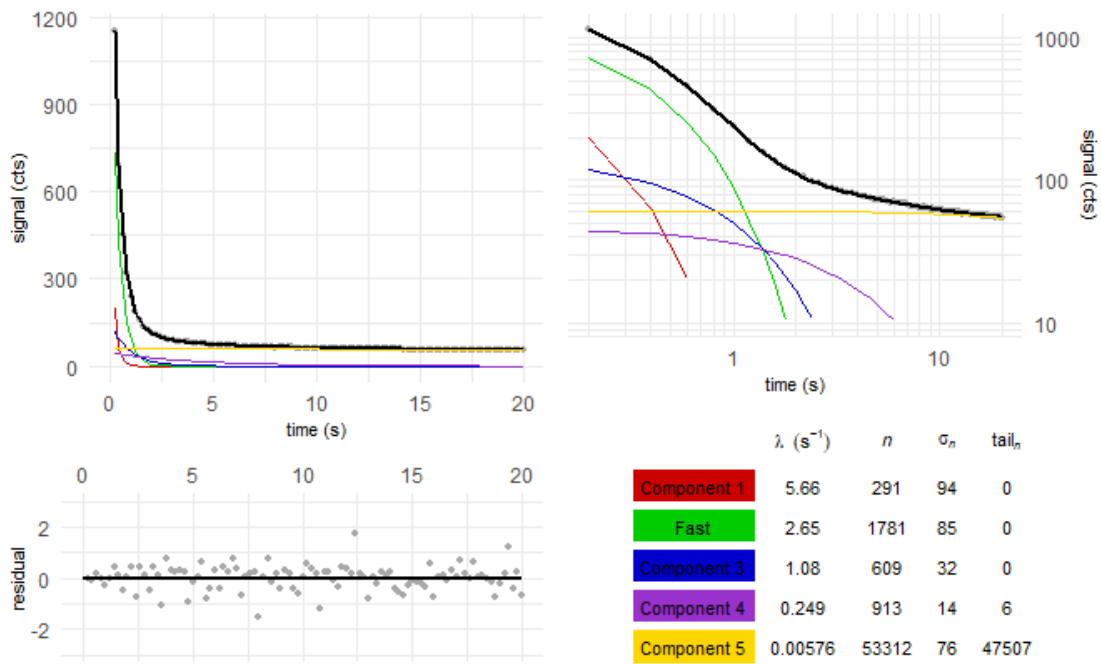


Figure 7: Global mean curve fit with  $K = 5$  components

### F-test

But which of these fittings gives back a sufficient model of the global mean curve, without over-fitting it? We solve this by comparing the residual square sum (RSS) of each fitting with the RSS value of the previous fitting. Bluszcz & Adamiec (2006) propose to use a F-test:

$$F_K = \frac{(RSS_{K-1} - RSS_K)/2}{RSS_K(N - 2K)}$$

If  $F_K$  falls below the preset threshold value of  $F_{threshold} = 50$ , the new fitting model with  $K$  components is apparently not significantly better than the  $K - 1$  model.

Table 1: Decay constants and fit quality parameters for multi-exponential decay fitting with  $K$  components

K	$\lambda_1 (s^{-1})$	$\lambda_2 (s^{-1})$	$\lambda_3 (s^{-1})$	$\lambda_4 (s^{-1})$	$\lambda_5 (s^{-1})$	RSS	$F_K$
1	1.76					3.99e+05	
2	2.54	0.0333				4.84e+03	3.91e+03
3	3.17	0.796	0.0164			216	1.01e+03
4	4.34	2.03	0.353	0.00885		27.1	320
5	5.66	2.65	1.08	0.249	0.00576	24	5.79

The fitting with  $K = 4$  components is found to be the best suiting model to describe the given sample. Signal components with not-first-order kinetics, however, can lead to over-fitting. It is recommended to take the results of the  $K = 3$  fitting model also into consideration.

If the sample was measured with a stimulation light wavelength of about 470 nm and a stimulation light intensity of  $50 \text{ mW cm}^{-2}$  as presetted, the photoionisation cross-sections of the components can be calculated. These can be compared with the quartz LM-OSL findings given in literature.

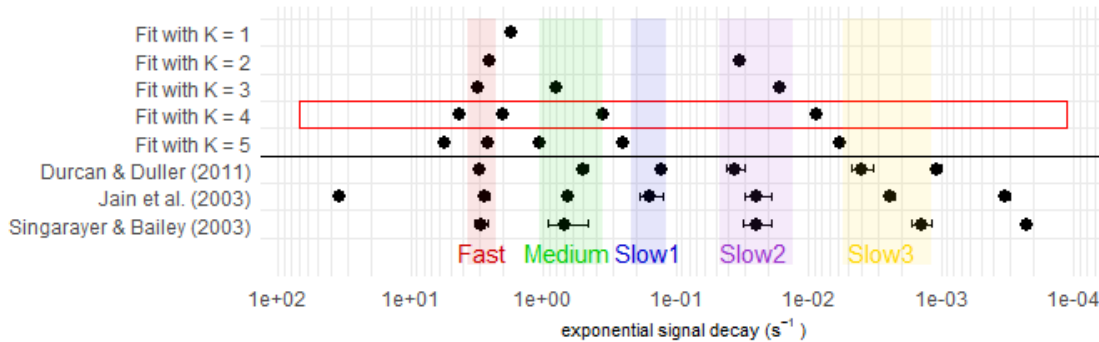


Figure 8: Comparison of decay constants between fitting cases and comparison with reference values. Red square: Best fit

## Step 2 – Single curve decomposition

In Step 2, we decompose each OSL curve into its signal components. We set the decay constants found in Step 1 as fixed values for all OSL curves of the data set. This allows us to apply the following signal decomposition method:

1. Divide the measurement time into  $K$  intervals. These intervals are calculated and optimized globally by **calc\_OSLintervals()**.
2. Integrate the signal curve of each OSL record over these intervals. From the integration values and the fitting model found in Step 1, build one equation system with  $K$  equations for each OSL record.
3. Solve the equation system by an analytic determinant based method, called 'Cramer's rule', and get the area under the component curve or 'intensity'  $n_k$  for each signal component
4. To enhance stability and precision of the method, refine the set of  $n_k$  values in a quasi-linear regression using **base::nls()**. If this refining-fit fails, go on with the Cramer's rule achieved values.
5. Calculate the standard deviation of the integration values from step 2 by the residuals between fit-model OSL curve and real data points
6. Apply the propagation of uncertainty method onto Cramer's rule and calculate the uncertainty  $\sigma_k$  for each component intensity value  $n_k$

All steps, beside the first step, are realized in **decompose\_OSLcurve()**. The table in figure 9 displays the particular outcome of this method for the  $K = 4$  model applied at the first OSL curve of the first aliquot as example. The parameter  $tail_n$  gives back the area under the component which is not displayed in the OSL diagram. If the measurement was not cutted in the data-pretreatment and an appropriate background correction was performed,  $tail_n$  equals the not-released signal of the component.

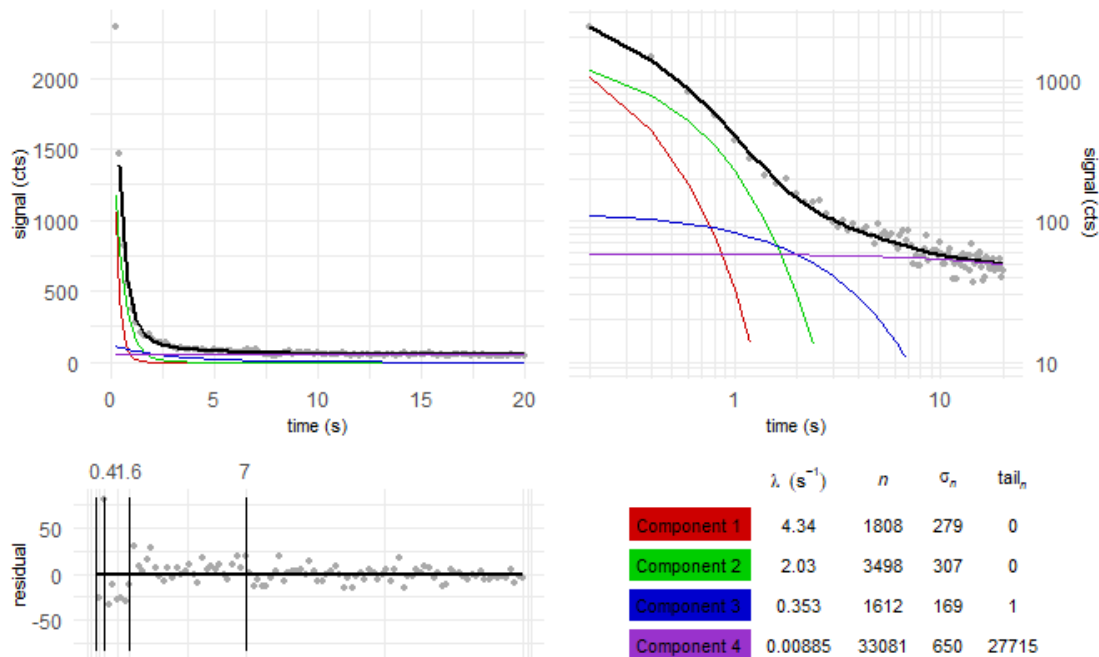


Figure 9: 4-component decomposition of the first OSL record in the data set. The vertical lines in the residual diagram show the integration intervals



## L/T table

We assume the data set is measured in accordance to the SAR protocol defined by Murray and Wintle (2000). Then every OSL measurement is followed by the regeneration of a fixed test-dose (here 0 Gy) and the measurement of the OSL signal related to this test-dose. The testdose-related OSL signal is indicated by the variable  $T_n$ , the natural and regenerated dose OSL signal is indicated by the variable  $L_i$ . The normalized OSL signal is therefore given by  $L_i/T_i$ .

A L/T table provides a structure for the signal values and dose regeneration points we need to build dose-signal curves in Step 3 and to test for signal behaviour criteria. One L/T table per signal component and aliquot is built. To avoid some potential issues in Step 3, we apply the following conditions when assigning the signal values to the table:

- If the measurement time was not cutted: Subtract the value of  $tail_n$  from the  $n_k$  value of the subsequent OSL measurement. This enables correctly built L/T tables for slow decaying components.
- If the measurement time was cutted: Do not build L/T tables of a component, when more than 1% of the components signal would be transferred into  $tail_n$ . So the component can not be further evaluated and misleading conclusions are avoided.
- Set negative  $L_i/T_i$  values to  $L_i/T_i = 0$  to avoid calculation issues although negative values are mathematically and physically possible (due to photo-transfer).

Table 2: L/T table of fastest decaying component of first aliquot for the  $K = 4$  case. Test dose for generating all  $T_i$  is:  $D_T = 0$  Gy

$i$	dose (Gy)	$L_i/T_i$	$\sigma_{L_i/T_i}$	$L_i$	$\sigma_{L_i}$	$T_i$	$\sigma_{T_i}$
0	natural	3.13	0.16	5638	99	1801	86
1	19.3593	1.08	0.05	1984	46	1831	70
2	48.3296	2.32	0.13	4444	116	1914	93
3	83.8903	3.63	0.11	7192	187	1979	34
4	103.2496	3.96	0.17	8527	271	2154	65
5	19.3593	1.15	0.05	2625	92	2289	64
6	0	0.00	0.02	-26	49	2311	72

### Step 3 – Equivalent dose calculation

From the L/T table, we create a signal dose curve or “growth curve” by calling the function **Luminescence::plot\_GrowthCurve()** programmed by Kreutzer and Dietze (2019). The function plots the luminescence signal values  $y = L_i/T_i$  against the regeneration doses  $x = D_i$ . Several fitting models are selectable. We will use the default model:

$$y(x) = a(1 - e^{-(x+c)/b})$$

Here  $a$ ,  $b$  and  $c$  are fitting factors. The natural or ‘equivalent’ dose  $D_e$  related to the natural luminescence signal is calculated by solving  $y(D_e) = L_0/T_0$ . The uncertainty of the equivalent dose  $D_e$  is calculated by a Monte Carlo simulation assuming normal distributed  $L_i/T_i$  values with a standard deviation equal to  $\sigma_{L_i/T_i}$ .

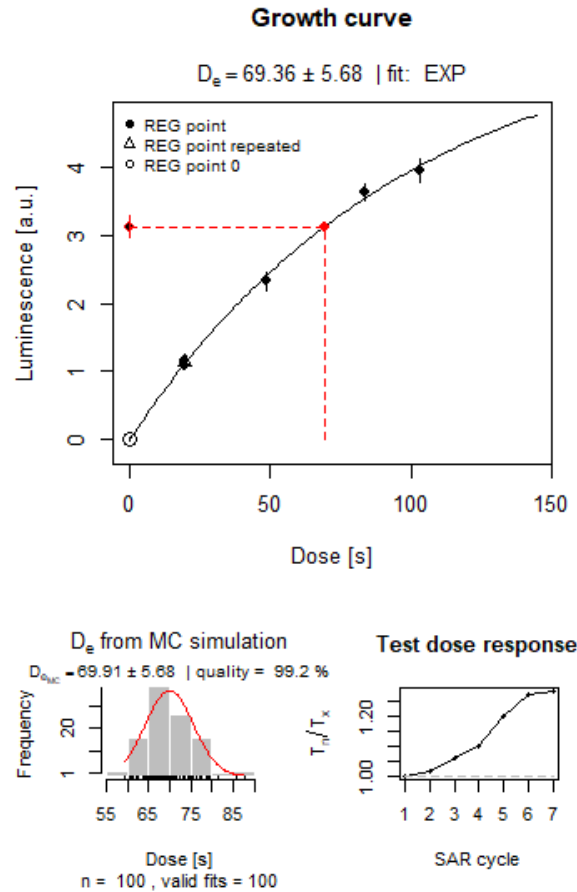


Figure 10: Signal-dose curve of the fastest decaying component of the first aliquot, plotted by **Luminescence::plot\_GrowthCurve()**. Lower left: Distribution of Monte Carlo simulated  $D_e$  values, used to calculate the  $D_e$  error value. Lower right: Variation of the normalized Test dose signal over the measurement sequence, useful to display luminescence sensitivity changes.

We calculate the equivalent doses  $D_e$  for all aliquots and all components for which L/T tables were built. We do this not just for the  $K = 4$  case we selected per  $F$ -test in Step 1 but also for all  $K < 4$  cases. This way, we gain dose information even if the  $K = 4$  doses aren’t successfully evaluated due to low signal-to-noise ratio or over-fitting in Step 1.

### Classic signal calculation approaches

For comparison, we also calculate  $D_e$  values by late light background subtraction and early light background subtraction. The late light background subtraction approach or short ‘late background’ approach was defined by Murray & Wintle (2000) in their definition of the standard SAR protocol. Here, the function

`calc_classisOSLsignal()` performs the signal calculation and sets the integration intervals following the rules by Murray & Wintle (2000). The ‘early background’ approach introduced by Cunningham and Wallinga (2010) try to remove not-Fast-signal components by subtraction the signal directly after the Fast signal decayed.

For this data set, the following signal and background intervals hat been determined:

	Signal interval	Background interval
Late light background subtraction	0 to 0.6 s	14 to 20 s
Early light background subtraction	0 to 0.4 s	0.4 to 1.4 s

The simplest way to estimate the stored dose information is by calculating the medians of the  $D_e$  populations.

Table 4: Medians of the  $D_e$ -distributions from 24 aliquots from different signal calculation approaches. The first line lists the median values of the fastest decaying signal component, the second line the second fastest, etc.. The value inside the brackets () shows the number of successful calculated  $D_e$ 's.

comp.	late b.	early b.	K = 1	K = 2	K = 3	K = 4
1	60 Gy (24)	67 Gy (24)	61 Gy (24)	60 Gy (24)	75 Gy (22)	71 Gy (20)
2				97 Gy (23)	34 Gy (23)	59 Gy (20)
3					131 Gy (22)	18 Gy (23)
4						188 Gy (20)

Note, that fit failures are common and can happen if the  $L_i/T_i$  values have to large errors or don't follow a growth curve or if  $L_0/T_0$  is larger than the fit parameter  $a$ .

Table 4 vizualized in a series of box plots, we get:

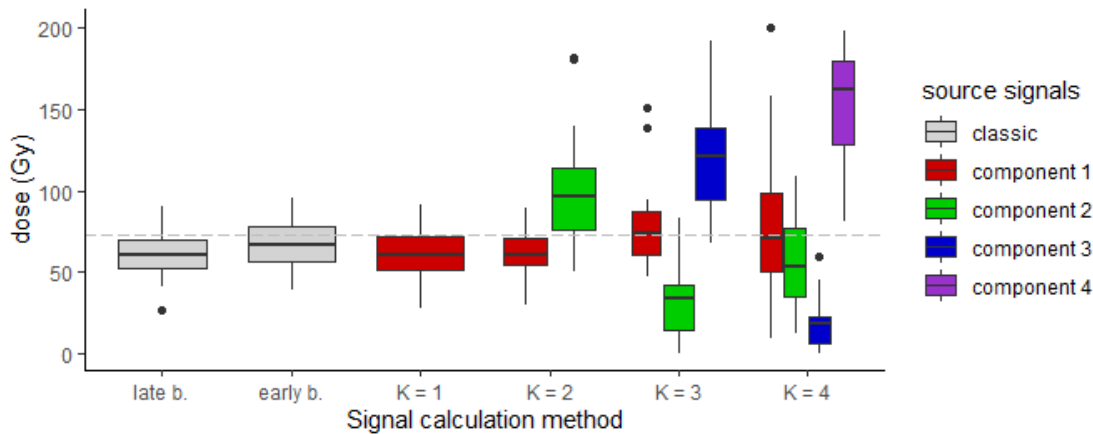


Figure 11: Box plots of the  $D_e$ -distributions from 24 aliquots from different signal calculation approaches. The dashed line shows the expected does. Box plot rules: The whiskers enclose all four quartiles besides outlier. The rectangles enclose the second and third quartile. The middle line shows the median

### **Rejection criteria**

The equivalent doses calculated so far, are not necessarily physical meaningful. Murray and Wintle introduced two tests to detect and reject not trustworthy  $D_e$  values.

### **Recycling ratio test**

In the SAR protocol, the first and the last dose regeneration cycle apply usually the same dose (=recycled dose). The generated normalized luminescence signals  $L_1/T_1$  and  $L_{last}/T_{last}$  should be about equal. If the ratio between both differs significantly from one, it implicates that the applied doses cannot be monitored precisely.

*Table 5: Mean and standard deviation of the recycling ratios from all successfully fitted aliquots*

comp.	late b.	early b.	K = 1	K = 2	K = 3	K = 4
1	$0.96 \pm 0.1$	$0.99 \pm 0.16$	$0.94 \pm 0.08$	$0.95 \pm 0.12$	$0.99 \pm 0.2$	$1.08 \pm 0.83$
2				$0.92 \pm 0.13$	$0.97 \pm 0.83$	$1.22 \pm 0.88$
3					$1.05 \pm 0.39$	$0.89 \pm 0.54$
4						$2.26 \pm 2.11$

Be aware, that the recycling ratio calculation is quite noise-sensitive, especially if small test doses are chosen. For low-SNR data sets, false positive as well as false negative aliquot rejections are likely.

### **Recuperation test**

In the regeneration cycle after the cycle with the largest applied dose, usually no dose is applied before measuring  $L_i$ . If no dose is applied, the corresponding normalized luminescence signal  $L_i/T_i$  should be about zero. The occurrence of significant luminescence signal hints towards the appearance of charge transfer into the observed OSL traps unrelated to dose regeneration.

*Table 6: Mean and standard deviation of the recuperation rates from all successfully fitted aliquots*

comp.	late b.	early b.	K = 1	K = 2	K = 3	K = 4
1	$0.016 \pm 0.014$	$0.009 \pm 0.011$	$0.111 \pm 0.058$	$0.001 \pm 0.002$	$0.011 \pm 0.015$	$0.024 \pm 0.04$
2				$0.265 \pm 0.108$	$0.037 \pm 0.104$	$0.046 \pm 0.109$
3					$0.082 \pm 0.076$	$0.492 \pm 1.312$
4						$0.005 \pm 0.017$

We use the range of acceptance proposed by Murray and Wintle (2000) for both tests:

	Formula	Range of acceptance
Recycling ratio	$r_{recycling} = \frac{L_1/T_1}{L_{last}/T_{last}}$	$0.9 < r_{recycling} < 1.1$
Recuperation rate	$r_{recuperation} = \frac{L_{D_i=0}/T_i}{L_0/T_0}$	$r_{recuperation} < 0.05$

How many aliquots fullfill these criteria?

Table 7: Number of aliquots which passed rejection criteria successfully.

comp.	late b.	early b.	K = 1	K = 2	K = 3	K = 4
1	13 of 24	14 of 24	2 of 24	11 of 24	9 of 24	1 of 24
2				1 of 24	3 of 24	4 of 24
3					1 of 24	1 of 24
4						9 of 24

Applying the test criteria should reject the majority of inaccurate  $D_e$  measurements. How does this change the  $D_e$  dose distribution?

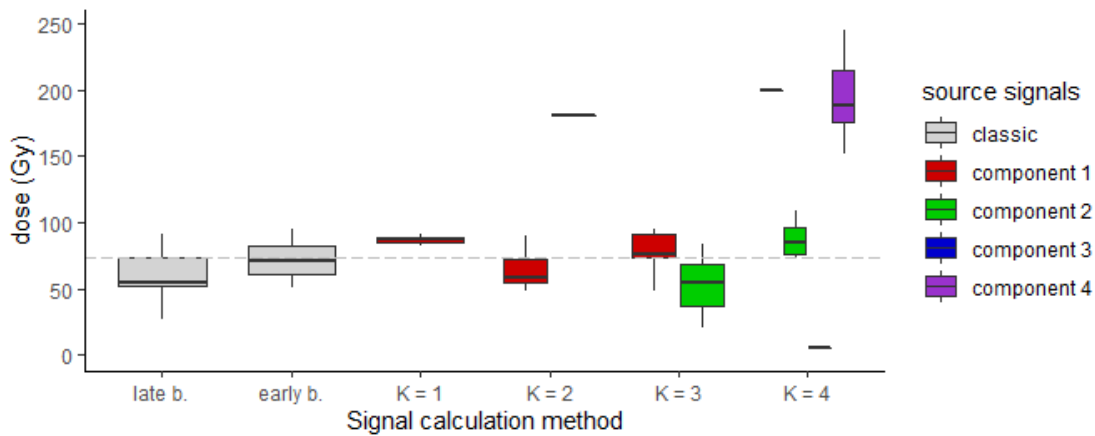


Figure 12: Box plots of the  $D_e$ -distributions from 24 aliquots which passed the rejection criteria.

## Paleodose and age estimation

We will use two approaches to calculating the burial age from a distribution of equivalent dose values which are common in the geoscientific community: The central age model and the minimum age model. Both models were introduced by Galbraith et al. (1999) and are comprehensively summarized in Galbraith and Roberts (2012). We will use this step also to transform the dose values into age values, given an environmental dose rate was given at the beginning of this script.

### Central age model

The central age model (short: 'CAM') proposed by Galbraith et al. (1999) assumes that the logarithmic values of the  $D_e$ 's are about normal distributed. But this normal distribution arises not just from measurement errors of the  $D_e$ -evaluation but also from unknown geologic or physical uncertainties. The CAM algorithm try to calculate a variance-weighted arithmetic mean from the  $\log(D_e)$  values but includes an unknown uncertainty parameter in the weighing term, called 'overdispersion'. The overdispersion  $\sigma_b$  is used as second fitting parameter besides the paleodose. In case the  $D_e$ -distribution is just caused by instrumental errors, the overdispersion should be around zero. For geologic samples, overdispersions up to  $\sigma_b = 0.5$  are common. We calculate the CAM paleodoses using `Luminescence::calc_CentralDose()` programmed by Burow (2019a).

In a nutshell: The CAM resulting paleodose is a kind of weighted geometric mean of the equivalent doses with an extra property (the overdispersion) indicating the pre-measurement dose uncertainty.

*Table 8: Central age model obtained paleodoses. In the brackets: overdispersion.*

comp.	late b.	early b.	K = 1	K = 2	K = 3	K = 4
1	$20 \pm 1.7$ ka (0.3)	$24.1 \pm 1.5$ ka (0.17)	$30.6 \pm 6.6$ ka (0)	$22.2 \pm 1.4$ ka (0.17)	$28.9 \pm 1.3$ ka (0.04)	-
2				-	$19.6 \pm 3.3$ ka (0)	$32.1 \pm 5.4$ ka (0)
3					-	-
4						$72.7 \pm 5.4$ ka (0.15)

### Minimum age model

The central age model does not take into account that the sample might be bleached incompletely before the burial event. For that case, Galbraith et al. (1999) assume a truncated normal distribution of the  $D_e$  values spreaded towards higher doses. The central age model would lead to over-estimated paleodoses, so they added one more fitting parameter to the CAM approach to compensate for the spreading. If the MAM paleodose is significantly lower than the CAM paleodose, incomplete bleaching before burial is likely. We calculate the MAM paleodoses using `Luminescence::calc_CentralDose()` programmed by Burow (2019b).

*Table 9: Minimum age model obtained paleodoses.  $\sigma_b = 0.2$ .*

comp.	late b.	early b.	K = 1	K = 2	K = 3	K = 4
1	$15.7 \pm 2.7$ ka	$24 \pm 2.6$ ka	$30.5 \pm 11.2$ ka	$22.1 \pm 2.5$ ka	$26.8 \pm 3.5$ ka	$68.5 \pm 363016.8$ ka
2				$62 \pm 21.3$ ka	$19.6 \pm 6.5$ ka	$31.3 \pm 8.5$ ka
3					$312.6 \pm 138$ ka	$1.8 \pm \text{Inf}$ ka
4						$73.2 \pm 10.4$ ka

In the MAM algorithm the overdispersion  $\sigma_b$  becomes an input parameter. In lack of experimental obtained  $\sigma_b$  (a fully bleached sample is needed), we set  $\sigma_b = 0.2$  per default, as proposed by Galbraith and Roberts (2012).

**Summary**

Signal-component wise dose evaluation of the file **BT594\_607\_608\_612\_619.BIN**:

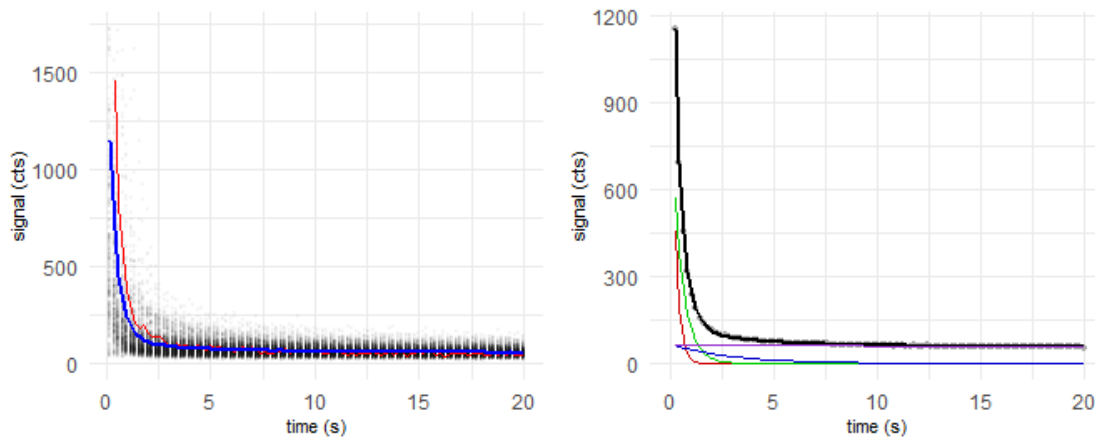


Figure 13: Left: Data points of whole data set with first curve (red) and global mean curve (blue). Right: Global mean curve (grey) fitted (black) with 4 components (colored)

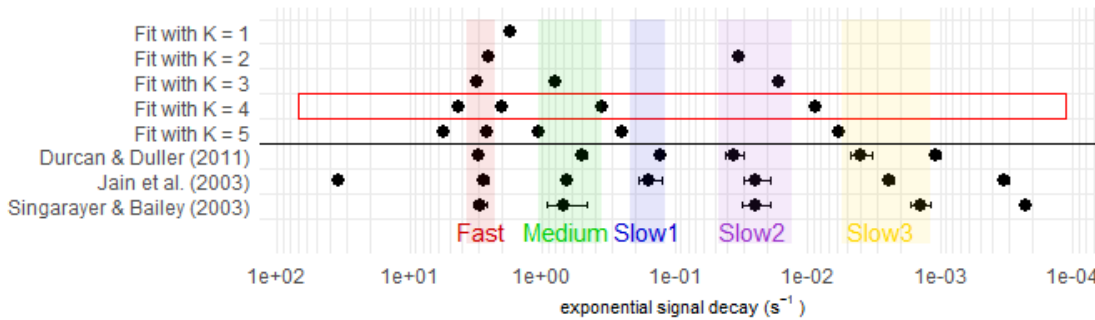


Figure 14: Evolution of the decay constants with increasing number of components K. Red square: Best fit chosen through F-test

Table 10: Result overview. Mean intensity: Area under the signal component curve in the global mean OSL curve. Passed aliquots: How many aliquots with successfully obtained  $D_e$  value passed the rejection criteria? CAM and MAM use just passed aliquots. CAM: Overdispersion ratio in brackets. MAM: Overdispersion ratio is assumed to be 0.2.

Method	Component	Decay constant	Mean intensity	Passed aliquots	Central age model	Minimum age model
late b.				13 of 24	$20 \pm 1.7$ ka (0.3)	$15.7 \pm 2.7$ ka
early b.				14 of 24	$24.1 \pm 1.5$ ka (0.17)	$24 \pm 2.6$ ka
K = 3	Fast	$3.2 \text{ s}^{-1}$	$1.9\text{e}+03$	9 of 24	$28.9 \pm 1.3$ ka (0.04)	$26.8 \pm 3.5$ ka
K = 3	Medium	$0.8 \text{ s}^{-1}$	$1.1\text{e}+03$	3 of 24	$19.6 \pm 3.3$ ka (0)	$19.6 \pm 6.5$ ka
K = 3	Slow2	$0.016 \text{ s}^{-1}$	$2.3\text{e}+04$	1 of 24	-	$312.6 \pm 138$ ka
K = 4	Component 1	$4.3 \text{ s}^{-1}$	$7.8\text{e}+02$	1 of 24	-	$68.5 \pm 363016.8$ ka
K = 4	Component 2	$2 \text{ s}^{-1}$	$1.7\text{e}+03$	4 of 24	$32.1 \pm 5.4$ ka (0)	$31.3 \pm 8.5$ ka

K = 4	Component 3	$0.35 \text{ s}^{-1}$	$9.1\text{e}+02$	1 of 24	-	$1.8 \pm \text{Inf ka}$
K = 4	Component 4	$0.0088 \text{ s}^{-1}$	$3.7\text{e}+04$	9 of 24	$72.7 \pm 5.4 \text{ ka}$ (0.15)	$73.2 \pm 10.4 \text{ ka}$

Computing time: 10.60348 mins



## C.2 BT1214 analysis summary

Signal-component wise dose evaluation of the file **BT1214\_all\_FKQ\_mx.BIN**:

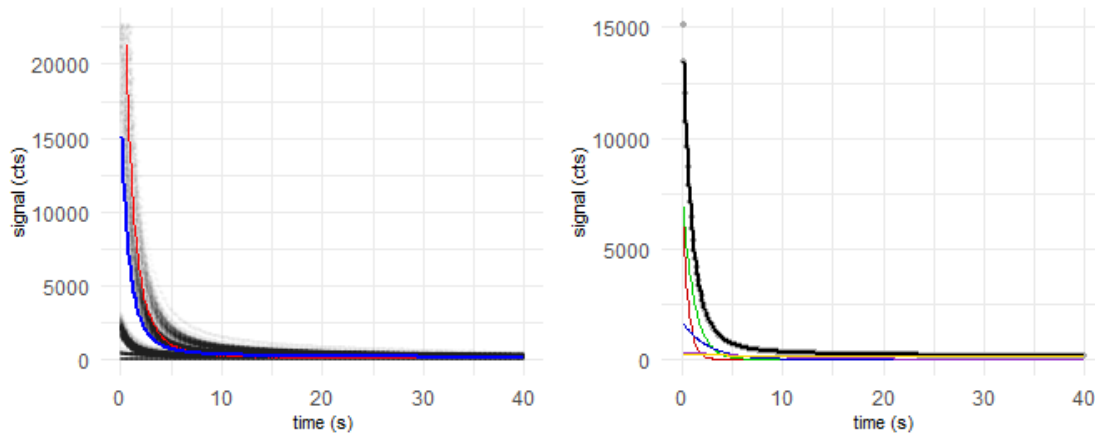


Figure: Left: Data points of whole data set with first curve (red) and global mean curve (blue). Right: Global mean curve (grey) fitted (black) with 5 components (colored)

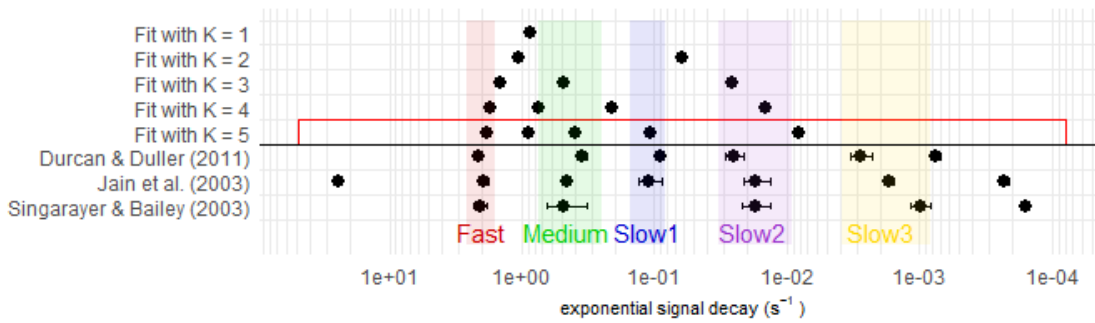


Figure: Evolution of the decay constants with increasing number of components  $K$ . Red square: Best fit chosen through F-test

Table: Result overview

Method	Component	Decay constant	Mean intensity	Passed aliquots	Central age model	Minimum age model
late b.				29 of 30	$50.9 \pm 0.3$ ka (0.02)	$51 \pm 2$ ka
early b.				24 of 30	$50 \pm 0.7$ ka (0)	$50.5 \pm 2.2$ ka
K = 3	Component 1	$1.5 \text{ s}^{-1}$	$7.7\text{e}+04$	24 of 30	$51 \pm 0.8$ ka (0)	$51.4 \pm 2.3$ ka
K = 3	Medium	$0.49 \text{ s}^{-1}$	$8.8\text{e}+04$	26 of 30	$39 \pm 0.6$ ka (0)	$39.2 \pm 1.7$ ka
K = 4	Fast	$1.7 \text{ s}^{-1}$	$4.6\text{e}+04$	8 of 30	$45.9 \pm 2.8$ ka (0)	$46.5 \pm 6.1$ ka
K = 4	Component 2	$0.75 \text{ s}^{-1}$	$9.3\text{e}+04$	22 of 30	$48.6 \pm 1.4$ ka (0)	$49.6 \pm 2.7$ ka
K = 4	Component 3	$0.21 \text{ s}^{-1}$	$3.8\text{e}+04$	2 of 30	$45.2 \pm 7.3$ ka (0)	$47.2 \pm 15$ ka
K = 5	Fast	$1.8 \text{ s}^{-1}$	$3.6\text{e}+04$	3 of 30	$74.4 \pm 22.3$ ka (0)	$75.2 \pm 33.2$ ka
K = 5	Component 2	$0.89 \text{ s}^{-1}$	$8.1\text{e}+04$	10 of 30	$40.5 \pm 4.6$ ka (0.19)	$40.6 \pm 7.3$ ka
K = 5	Medium	$0.4 \text{ s}^{-1}$	$4.1\text{e}+04$	7 of 30	$50.9 \pm 8.5$ ka (0.3)	$42.7 \pm 11.3$ ka

### C.3 BK8 analysis summary

Signal-component wise dose evaluation of the file **BK-8\_1295-1280\_63-40um\_2mm\_Qz1\_ed.BIN**:

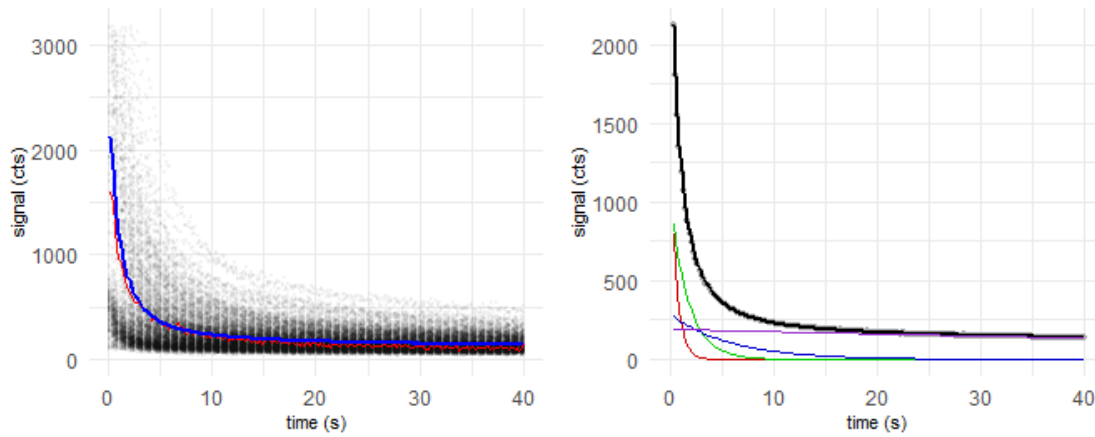


Figure: Left: Data points of whole data set with first curve (red) and global mean curve (blue). Right: Global mean curve (grey) fitted (black) with 4 components (colored)

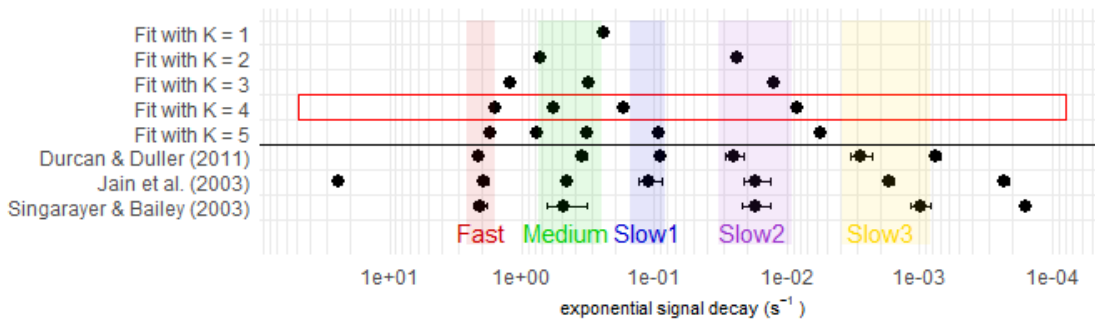


Figure: Evolution of the decay constants with increasing number of components  $K$ . Red square: Best fit chosen through  $F$ -test

Table: Result overview

Method	Component	Decay constant	Mean intensity	Passed aliquots	Central age model	Minimum age model
late b.				16 of 20	$31 \pm 2$ ka (0.27)	$25 \pm 3$ ka
early b.				9 of 20	$31 \pm 2$ ka (0.03)	$32 \pm 5$ ka
K = 3	Component 1	$1.2 \text{ s}^{-1}$	$5.6\text{e}+03$	10 of 20	$31 \pm 2$ ka (0.14)	$31 \pm 4$ ka
K = 3	Medium	$0.31 \text{ s}^{-1}$	$1.1\text{e}+04$	7 of 20	$26 \pm 2$ ka (0.03)	$25 \pm 4$ ka
K = 4	Fast	$1.6 \text{ s}^{-1}$	$3\text{e}+03$	4 of 20	$27 \pm 7$ ka (0.3)	$21 \pm 10$ ka
K = 4	Component 3	$0.17 \text{ s}^{-1}$	$8.1\text{e}+03$	8 of 20	$65 \pm 16$ ka (0.15)	$65 \pm 24$ ka

## C.4 Oy7 analysis summary

Signal-component wise dose evaluation of the file **Oy7-01-14\_63-100\_1mm\_Qz1-1\_ed.BIN**:

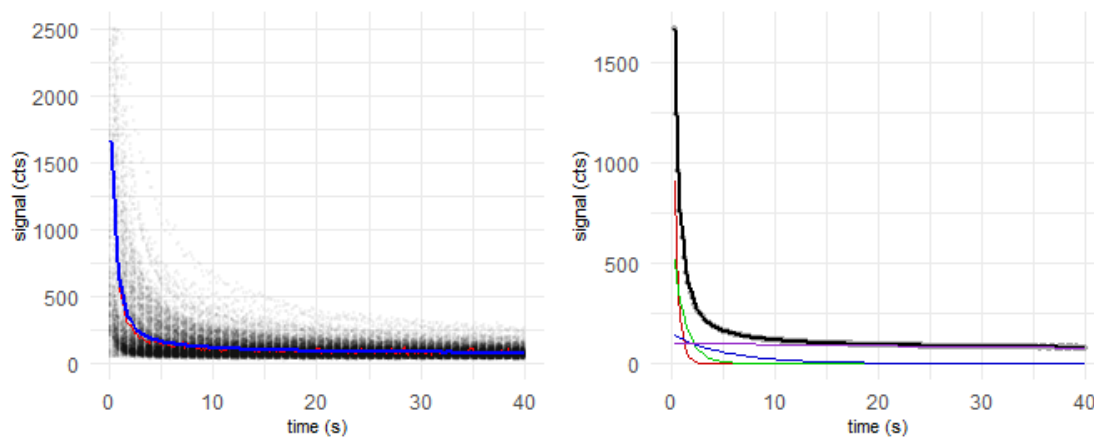


Figure: Left: Data points of whole data set with first curve (red) and global mean curve (blue). Right: Global mean curve (grey) fitted (black) with 4 components (colored)

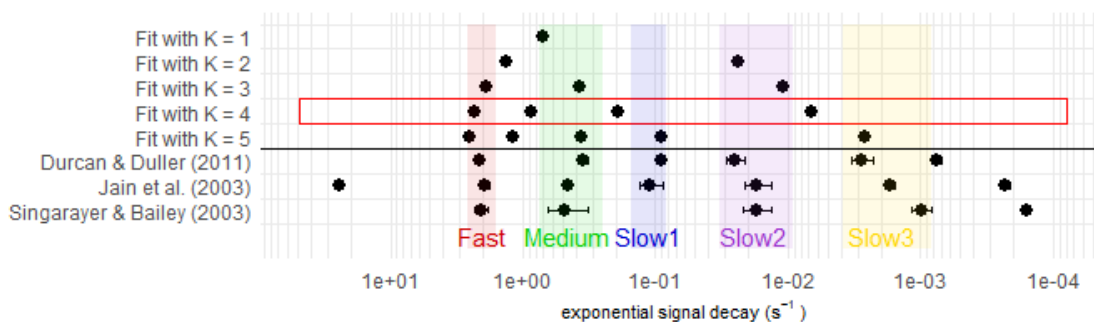


Figure: Evolution of the decay constants with increasing number of components K. Red square: Best fit chosen through F-test

Table 10: Result overview

Method	Component	Decay constant	Mean intensity	Passed aliquots	Central age model	Minimum age model
late b.				15 of 20	$97 \pm 5$ ka (0.2)	$97 \pm 10$ ka
early b.				10 of 20	$112 \pm 17$ ka (0.38)	$75 \pm 21$ ka
K = 3	Fast	$1.9 \text{ s}^{-1}$	$3.9\text{e}+03$	8 of 20	$124 \pm 12$ ka (0.1)	$128 \pm 21$ ka
K = 3	Medium	$0.37 \text{ s}^{-1}$	$4.5\text{e}+03$	4 of 20	$62 \pm 13$ ka (0.23)	$59 \pm 20$ ka
K = 4	Fast	$2.3 \text{ s}^{-1}$	$2.5\text{e}+03$	6 of 20	$99 \pm 17$ ka (0)	$99 \pm 29$ ka
K = 4	Component 2	$0.86 \text{ s}^{-1}$	$3.3\text{e}+03$	4 of 20	$107 \pm 22$ ka (0)	$106 \pm 32$ ka
K = 4	Component 3	$0.19 \text{ s}^{-1}$	$3.7\text{e}+03$	2 of 20	$105 \pm 53$ ka (0)	-

## C.5 Batagai analysis summary

Signal-component wise dose evaluation of the file **Batagai\_2-7\_B-2-47\_OSL\_63-100\_2mm\_Qz1\_ed.BIN**:

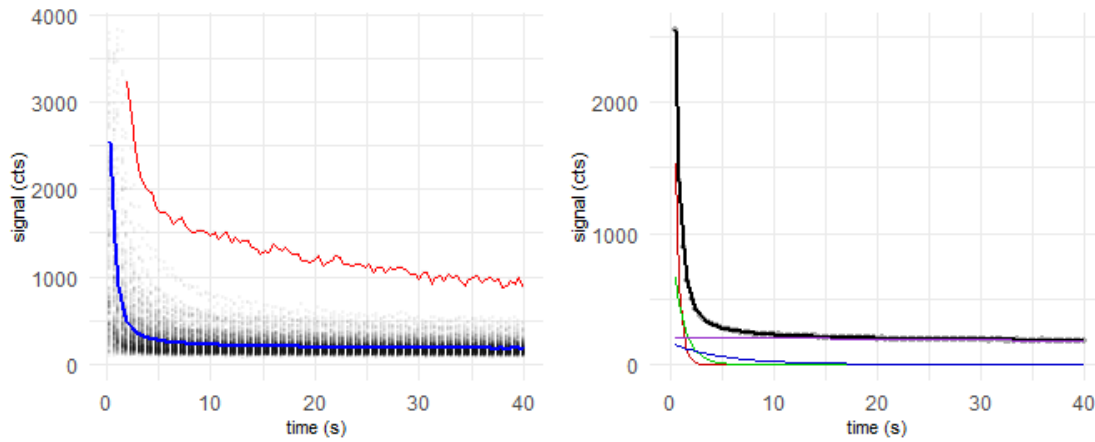


Figure: Left: Data points of whole data set with first curve (red) and global mean curve (blue). Right: Global mean curve (grey) fitted (black) with 4 components (colored)

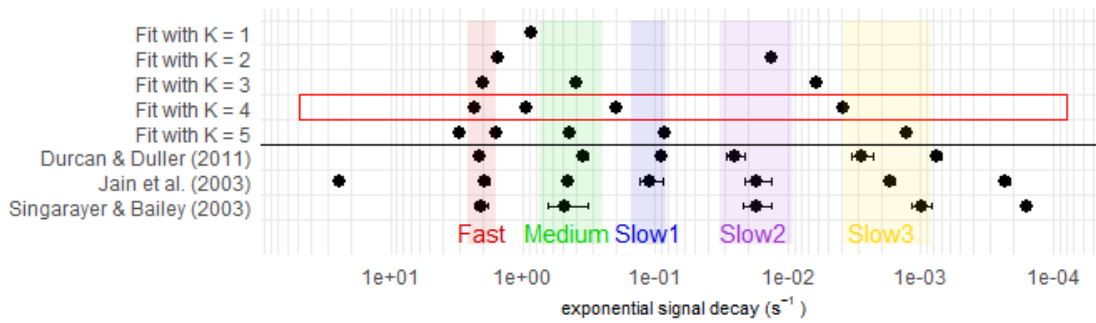


Figure: Evolution of the decay constants with increasing number of components K. Red square: Best fit chosen through F-test

Table: Result overview

Method	Component	Decay constant	Mean intensity	Passed aliquots	Central age model	Minimum age model
late b.				14 of 20	155 ± 25 ka (0.57)	99 ± 16 ka
early b.				4 of 20	168 ± 36 ka (0.3)	-
K = 3	Fast	2 s <sup>-1</sup>	3.6e+03	8 of 20	157 ± 31 ka (0.49)	103 ± 24 ka
K = 3	Medium	0.39 s <sup>-1</sup>	2.5e+03	6 of 20	62 ± 15 ka (0.37)	49 ± 18 ka
K = 4	Fast	2.3 s <sup>-1</sup>	2.5e+03	4 of 20	317 ± 96 ka (0)	317 ± 156 ka
K = 4	Component 2	0.93 s <sup>-1</sup>	2.1e+03	2 of 20	57 ± 27 ka (0)	-
K = 4	Component 3	0.2 s <sup>-1</sup>	2e+03	5 of 20	131 ± 95 ka (0)	130 ± 144 ka

# D OSL dating without heating

## D.1 FB standard SAR protocol analysis summary

Signal-component wise dose evaluation of the file `FB_10Gy_SAR_classic.bin`:

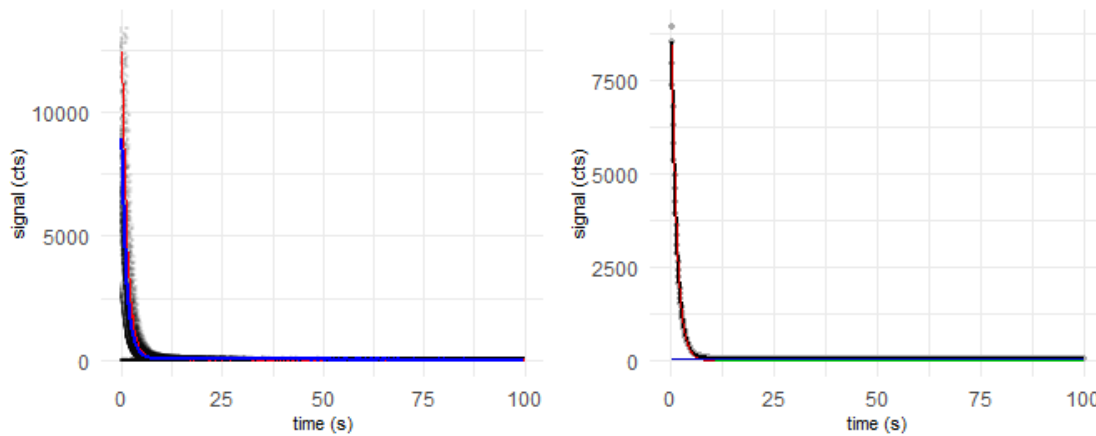


Figure: Left: Data points of whole data set with first curve (red) and global mean curve (blue). Right: Global mean curve (grey) fitted (black) with 3 components (colored)

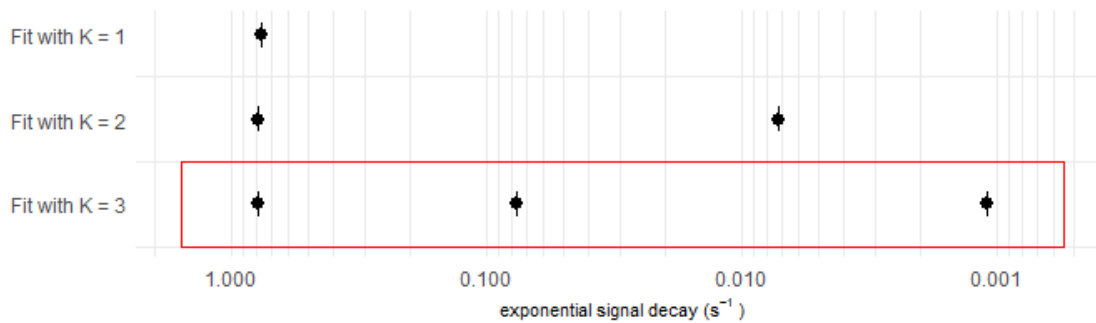


Figure: Evolution of the decay constants with increasing number of components K. Red square: Best fit chosen through F-test

Table: Result overview

Method	Component	Decay constant	Mean intensity	Passed aliquots	Central age model	Minimum age model
late b.				10 of 10	$8.7 \pm 0.1$ Gy (0.02)	$8.7 \pm 0.6$ Gy
early b.				10 of 10	$8.8 \pm 0.1$ Gy (0)	$8.8 \pm 0.6$ Gy
K = 3	Component 1	$0.79 \text{ s}^{-1}$	1.2e+05	10 of 10	$8.7 \pm 0.1$ Gy (0.01)	$8.7 \pm 0.6$ Gy
K = 3	Component 2	$0.077 \text{ s}^{-1}$	6e+03	2 of 10	$7.9 \pm 0.4$ Gy (0)	$7.7 \pm 1.7$ Gy
K = 3	Component 3	$0.0011 \text{ s}^{-1}$	3e+05	2 of 10	$8.4 \pm 3.4$ Gy (0.48)	$5.3 \pm 2.9$ Gy

## D.2 FB no-heating protocol analysis summary

Signal-component wise dose evaluation of the file **FB\_10Gy\_SAR\_RT.bin**:

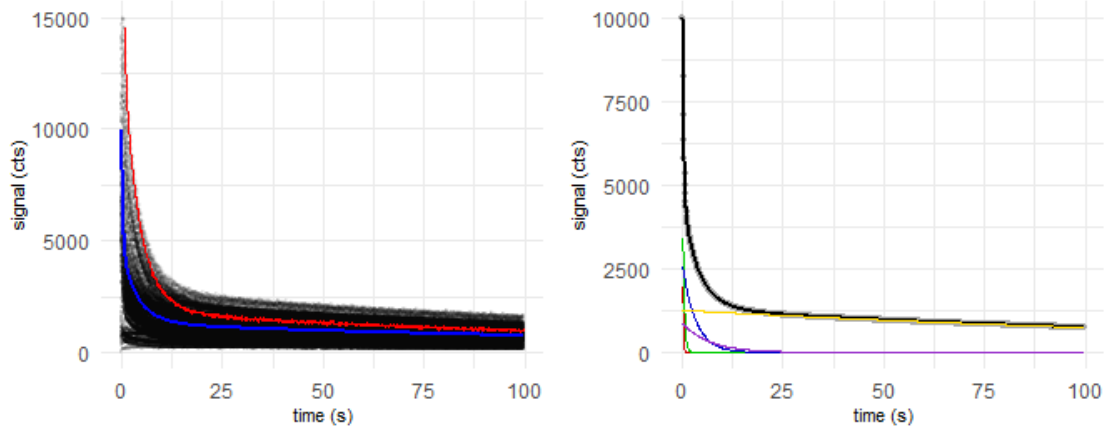


Figure: Left: Data points of whole data set with first curve (red) and global mean curve (blue). Right: Global mean curve (grey) fitted (black) with 5 components (colored)

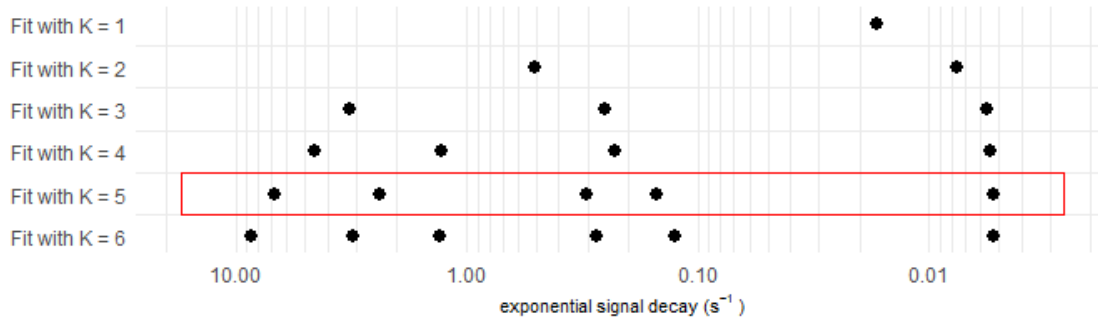


Figure: Evolution of the decay constants with increasing number of components K. Red square: Best fit chosen through F-test

Table: Result overview

Method	Component	Decay constant	Mean intensity	Passed aliquots	Central age model	Minimum age model
K = 3	Component 1	$3.2 \text{ s}^{-1}$	$1.9\text{e}+04$	10 of 10	$0.6 \pm 0.2 \text{ Gy (0)}$	$0.6 \pm 0.2 \text{ Gy}$
K = 3	Component 2	$0.25 \text{ s}^{-1}$	$1.3\text{e}+05$	10 of 10	$7.8 \pm 0.1 \text{ Gy (0.01)}$	$7.8 \pm 0.5 \text{ Gy}$
K = 3	Component 3	$0.0057 \text{ s}^{-1}$	$2.3\text{e}+06$	10 of 10	$4.4 \pm 0.2 \text{ Gy (0.12)}$	$4.4 \pm 0.4 \text{ Gy}$
K = 4	Component 1	$4.6 \text{ s}^{-1}$	$1\text{e}+04$	1 of 10	-	$0.7 \pm 23.6 \text{ Gy}$
K = 4	Component 2	$1.3 \text{ s}^{-1}$	$1.6\text{e}+04$	5 of 10	$4.6 \pm 1.9 \text{ Gy (0)}$	-
K = 4	Component 3	$0.23 \text{ s}^{-1}$	$1.3\text{e}+05$	10 of 10	$7.9 \pm 0.1 \text{ Gy (0)}$	$7.9 \pm 0.6 \text{ Gy}$
K = 4	Component 4	$0.0055 \text{ s}^{-1}$	$2.3\text{e}+06$	10 of 10	$4.1 \pm 0.2 \text{ Gy (0.12)}$	$4.1 \pm 0.4 \text{ Gy}$
K = 5	Component 1	$6.8 \text{ s}^{-1}$	$3.9\text{e}+03$	3 of 10	$1.5 \pm 3.4 \text{ Gy (0)}$	-
K = 5	Component 2	$2.4 \text{ s}^{-1}$	$1.6\text{e}+04$	3 of 10	$0.8 \pm 1.5 \text{ Gy (0)}$	-
K = 5	Component 3	$0.31 \text{ s}^{-1}$	$8.5\text{e}+04$	7 of 10	$10.2 \pm 0.5 \text{ Gy (0)}$	$10.4 \pm 1.3 \text{ Gy}$
K = 5	Component 4	$0.15 \text{ s}^{-1}$	$5.8\text{e}+04$	4 of 10	$6 \pm 0.8 \text{ Gy (0.14)}$	$5.8 \pm 1.4 \text{ Gy}$
K = 5	Component 5	$0.0053 \text{ s}^{-1}$	$2.4\text{e}+06$	10 of 10	$3.9 \pm 0.2 \text{ Gy (0.12)}$	$3.9 \pm 0.4 \text{ Gy}$

## D.3 BT1713 standard SAR protocol analysis summary

Signal-component wise dose evaluation of the file **BT1713\_SAR\_classic.bin**:

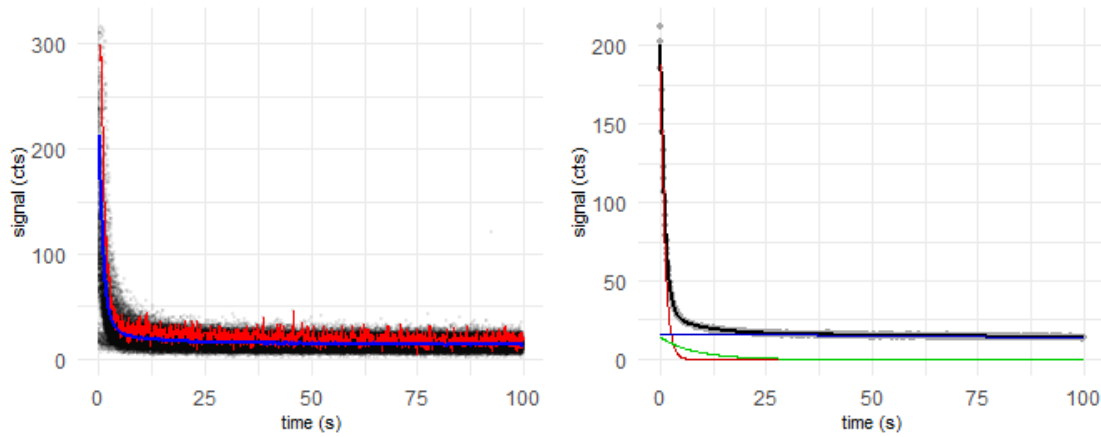


Figure: Left: Data points of whole data set with first curve (red) and global mean curve (blue). Right: Global mean curve (grey) fitted (black) with 3 components (colored)

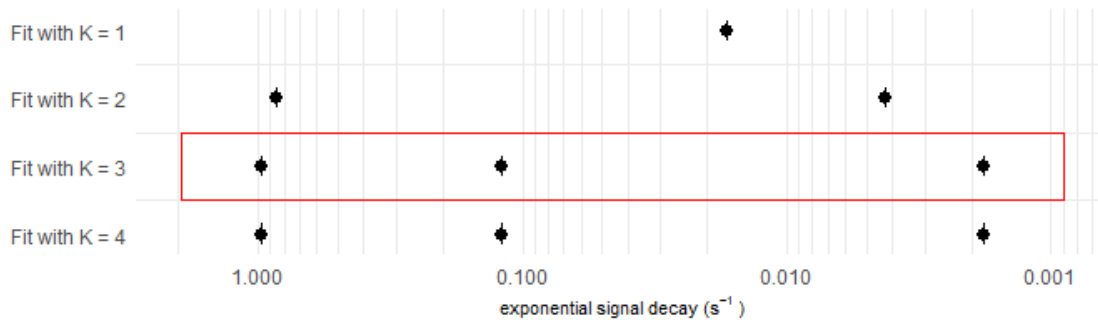


Figure: Evolution of the decay constants with increasing number of components K. Red square: Best fit chosen through F-test

Table: Result overview

Method	Component	Decay constant	Mean intensity	Passed aliquots	Central age model	Minimum age model
late b.				6 of 10	$11.1 \pm 1.4$ Gy (0.3)	$9.7 \pm 1.6$ Gy
early b.				2 of 10	$20.9 \pm 4.1$ Gy (0)	$21.6 \pm 7.4$ Gy
K = 3	Component 1	$0.98 \text{ s}^{-1}$	2e+03	6 of 10	$12.3 \pm 1.7$ Gy (0.33)	$10.5 \pm 1.8$ Gy
K = 3	Component 3	$0.0018 \text{ s}^{-1}$	9.2e+04	1 of 10	-	$455.5 \pm 265.9$ Gy

## D.4 BT1713 no-heating protocol analysis summary

Signal-component wise dose evaluation of the file **BT1713\_SAR\_RT.bin**:

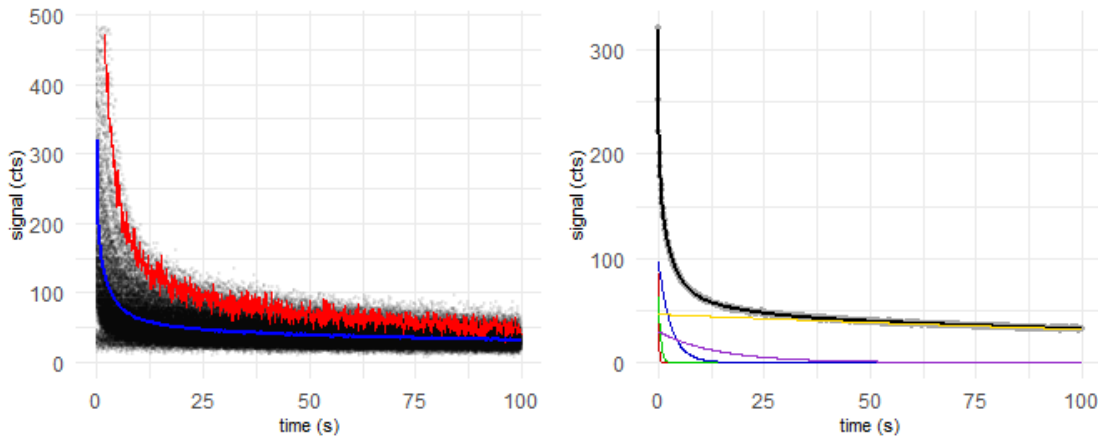


Figure: Left: Data points of whole data set with first curve (red) and global mean curve (blue). Right: Global mean curve (grey) fitted (black) with 5 components (colored)

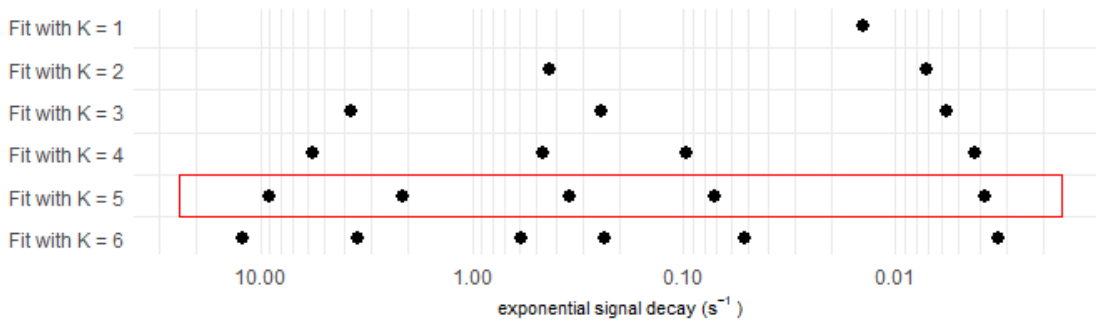


Figure: Evolution of the decay constants with increasing number of components K. Red square: Best fit chosen through F-test

Table: Result overview.

Method	Component	Decay constant	Mean intensity	Passed aliquots	Central age model	Minimum age model
K = 3	Component 1	$3.7 \text{ s}^{-1}$	$4.7\text{e}+02$	4 of 10	$34.8 \pm 8.7 \text{ Gy (0)}$	$35.5 \pm 12.7 \text{ Gy}$
K = 3	Component 2	$0.24 \text{ s}^{-1}$	$4.6\text{e}+03$	6 of 10	$57 \pm 11 \text{ Gy (0.28)}$	$45.9 \pm 15 \text{ Gy}$
K = 4	Component 1	$5.6 \text{ s}^{-1}$	$3\text{e}+02$	3 of 10	$35.4 \pm 13.2 \text{ Gy (0)}$	$35.5 \pm 18.6 \text{ Gy}$
K = 4	Component 3	$0.097 \text{ s}^{-1}$	$4.1\text{e}+03$	3 of 10	$54.7 \pm 17.3 \text{ Gy (0.4)}$	$36.9 \pm 22.1 \text{ Gy}$
K = 5	Component 2	$2.1 \text{ s}^{-1}$	$3.3\text{e}+02$	3 of 10	$39.9 \pm 23.1 \text{ Gy (0)}$	$39.8 \pm 32 \text{ Gy}$
K = 5	Component 3	$0.35 \text{ s}^{-1}$	$2.8\text{e}+03$	1 of 10	-	$31.8 \pm 38.1 \text{ Gy}$
K = 5	Component 4	$0.072 \text{ s}^{-1}$	$4.1\text{e}+03$	4 of 10	$50.8 \pm 11.4 \text{ Gy (0.1)}$	$49.7 \pm 17.5 \text{ Gy}$

**Note:** The allowed recuperation rate and the allowed recycling ration deviation were both set to 0.2 to increase number of passed aliquots.



# Erklärung

Hiermit versichere ich, dass ich die vorliegende Masterarbeit ohne unzulässige Hilfe und ohne Benutzung anderer als der angegebenen Hilfsmittel angefertigt habe. Die aus fremden Quellen direkt oder indirekt übernommenen Gedanken sind als solche kenntlich gemacht. Diese Arbeit wurde bisher weder im Inland noch im Ausland in gleicher oder ähnlicher Form einer anderen Prüfungsbehörde vorgelegt.

Dirk Mittelstraß

Dresden den 27. November 2019